

Aus dem Institut für Schlaganfall und Demenzforschung  
der Ludwig-Maximilians-Universität München

Vorstand: Prof. Dr. Martin Dichgans

## **The effect of age on neuro-vascular reactivity in mice**

Dissertation

zum Erwerb des Doktorgrades der Medizin

an der Medizinischen Fakultät der

Ludwig-Maximilians-Universität zu München

vorgelegt von

Ziyu Fan

aus

Anyang, Henan, China

2021

Mit Genehmigung der Medizinischen Fakultät der Universität München

Berichterstatter: Prof. Dr. Nikolaus Plesnila

Mitberichterstatter: Prof. Dr. Inga Koerte

PD Dr. Guido Böning

Mitbetreuung durch die

promovierte Mitarbeiterin: Dr. Burcu Seker

Dekan: Prof. Dr. med. dent. Reinhard Hickel

Tag der mündlichen Prüfung: 04.03.2021

# Table of contents

1. Introduction.....	7
1.1. Autoregulation of cerebral blood flow .....	7
1.2. Functional hyperemia .....	8
1.3. Neurovascular unit.....	9
1.4. Cellular basis of Neurovascular coupling .....	10
1.4.1. Neurons.....	12
1.4.2. Astrocytes .....	13
1.4.3. Endothelial cells .....	14
1.4.4. Smooth muscle cells and pericytes.....	14
1.4.5. Summary of possible mechanisms.....	15
1.5. Aging.....	15
1.6. Aim .....	17
2. Materials and methods .....	19
2.1. Materials .....	19
2.1.1. Equipment.....	19
2.1.2. Surgery tools .....	20
2.1.3. Automatic whisker stimulator .....	21
2.1.4. Drugs and chemicals .....	21
2.1.5. Software.....	22
2.2. Experimental Animals .....	22
2.3. Experimental design.....	23
2.3.1. Forepaw stimulation and Laser Doppler flowmetry (LDF).....	23
2.3.2. Forepaw stimulation and Laser speckle imaging (LSI) .....	23
2.3.3. Whisker stimulation, LSI and two-photon microscopy.....	23

2.4. Forepaw stimulation and LDF .....	24
2.4.1. Anesthesia and intubation .....	24
2.4.3. Femoral artery catheterization .....	25
2.4.4. Forepaw stimulation and LDF .....	25
2.5. Forepaw stimulation and LSI .....	26
2.5.1. Chronic window surgery .....	27
2.5.2. Forepaw stimulation and LSI .....	28
2.5.3. CO <sub>2</sub> inhalation and LSI .....	29
2.5.4. Neuronal activity during forepaw stimulation .....	29
2.6. Whisker stimulation .....	30
2.6.1. Chronic window surgery .....	30
2.6.2. Whisker stimulation and LSI .....	30
2.6.3. CO <sub>2</sub> inhalation and LSI .....	31
2.6.4. Whisker stimulation and CO <sub>2</sub> inhalation: two-photon microscopy .....	31
2.7. Barnes maze .....	32
2.8. Imaged analysis of two-photon images .....	33
2.9. Statistics .....	34
3. Results .....	35
3.1. Forepaw stimulation and LDF .....	35
3.2. Neuronal activity during forepaw stimulation .....	35
3.3. Forepaw stimulation and LSI .....	36
3.3.1. Forepaw stimulation .....	36
3.3.2. CO <sub>2</sub> response .....	41
3.3.3. Whisker stimulation .....	43
3.3.4. CO <sub>2</sub> response .....	46

3.4. Whisker stimulation and two-photon microscopy .....	48
3.4.1. Whisker stimulation.....	48
3.4.1.1. Pial arteries.....	48
3.4.1.2. Penetrating arteries.....	49
3.4.1.3. Capillaries.....	50
3.4.2. CO <sub>2</sub> response.....	52
3.4.2.1. Pial arteries.....	52
3.4.2.2. Penetrating arteries.....	53
3.4.2.3. Capillaries.....	54
3.5. Barnes maze.....	55
4. Discussion.....	57
4.1. Discussion of method.....	58
4.1.1. In vitro method.....	58
4.1.2. In vivo method.....	58
4.1.2.1. Laser Doppler based imaging.....	58
4.1.2.2. Fluorescent based imaging.....	60
4.1.3. Sensory stimulation.....	61
4.1.3.1. Forepaw stimulation.....	61
4.1.3.2. Whisker stimulation.....	62
4.1.4. Anesthesia.....	63
4.2. Discussion of result.....	63
5. Summary.....	69
5.1. English summary.....	69
5.2. Zusammenfassung und Ausblick.....	70
6. References.....	72

7. Abbreviations ..... 97

8. Acknowledgments ..... 100

## **1. Introduction**

In comparison to its weight the brain needs extensive amounts of blood to supply oxygen and glucose to glia and neurons and to eliminate metabolic waste. Although brain weight accounts for only 2% of the body weight, it consumes about 20% of the whole body energy<sup>1</sup>. Thus, brain tissue is extremely vulnerable to hypoxia and consequently neuronal cells can quickly develop ischemia. Therefore, a healthy cerebrovascular adaptation system is essential to supply sufficient cerebral blood flow (CBF) to the brain in order to maintain the required cerebral oxygen and glucose concentrations and to maintain brain function at rest and during phases of activity.

When neurons start firing, local CBF increases (hyperemia) to deliver more energy substrates and oxygen to activated neurons. This phenomenon is called “neurovascular coupling (NVC)” or “functional hyperemia”<sup>2</sup>. Functional hyperemia has been studied in detail in the past. In 1840, Sherrington and colleagues recorded an increase in CBF upon application of brain extract to dogs<sup>3</sup>. In 1938, Schmidt et al. found that visual stimulation increased visual cortex temperature, as a surrogate marker for increased CBF, in cats<sup>4</sup>. Subsequently, the concept of functional hyperemia was established, namely that increased brain function is followed by a consecutive increased in blood flow in order to match increased cerebral metabolism.

### **1.1. Autoregulation of cerebral blood flow**

The cerebral circulation has an autoregulation system. Basically, cerebral vessels can constrict or dilate in response to increased or decreased blood pressure, thus maintaining CBF stable during different physiological conditions<sup>5</sup>. The myogenic response of smooth muscle cell (SMC) is considered to control autoregulation<sup>6</sup> and thus large vessels account for 40% of cerebral vascular resistance<sup>7</sup>. When the pressure in the vessel lumen is increased, SMCs will constrict so that the increased pressure does not reach downstream vessels. This is supported by the in vitro isolated rabbit pial vessel experiment<sup>8</sup> as well as

the in vivo recording of Laser Doppler flowmetry (LDF) from patients<sup>9</sup>. In the normal hypertensive state, CBF can still remain relatively stable due to autoregulation<sup>10</sup>. This is especially important for the protection of some micro cerebral vessels like lenticulostriate arteries which are vulnerable in hypertension. The constriction of SMC is related to 20-Hydroxyeicosatetraenoic acid (20-HETE)<sup>11</sup>. Mechanical stress from increased pressure increases the catalyzation of phospholipase A2 (PLA2) on SMCs which increases the production of 20-HETE<sup>12</sup>. 20-HETE further increases calcium, depolarizes and constricts SMCs. There is also evidence that the sympathetic and parasympathetic nerves are involved in autoregulation<sup>13</sup>.

## **1.2. Functional hyperemia**

In addition to autoregulation, a functional regulation is also needed in the brain in order to adjust blood flow to brain activity and to remove metabolic by-products such as CO<sub>2</sub>, lactate, or even amyloid- $\beta$  and tau<sup>14</sup>. To date, mainly two theories are discussed how CBF is regulated within the brain parenchyma. One is the feedback theory and the other is the feed-forward theory.

The feedback theory is based on the fact that metabolic by-products like CO<sub>2</sub> and lactate and hypoxia evoke CBF responses<sup>15,16</sup>. It was reported that decreased oxygen in rat brain slices increased astrocytic calcium and dilated vessels<sup>17</sup>. However, other evidence indicates that feedback mechanism cannot solely evoke hemodynamic responses. The increase in CBF was shown to be related to the release of lactate, but the response was much smaller as compared to task-evoked CBF response<sup>18</sup>. In another study, the CBF response following forepaw stimulation remained unchanged under the condition of excess energy supply like hyperbaric hyperoxia suggesting that the CBF response may not only be driven by local metabolites<sup>19</sup>.

The feed-forward theory was proposed based on the observation that release of neurotransmitters by neurons during activity, e.g. glutamate, potassium (K<sup>+</sup>), or nitric

oxide (NO), directly elicit a CBF response<sup>20</sup>. For example, extracellular K<sup>+</sup> can directly dilate cerebral capillaries as well as upstream arterioles<sup>21</sup>. The feedback and feed-forward theory, however, may not be contradictory but seems to work together. On one hand, neural activity releases transmitters which directly increase CBF to a maximal level, subsequently the feedback control tends to decrease the CBF and fine-tunes the response based on the need for energy supply<sup>22,23</sup>.

### **1.3. Neurovascular unit**

To understand how neuronal signals evoke vessel dilation, the concept of the neurovascular unit (NVU) should be introduced in detail. The NVU was first proposed in 2001 with the advancement of biomedical technologies and emerging brain imaging skills to study brain structure<sup>24</sup>. Cerebral vessels and different types of brain cells are in close contact with each other structurally and functionally<sup>25,26</sup>. Brain blood supply mainly originates from the internal carotid arteries and vertebral artery. They form a communicating circle called Willis' circle at the base of the brain. As shown in Figure 1, the branch of the cerebral artery from Willis' circle extending on the surface of the brain is called "pial artery" and it is located in the subarachnoid space. A pial artery has a classical vessel structure like other big vessels in the body. It consists of thick layers of SMC in the outer layer, an endothelial cell lining the inner layer and an internal elastic membrane in the middle layer<sup>27</sup>. At the pial artery level, there is also perivascular nerve innervation, mainly from the sympathetic and parasympathetic system and peripheral ganglion<sup>28,29</sup>. These perivascular nerves release neuropeptides and transmitters which control vessel dilation or constriction<sup>30</sup>. For example, treatment with the inhibitor of 20-HETE synthesis reduce oxidative stress and cerebrovascular inflammation in spontaneously hypertensive rats<sup>20</sup>. After pial artery dives into the brain parenchyma, it forms "penetrating arterioles" which have fewer SMCs and a thinner elastic membrane. There is a perivascular space between penetrating vessels and the glia limitans which is called Virchow-Robin space<sup>31,32</sup>.

As the artery penetrates deeper into the brain, it starts to become thinner having a single layer SMCs and not having an elastic membrane anymore. These vessels are called “Intraparenchymal arterioles”. Intraparenchymal arterioles have a direct contact with astrocytes and neurons so that there is no longer Virchow-Robin space in between. Eventually, at the level of the capillary, the SMC is replaced by “pericytes”, perivascular cells which express alpha smooth muscle actin ( $\alpha$ -SMA) and can also constrict. Therefore, pericytes most likely adjust the diameter of capillaries<sup>33</sup>.

#### **1.4. Cellular basis of Neurovascular coupling**

Different cells are involved in NVC. Neurons are the initiator of the NVC process. They generate signals and transfer the signal to astrocytes. Astrocytes are the linker between neurons and vessels where the signaling is controlled and modified. Besides astrocytes, endothelial cells are also involved in signal propagation. Finally, SMCs and pericytes are the contractile apparatus to constrict or dilate the vessel.

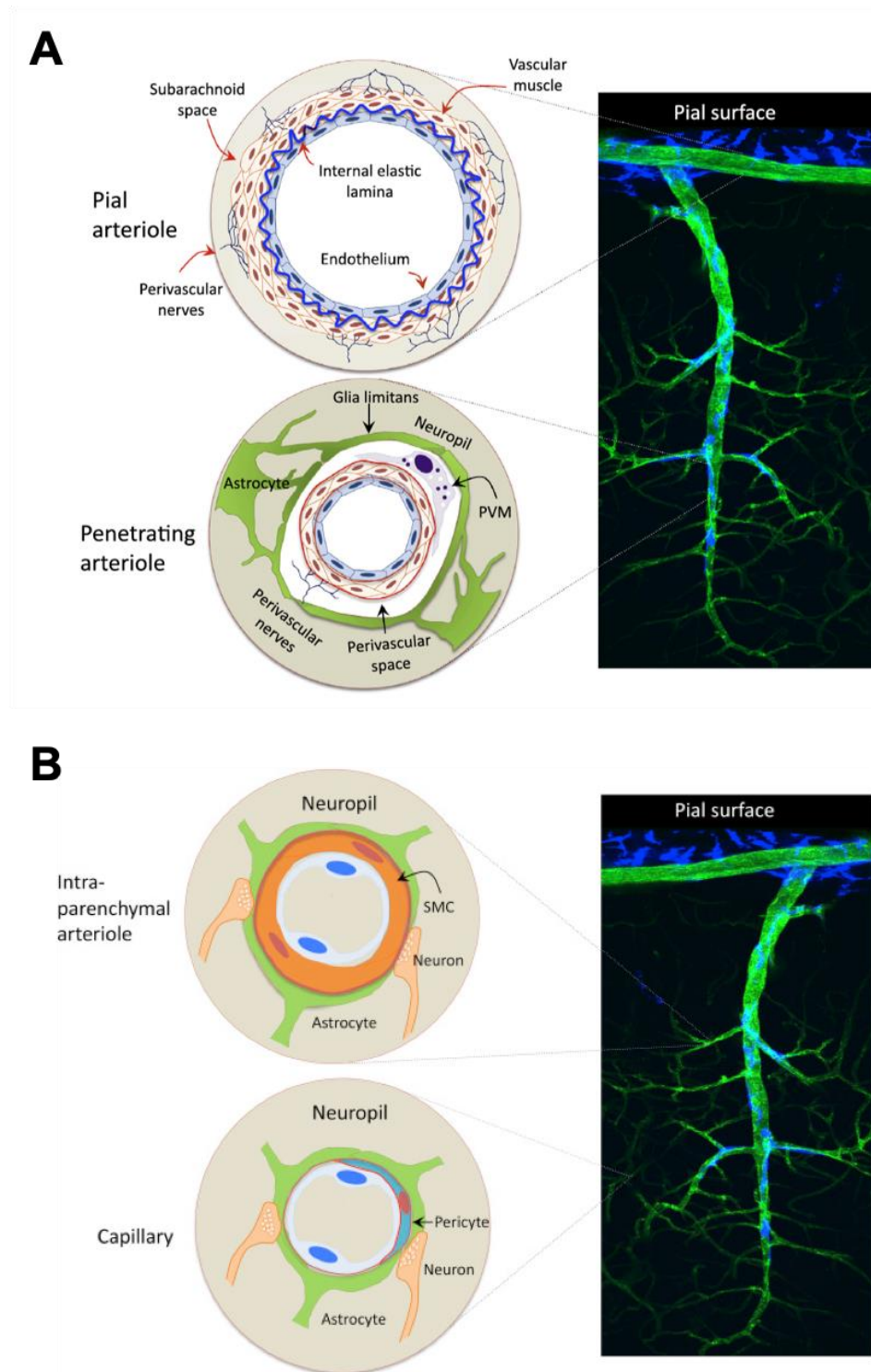


**Figure 1:** The structure of the neurovascular unit. (A) Pial and penetrating artery; (B) Intraparenchymal artery and capillary<sup>24</sup>.

### 1.4.1. Neurons

Neurons are responsible for initiating NVC. They communicate to astrocytes and transfer signals to them which then results in vessel dilatation<sup>34</sup>. There are two types of neurons involved in the process: pyramidal neurons and interneurons. Pyramidal neurons are the main source of signal output. The activation of pyramidal neurons releases glutamate which binds to N-methyl-D-aspartate (NMDA) and  $\alpha$ -amino-3-hydroxy-5-methyl-4-isoxazole propionic acid (AMPA) receptors thereby causing the release of vasoactive agents like NO or adenosine<sup>20,35,36</sup>. At the same time, glutamate binds to glutamate receptors on astrocytes, leading to an increase in cytosolic calcium<sup>37,38</sup>. The increase of cytosolic calcium will then activate calcium-dependent enzymes like neuronal nitric oxide synthase (nNOS) or cyclooxygenase 2 (COX-2) which then release the vasoactive agents<sup>39</sup>. nNOS deficient mice have an attenuated NVC response upon electrical limb stimulation or superfusion with glutamate<sup>40</sup>. Application of indomethacin or other cyclooxygenase-1 inhibitors attenuated NVC evoked by the specific release of calcium in astrocytes<sup>41</sup>.

Besides nNOS/COX2-mediated signaling in pyramidal neurons,  $\gamma$ -aminobutyric acid (GABA)-ergic interneurons also play a role in NVC<sup>42</sup>. Inhibition of glutamatergic signaling by NBQX or MK-801 attenuated NVC<sup>43</sup>, however, the CBF response was maintained when interneurons were blocked pharmacologically<sup>35</sup>. This indicates that interneurons may play a role for NVC in parallel to pyramidal neurons. The mechanism of interneuron-mediated NVC may be related to the release of vasoactive peptides like intestinal peptide (VIP)<sup>44</sup> or neuropeptide Y (NPY)<sup>45</sup>. In brain slices, VIP superfusion caused vessel dilation and NPY perfusion caused vessel constriction<sup>46</sup>, however, the underlying mechanisms are unclear yet<sup>47</sup>.

Neurons located in subcortical nuclei may also play a role in NVC. They have long projections which are in contact with perivascular astrocyte end-feet near arterioles and release cholinergic and adrenergic neurotransmitters, such as acetylcholine, serotonin,

and noradrenaline<sup>48</sup>. Activation of these subcortical nuclei has shown to increase blood flow and inhibition of the cholinergic system suppressed NVC in response to whisker stimulation<sup>49,50</sup>. Hence subcortical nuclei are suggested to maintain vascular tone and modulate NVC<sup>24</sup>.

#### **1.4.2. Astrocytes**

Astrocytes are mediators between neurons and vessels and play an important role in NVC. The main hypothesis of how astrocytes are involved in NVC is related to cytosolic calcium. As pointed out above, activated neurons release glutamate into the synaptic cleft. Glutamate then binds to glutamate receptors on astrocytes and increases cytosolic calcium through the inositol trisphosphate (IP3) pathway<sup>51</sup>. The calcium signal propagates from peri-synaptic astrocytic end-feet to peri-vascular astrocytic end-feet where it causes release of vasoactive factors such as 20-HETE or Prostaglandin E<sub>2</sub> (PGE<sub>2</sub>)<sup>52</sup>. However, this sequence of events has been challenged by experiments showing that a selective increase in cytosolic calcium in astrocytes does not evoke NVC upon visual stimulation<sup>53</sup>. These results suggest that an increase in cytosolic calcium in astrocyte is not the cause for functional hyperemia, but rather its result. Also, the role of astrocytic glutamate and IP3 receptors for NVC was challenged since metabotropic glutamate receptor 5 does not exist in adults<sup>54</sup> and NVC remained intact in mice lacking the IP3 receptor<sup>55</sup>. Thus it is believed that astrocyte derived vasoactive factors have a rather tonic, steady-state effect on CBF<sup>56</sup>. These results indicate that astrocytes mediate NVC through alternative, so far unknown mechanisms. Potassium signaling may be a suitable candidate since astrocytic end-feet express large-conductance Ca<sup>2+</sup>-sensitive potassium BK channels<sup>57</sup> and neural activity activates these channels thereby causing vessel dilatation through activation inward-rectifier potassium (K<sub>ir</sub>) channels on SMC<sup>58</sup>.

### **1.4.3. Endothelial cells**

Endothelial cells seem to be involved in the retrograde spreading of NVC from capillaries to more upstream arterioles along the vascular tree<sup>59</sup>. Blood oxygenation level-dependent (BOLD) functional magnetic resonance imaging (fMRI) data indicate that following forepaw stimulation, deeper regions in the rat brain respond first and the signal propagates in a retrograde manner through the cortex<sup>60</sup>. This suggests that capillaries in the parenchyma dilate before pial arteries. The underlying mechanisms seem, again, to be mediated by potassium ions. When  $K^+$ -ions were injected around capillaries in vivo, capillaries dilated before upstream arterioles<sup>61</sup>. This process was blocked in  $K_{ir}$  knockout mice, therefore  $K_{ir}$  channels expressed on endothelial cells are believed to be crucial for this process<sup>61</sup>. This is supported by reports describing that retrograde vessel dilation was abolished when the endothelium of pial vessels was lesioned<sup>62</sup>. Experiments using Cx40(BAC)-GCaMP2 transgenic mice indicated that endothelial gap junctions were involved in the bidirectional propagation of  $K^+$ -ions along the neurovascular tree<sup>63</sup>.

### **1.4.4. Smooth muscle cells and pericytes**

The ability to contract makes SMCs and pericytes the final controllers of vessel diameter and, hence, capillary blood flow. SMCs are located on larger vessel, e.g. pial arterioles, while pericytes are located on capillaries<sup>64</sup>. SMCs do not only control functional hyperemia but are also involved in autoregulation of CBF upon changes in systemic blood pressure<sup>65</sup>. The contractile apparatus of SMCs is similar to that of skeletal muscle cells<sup>66</sup>. They contain myosin and  $\alpha$ -SMA, which slide together causing constriction upon increase of cytosolic calcium<sup>67</sup>.

More recently pericytes emerged as key elements of controlling cerebral blood flow at the level of the capillary. Pericytes sit on the parenchymal side of the endothelial cell layer and stretch out long processes along the capillary network. They are in direct contact with endothelial cells, astrocyte end-feet, and neuronal terminals. Although specific markers

for pericytes are still lacking, they can be identified by their localization on the capillary level together with the expression of marker proteins like platelet-derived growth factor receptor  $\beta$  (PDGFR- $\beta$ ) and neuron-gial antigen 2 (NG2). In the brain, pericytes maintain vessel morphology and the proper function of the blood-brain-barrier (BBB)<sup>68,69</sup> and control capillary blood flow through their ability to constrict<sup>70</sup>. Similar to SMC, pericytes are able to constrict by expression of  $\alpha$ -SMA as recently demonstrated by immunostaining<sup>71</sup>.

An in vivo study using NG2-DsRed transgenic mice showed that whisker stimulation dilates capillaries rather than arterioles and that capillaries with more pericytes dilate more pronounced<sup>70</sup>. In partly pericyte-deficient mice, the CBF increase induced by hindpaw stimulation was smaller compared to control mice<sup>72</sup>. Even though the debate about the precise role of pericyte for NVC is still ongoing, these data clearly suggest that pericytes are part of the cells involved in the network responsible for NVC.

#### **1.4.5. Summary of possible mechanisms**

Taken together, NVC is initiated by neuronal activity and the subsequent release of  $K^+$  ions which act through  $K_{ir}$  channels on endothelial cells and pericytes. Hyperpolarization of endothelial cells retrogradely propagates to upstream SMCs which dilate penetrating and pial arterioles. In addition, perivascular nerves and interneurons modulate vessel tone. The role of astrocytes remains to be fully elucidated.

#### **1.5. Aging**

The effect of aging on the central neural system can be reflected on both the morphological and functional side. One of the most prominent changes in the aged brain is brain atrophy which can be detected by gross autopsy<sup>73</sup>. Magnetic resonance imaging (MRI) shows a decrease in grey matter volume in various brain regions with aging<sup>74</sup>. As for the white matter, which is evaluated by diffusion tensor imaging (DTI), atrophy is also

observed in aged citizens<sup>75</sup>. In parallel to morphological changes, aging causes cognitive decline in laboratory animals or humans<sup>76,77,78</sup>.

Aging affects the normal structure and function of the NVU. Aged mice show decreased astrocyte end-feet density, pericyte coverage in the hippocampus and also more microglial proliferation as compared to young mice<sup>79,80</sup>. Aging also contributes to neural death and synaptic dysfunction<sup>81</sup>. Neurons and synaptic density are mostly reduced in the hippocampus and prefrontal cortex in aged brain<sup>82</sup>. The synaptic function can be measured by long-term potentiation (LTP). Aged mice have impaired induction and maintenance of LTP. Moreover, aging also increases blood-brain barrier (BBB) permeability which affects the homeostasis of NVU and cell to cell interaction<sup>83</sup>.

Aging can also affect the cerebral vascular system. At the anatomical level, aging reduces the capillary density and leads to abnormal microvessel structure<sup>84</sup>. It can promote atherosclerosis in large cerebral vessels<sup>85</sup>. Further, aging may increase artery stiffness, mainly in big arteries, which can impair CBF autoregulation<sup>86</sup>. The myogenic response to increased blood pressure is impaired thereby making the brain vulnerable to hypertensive encephalopathy and hypoperfusion<sup>87</sup>. The change of structure in the aging brain leads to reduced cerebral blood flow<sup>88,89</sup>. Moreover, aging impairs NVC in animals and humans<sup>90,91,92,93</sup>. When stimulating CBF by forepaw stimulation, the CBF response of the somatosensory cortex is decreased in mice<sup>94</sup>. In humans, the BOLD signal of fMRI is decreased in old as compared to young people<sup>95</sup>. The mechanism of how aging affects NVC is still poorly understood. But it is generally agreed that it might be related to endothelial dysfunction and oxidative stress<sup>96</sup>.

Oxidative stress is believed to be one of the main reasons for endothelial dysfunction during aging<sup>97</sup>. Nicotinamide adenine dinucleotide phosphate (NADPH) is the major source of free radicals in blood vessels<sup>98</sup>. Reactive oxygen species (ROS) scavenger or NADPH oxidase peptide inhibitor gp91ds-tat can rescue cerebrovascular impairment in

aged mice but failed in mice lacking the Nox2 subunit of NADPH oxidase<sup>99</sup>. Anti-oxidative treatment can also restore endothelial function. Treatment with the cytochrome P450  $\omega$ -hydroxylase inhibitor HET0016 attenuates cerebrovascular inflammation, oxidative stress, and improves vasomotor function in spontaneously hypertensive rats<sup>100</sup>. But anti-oxidative treatment may be only partially effective. Superfusion with a free radical scavenger can rescue NVC at three months but only partially at 18 months<sup>101</sup>.

Besides normal aging, neurovascular dysfunction also happens in pathological aging like Alzheimer's disease (AD). AD is an age-related progressive neurodegenerative disease characterized by cognitive decline and the accumulation of amyloid beta (A $\beta$ ) in the brain<sup>102</sup>. Age-associated NVC uncoupling also exists in AD<sup>103</sup>. In 18 months-old transgenic AD mice, glutamate-induced NVC was impaired<sup>104</sup>. In AD patients, NVC was also significantly reduced compared to healthy controls<sup>105</sup>. These changes are paralleled by degeneration of capillaries<sup>106</sup>. Even though in the AD brain there is no obvious decline in capillary density, the morphology of capillaries changes to a string shape<sup>107</sup>. Since, AD may be associated with atherosclerosis, the brain of AD patients may become particularly vulnerable to cerebral hypoperfusion<sup>108,109</sup>. The mechanisms for NV uncoupling in AD is similar to normal aging, i.e. by oxidative stress caused NADPH oxidase, especially the NOX subunit of NADPH oxidase<sup>110,111</sup>.

NVC uncoupling in aging means that the energy need of activated neurons cannot be satisfied and that metabolic waste cannot be removed effectively. This pathology leads to decline of higher cognitive function in animals and humans<sup>5,112</sup>. Similar findings are observed when NVC uncoupling is induced pharmacologically<sup>113</sup>, a process which can be reversed by treatment with antioxidants<sup>76</sup>.

## **1.6. Aim**

Aging causes a decline of NVC which was not often investigated experimentally and therefore the effect of age on NVC is poorly understood. With the limitation of sensory

stimulation or imaging platform, former studies in the past sometimes lack proper sensory stimulation in vivo or the specificity of the contribution of different vessel segments to the impact of aging on the NVC.

In order to study NVC, proper sensory stimulation is important. Former studies tended to use forepaw stimulation with LDF recording in aged mice<sup>114</sup>. The inappropriate setting of the forepaw stimulation can hyperpolarize sensory neurons and lead to the increase of mean artery pressure which increases the CBF mechanically and not functionally<sup>115</sup>. The aim of this project is, first of all, to establish an effective sensory stimulation protocol in vivo and combine it with an imaging system suitable to detect the hemodynamic change in aged mice. We used forepaw stimulation and whisker stimulation with laser speckle imaging (LSI). With an optimized stimulation protocol, the CBF response of mice can be recorded with LSI within different regions on the cortex. The temporal and spatial resolution of LSI is suitable to record the CBF response.

Former studies of NVC response in aged animal often focused on pial arteries<sup>94</sup>. There are studies investigating NVC of different vessel segments like pial artery, penetrating artery and capillary using two-photon microscopy, but usually only young mice were used<sup>116,117</sup>. Moreover, different stimulation methods, like forepaw stimulation, whisker pad stimulation, and whisker air puff were used<sup>118,119,120</sup>. In this project, we wanted to study the impact of aging on the hemodynamic response of different vessel segments by using two-photon microscopy. We build an automated whisker stimulation device which allowed us to perform the mechanical whisker stimulation under the two-photon microscope in light sedation. Using this experimental platform, we wanted to explore whether there is a decline of NVC in aged mice in different vessel segments. Finally, we wanted to correlate the neurovascular response with cognitive function.

## 2. Materials and methods

### 2.1. Materials

#### 2.1.1. Equipment

Li:Ti Laser, Chameleon	Co. Coherent (Scotland)
Two-photon microscope LSM 7 MP	Co. Carl Zeiss (Germany)
DS3 Isolated Constant Current Stimulator	Co. Digitimer (UK)
Laser speckle imager (PeriCam PSI)	Co. Perimed AB (Sweden)
Barnes maze software	Co. NoldusIT (USA)
LDF monitor (PeriFlux System 5000)	Co. Perimed AB (Sweden)
Leica M80 surgical microscope	Co. Leica (Germany)
X-cite 120 Fluorescence Illuminator	Co. Lumen Dynamics (USA)
Microcapnograph 340	Co. Hugo Sachs (Germany)
Minivent 845	Co. Hugo Sachs (Germany)
DC Temperature Control System	Co. FHC (USA)
Power Lab 8/35	Co. ADInstruments (Australia)
PhysioSuite PS-03	Co. Kent Scientific (USA)
Mouse Tail Illuminator Restrainer	Co. Braintree Scientific
MediHEAT Heater	Co. Peco Services (UK)
Pulse oximeter (PhysioSuite PS-03)	Co. Kent Scientific (USA)

### 2.1.2. Surgery tools

Dental Drill	Co. Rewatronik (Germany)
Drill tips (19007-05)	Co. FHC (USA)
Stereotactic Injection Platform	Co. Föhr Medical Instruments (Germany)
MicroSyringe Pump Controller	Co. World Precision Instruments (USA)
Intubation tube	Custom made
Venous Catheter (20G)	Co. BD Biosciences (USA)
Coverslips (2mm*2mm)	Co. Warner Instruments (USA)
Coverslips (4mm)	Co. Warner Instruments (USA)
Anesthetic Vaporizers	Co. Harvard Apparatus (USA)
Acupuncture needle (0.2mm)	Co. Suzhou medical appliance (China)
CO <sub>2</sub> gas bottle	Co. Linde (Germany)
Biopsy punch	Co. KAI medical
Micro Serrefine (1805504)	Co. Fine Science Tool (Switzerland)
Micro Serrefine Clamp Applying Forcep	Co. Fine Science Tool (Switzerland)
Sugi Sponge Points	Co. Kettenbach (Germany)

### **2.1.3. Automatic whisker stimulator**

Goose neck holder	Co. Hilitand (China)
Small engine (DC 6v 300rpm)	Co. Walfront (China)
Battery box	Co. KEESIN (China)
Cables	Co. DeFaYi (China)
Voltage controller	Co. Daifenni (China)

### **2.1.4. Drugs and chemicals**

Lidocaine (2% HCl)	Co. B. Braun (Germany)
Medetomidine	Co. Zoetis (USA)
Buprenorphine	Co.Reckitt Benckiser (UK)
Isoflurane	Co. CP-Pharma (Germany)
Dexpanthenol cream (Bepanthen)	Co. Zoetis (USA)
Fluorescein isothiocyanate (2000 kDa)	Co. Sigma-Aldrich (Germany)
Cyano Veneer	Co. Hager & Werken (Germany)
Cyano Veneer Powder	Co. Hager & Werken (Germany)
Cyanoacrylate Maxi-Cure	Co. Drechseln & Mehr (Germany)
Dexamethasone	Co. Sigma-Aldrich (Germany)
Enrofloxacin (Baytril)	Co. Bayer (Germany)
Special sponge-paper (Tachosil)	Co. Baxter Healthcare

### **2.1.5. Software**

LabChart 8 Reader	Co. ADInstruments (Australia)
SigmaPlot 13.0	Co. Systat (USA)
ZEN 2010	Co. Carl Zeiss (Germany)
ImageJ 1.52j	National Institute of Health (USA)
Graphpad Prism 7.0	Co. GraphPad Software (USA)
EthoVision® XT	Co. NoldusIT (Netherlands)

### **2.2. Experimental Animals**

6-8 weeks old C57BL/6N mice were purchased from Charles River Laboratories (Sulzfeld, Germany). 6-8 weeks old C57BL/6J mice were purchased from Jackson Laboratories (Bar Harbor, USA). 1 year-, 1.5 year-, and 2 year-old C57BL/6N mice were aged in the animal facility of the Institute of Stroke and Dementia Research. 1 year-old C57BL/6J mice were aged in the same condition which was used for the whisker stimulation experiment. All mice were housed in groups of five in isolated ventilated HEPA filtered cages with a 12-hour light/dark cycle with ad libitum access to food and water. All cages had standard enrichment. After cranial window surgery, mice were kept in single cages.

All forepaw and whisker stimulation experiments were performed with LDF and/or LSI. Mice at the age of 6-8 weeks were categorized as young and mice at the age of 1 year and 2 years were categorized as aged. For the experiment using forepaw stimulation and LDF 6-8 weeks old and 1 year-old mice were used. For experiments using whisker stimulation, LSI, and two-photon microscopy, 6-8 weeks-, 1 year-, and 2 year-old mice were studied. In the experiment using Barnes maze 6-8 weeks-, 1.5 year-, and 2 year-old aged mice were studied.

All procedures related which experimental animals were conducted according to institutional guidelines of the University of Munich and were approved by the Government of Upper Bavaria.

## 2.3. Experimental design

### 2.3.1. Forepaw stimulation and Laser Doppler flowmetry (LDF)

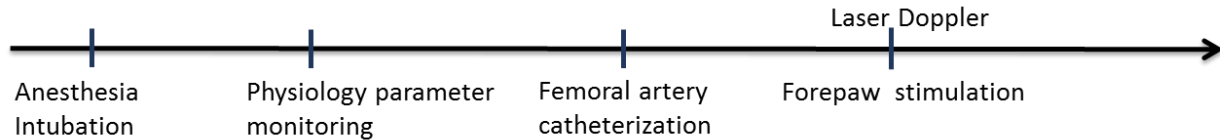


**Figure 2:** Experimental scheme of forepaw stimulation and CBF measurements with LDF.

### 2.3.2. Forepaw stimulation and Laser speckle imaging (LSI)

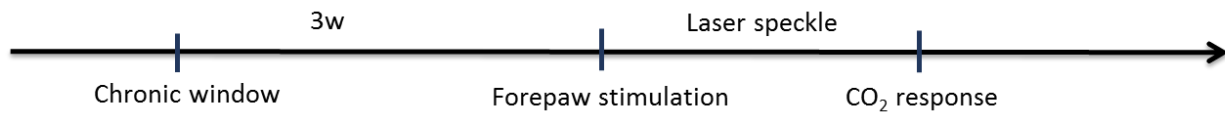


**Figure 3:** Experimental scheme of forepaw stimulation and CBF measurements with LSI.

### 2.3.3. Whisker stimulation, LSI and two-photon microscopy



**Figure 4:** Experimental scheme of whisker stimulation, CBF measurements with LSI, and two-photon microscopy.

## **2.4. Forepaw stimulation and LDF**

### **2.4.1. Anesthesia and intubation**

A perfectly balanced and maintained anesthesia is crucial for a reliable and consistent forepaw NVC response. To achieve this, a combination of isoflurane and ketamine anesthesia is needed. First of all, induction of anesthesia was achieved with 5% isoflurane with air. After loss of consciousness which was confirmed by checking the paw reflex, mice were moved to the intubation platform and anesthesia was maintained with 2% isoflurane mixed with 30% oxygen and 70% nitrogen using a tube fixed on the platform near the nose of the mouse. The glottis was exposed with forceps under a surgical microscope. A custom-made intubation tube was inserted into the trachea. The success of intubation and regular respiration wave pattern was continuously observed and recorded with a capnograph which was connected to a digital data acquisition system (AD Instruments).

### **2.4.2. Monitoring physiological parameters**

After intubation, mice were ventilated with a mechanical ventilator with 0.3 l/min O<sub>2</sub> and 0.7 l/min room air. The end-tidal partial pressure of carbon dioxide (end-tidal pCO<sub>2</sub>) was measured by connecting the intubation tube to a capnograph. The stroke volume was adjusted to 200 – 250 ml and ventilation frequency was adjusted to 180 – 220 strokes/min in order to receive an end-tidal CO<sub>2</sub> of 25 – 35 mmHg, a value resulting in physiological blood pCO<sub>2</sub> of 25 - 45 mmHg.

Mice were placed on a feedback-controlled heating pad on the stereotactic frame in a supine position. A temperature probe was lubricated with Bepanthen ointment and carefully inserted into the colon. Body temperature was maintained at 36°C. A pulse oximeter was clipped to the right hindpaw to monitor heart rate and systemic oxygen saturation. The eyes of the mouse were lubricated with Bepanthen to avoid drying of the corneal. All physiological parameters were recorded and stored with Powerlab and displayed in real time on a computer monitor (LabChart).

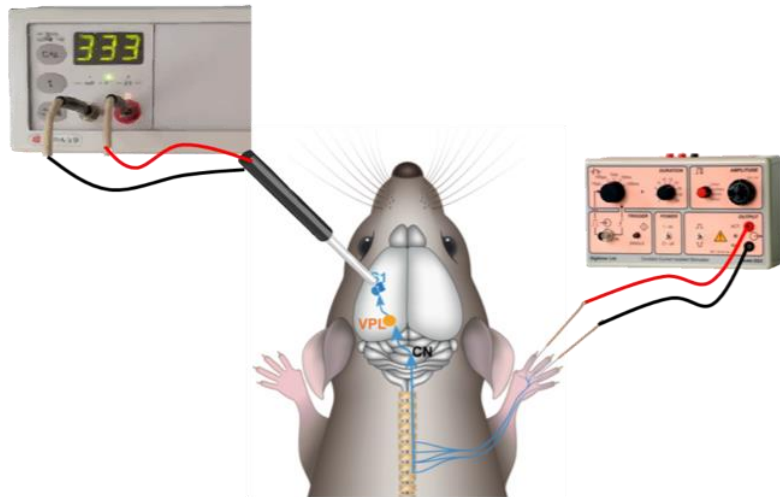
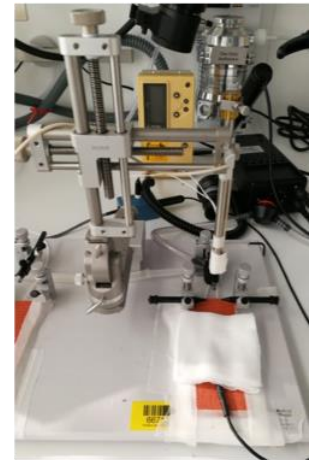
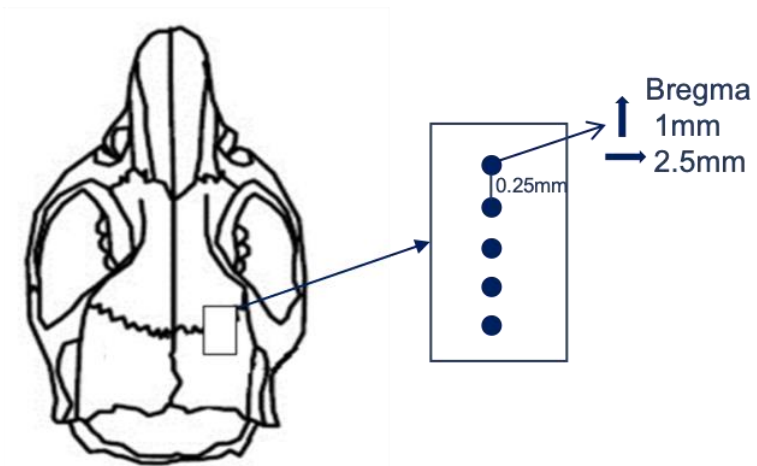
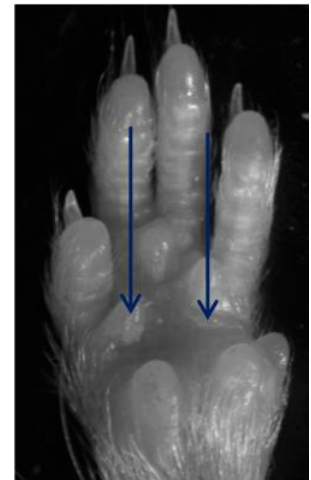
### **2.4.3. Femoral artery catheterization**

After all physiological parameters stabilized, the left femoral artery was catheterized for continuous ketamine infusion. A syringe driven by MicroSyringe Pump infusing saline at rate of 0.004 to 0.009 ml/min was connected to the catheter to avoid the reflux of blood. Blood pressure was measured with a pressure transducer (Harvard Apparatus, USA) and recorded using the LabChart software.

### **2.4.4. Forepaw stimulation and LDF**

After femoral artery catheterization, mice were placed in a prone position. Two acupuncture needle electrodes (0.2 mm) were subcutaneously inserted into the left forepaw. The skin of the head was incised to expose the skull (**Figure 5**). The nose was fixed to a stereotactic frame using a nose clamp. A LDF probe was attached to the stereotactic frame and positioned +1 mm anterior and +2.5 mm lateral to bregma over the forepaw somatosensory cortex. CBF values were continuously monitored (PeriFlux System 5000), recorded, and displayed (LabChart software).

To achieve a stable baseline CBF isoflurane was decreased to 0.3 to 1.0% and combined with ketamine (30 mg/kg/h). A constant current stimulator was used for electrical forepaw stimulation. The forepaw was stimulated with 10 trains of 96 pulses (length: 0.3 ms, intensity: 2 mA) at 6 Hz, i.e. for 16 seconds, every 40 seconds. Five areas of the somatosensory cortex were analyzed (**Figure 5c**) and the one with the strongest response was chosen for further analysis.

**A****B****C****D**

**Figure 5:** (A) Schematic forepaw stimulation with LDF; (B) Real picture of forepaw stimulation with LDF; (C) Location of LDF probe on the skull; (D) Illustration of insertion of needles.

## 2.5. Forepaw stimulation and LSI

Another method used to image the forepaw NVC response was LSI. With LSI CBF changes of a specific region can be observed through a cranial window.

### 2.5.1. Chronic window surgery

A chronic cranial window was implanted over the right parietal cortex three weeks before forepaw stimulation. Mice received buprenorphine (0.1 mg/kg) 30 minutes before surgery for analgesia and anesthesia was induced with 5% isoflurane and maintained with 2% isoflurane in 70% room air and 30% O<sub>2</sub> during surgery. A feedback-controlled heating pad was used to maintain body temperature at 36°C. Animals were fixed in a stereotactic frame using a nose clamp, lidocaine (2%) was applied topically on the skull as local anesthetic, and a 2 mm\*2 mm craniotomy exposing the forepaw somatosensory area was performed using a high speed drill (Co. Rewatronik, Germany). Afterward, the craniotomy was covered with a glass window and sealed with a mixture of dental cement and glue. After surgery mice were placed in a pre-heated wake-up box (32 °C) until all vital functions recovered and all mice received buprenorphine and enrofloxacin once a day during postoperative days 1-3.

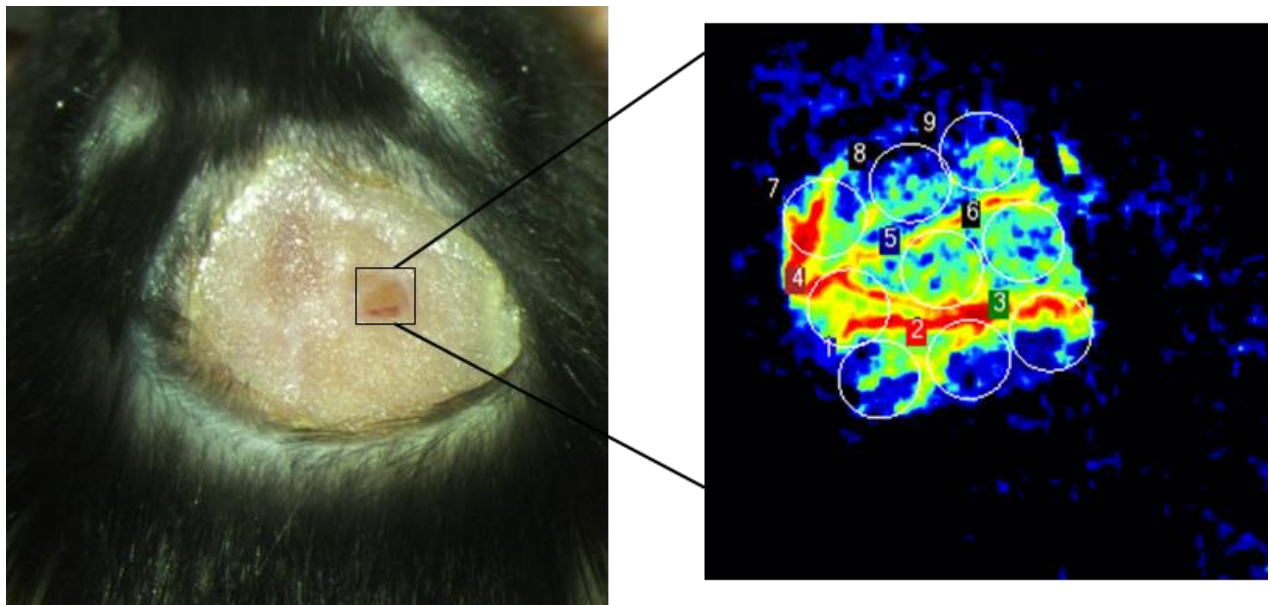


**Figure 6:** Cranial window and laser speckle image of the window.

### 2.5.2. Forepaw stimulation and LSI

Three weeks after the chronic window surgery, mice were injected with medetomidine (0.05 mg/kg) for light sedation and after 10 min anesthesia was initiated with 5% isoflurane. Mice were fixed in a stereotactic frame with a nose bar and isoflurane was gradually reduced to 0.75 - 1% in 70% room air and 30% O<sub>2</sub> before the start of forepaw stimulation. Two acupuncture needle electrodes were subcutaneously inserted in the left forepaw. A feedback-controlled heating pad was used to maintain body temperature at 36°C.

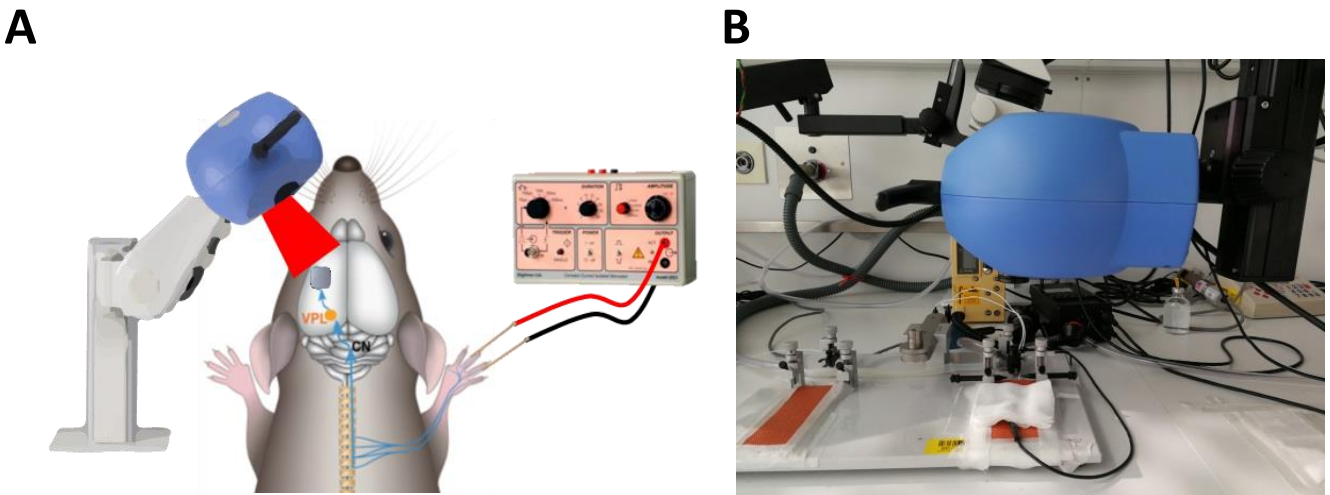


**Figure 7:** Schematic drawing (A) and a photograph (B) of the setup used for forepaw stimulation and CBF measurements with LSI.

A laser speckle imager (Perimed) was positioned 10.4 cm above the head of the mouse and a 0.3 mm x 0.3 mm field of the cortex was imaged at 4.4 Hz. Manual perfusion filter was used to show the vessels in good precision and contrast. The stimulation of the forepaw was performed as described above. The data was recorded and analyzed using the Pimsoft software. Nine regions of interest (ROI) were chosen for analysis.

### 2.5.3. CO<sub>2</sub> inhalation and LSI

After forepaw stimulation a CO<sub>2</sub> challenge was performed. Mice were ventilated with 10% CO<sub>2</sub> and 30% oxygen in room air for 3 min. The CO<sub>2</sub> concentration was measured with a capnography and recorded. The response of the whole cranial window was used for analysis.

### 2.5.4. Neuronal activity during forepaw stimulation

To explore the specificity of the stimulation, we measured neuronal field potentials during forepaw stimulation. Two needles were glued on the skull above the forepaw somatosensory cortex. Neuronal field potentials were measured during contralateral forepaw and ipsilateral hindpaw stimulation and recorded with the LabChart software.

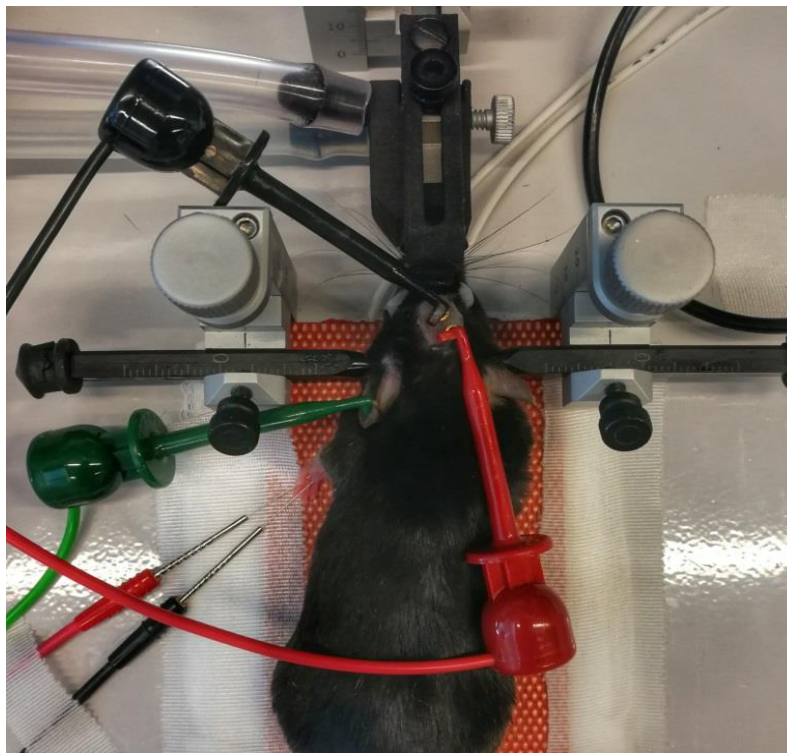


**Figure 8:** Neural field potential recording of forepaw stimulation

## **2.6. Whisker stimulation**

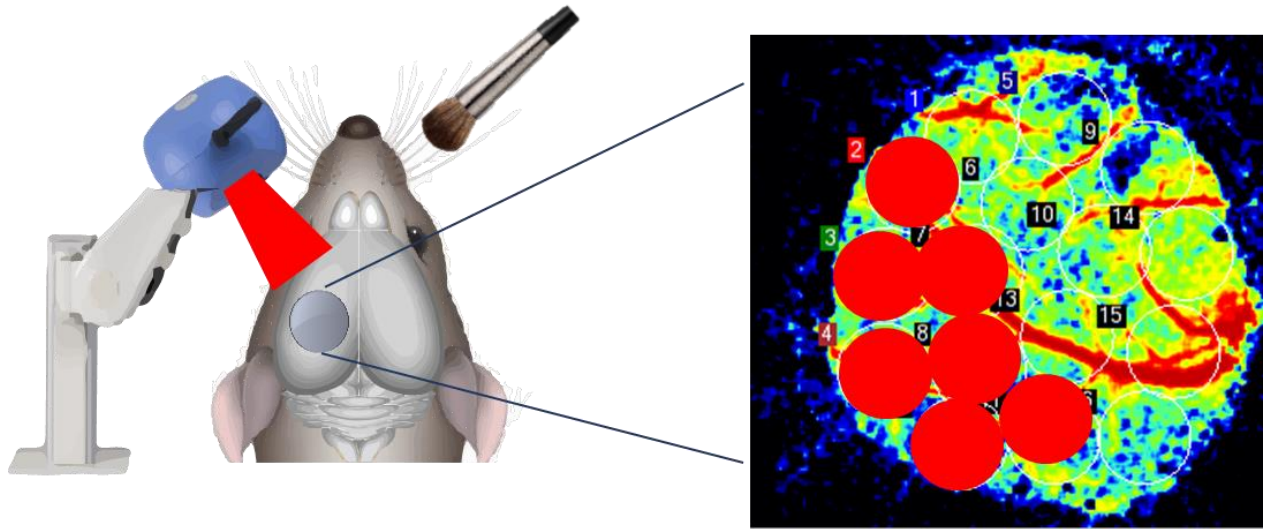
### **2.6.1. Chronic window surgery**

The same procedure was performed as for forepaw stimulation. Only the size of the window was changed from 2 x 2 mm square to 4 mm round in order to cover the bigger barrel cortex where the whisker pads are represented. A plastic ring (diameter: 1 cm; weight: 0.1 g) required to form a water reservoir for the two-photon water dipping objective was glued around the window.

After the operation, the mouse was placed in a pre-heated wake-up box (32°C) until all vital functions recovered and received buprenorphine and enrofloxacin once a day during postoperative days 1-3.

### **2.6.2. Whisker stimulation and LSI**

Three weeks after the chronic window surgery, mice were injected with medetomidine (0.05 mg/kg) for light sedation and after 10 min anesthesia was initiated with 5% isoflurane. Mice were fixed in a stereotactic frame with a nose bar and isoflurane was gradually reduced to 0.75 - 1% in 70% room air and 30% O<sub>2</sub> before the start of whisker stimulation. A feedback-controlled heating pad was used to maintain body temperature at 36°C. LSI was performed as described above. Whisker stimulation was performed for 1 minute by stroking the contralateral vibrissae with a brush at a frequency of 1-2 Hz and repeated three times with intervals of 2 minutes. The data was recorded and analyzed in Perimed software. Seven ROIs covering the barrel cortex were chosen (**Figure 9**). For the heat map data, 36 ROI matrices were placed on the image for analysis. For the slope data, the individual CBF value during the increase until the peak was selected, and the slope was calculated in Graphpad software.



Most responsive ROI was chosen

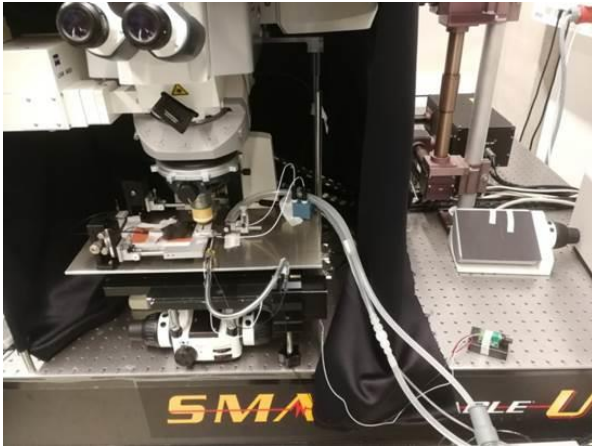
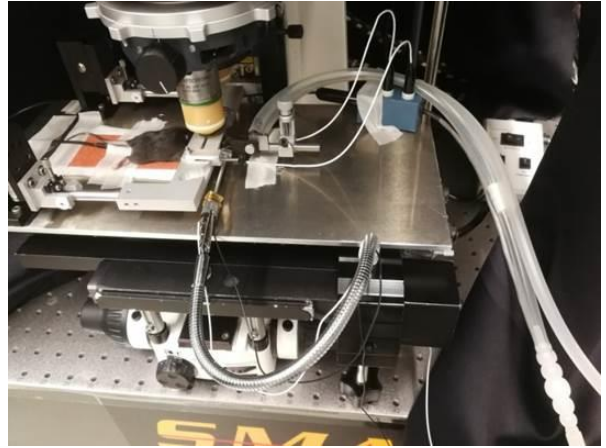
**Figure 9:** Schematic picture of whisker stimulation and LSI

### 2.6.3. CO<sub>2</sub> inhalation and LSI

The procedure was performed as described above (2.5.3.).

### 2.6.4. Whisker stimulation and CO<sub>2</sub> inhalation: two-photon microscopy

In order to perform mechanical whisker stimulation while imaging with two-photon microscopy, a custom-made automated whisker stimulation device was used. A 300 rpm (6 V) battery-powered motor was connected to a small brush and a voltage controller was used to change the frequency of the motor. A gooseneck holder was used to fix the motor on the two-photon microscopy imaging platform which allowed to fine-tune the angle of the brush.

**A****B**

**Figure 10:** (A) Two-photon microscopy set up for whisker stimulation; (B) Zoom-in view of the setup.

Mice were injected with medetomidine (0.05 mg/kg) 10 minutes before the experiment. For visualizing of the vasculature, a mouse tail illuminator was used to inject 0.1 ml fluorescein isothiocyanate (2000 kDa) into the tail vein. Then mice were fixed under the two-photon microscope using a nose holder and pial and parenchymal vessels in the region of whisker cortex were visualized at a depth of 50-100  $\mu\text{m}$  with a 10x Zeiss EC Plan-NeoFluar objective and a Li: Ti laser tuned to 800 nm (**Figure 10**). Before starting the stimulation, isoflurane was reduced to 0.75 - 1% in 70% room air and 30%  $\text{O}_2$ . The whisker stimulation protocol was followed by a  $\text{CO}_2$  challenge (see above) and imaging of the arterial vascular tree was repeated.

## 2.7. Barnes maze

The Barnes maze is a behavioral test used to quantify learning and memory of mice consisting of a round table with 16 holes, three visual clues for spatial orientation, and a digital camera system for recording and storage of the experiment (**Figure 11**). A home cage was placed under one of the holes. Animals were trained with the help of a glass

cylinder for 2 minutes to find the home cage in the morning of day 1 and 2. On days 1, 2, 3, 4, 6 in the afternoon mice were placed in the middle of the table and allowed to search for the home cage for 180 s. Each trial was recorded and analyzed with an investigator-independent software package for the latency to find the home cage and for walking speed (EthoVision®XT, Noldus).

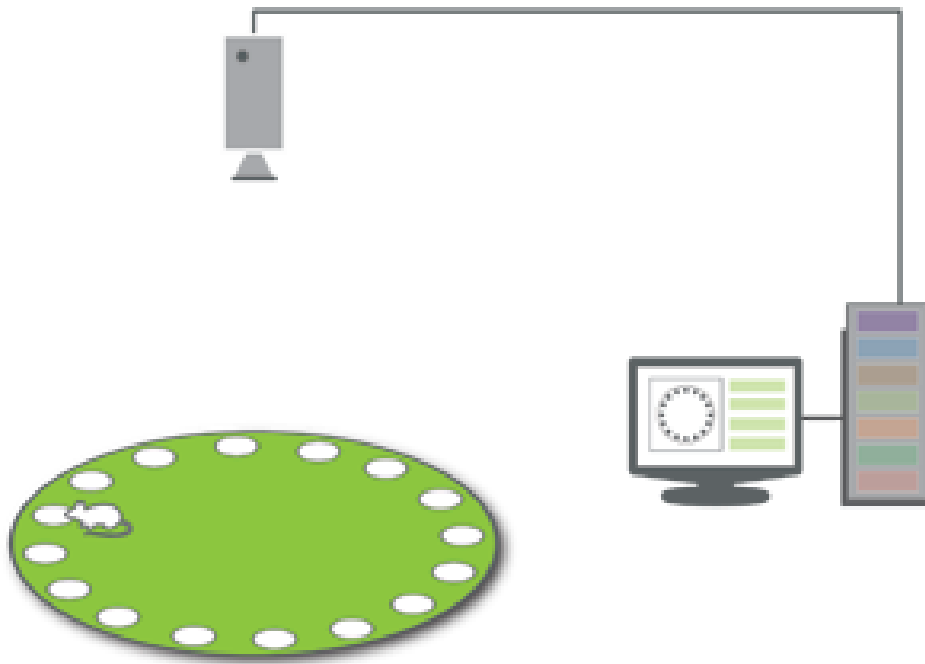


**Figure 11:** Schematic drawing of a Barnes maze (adapted from <https://www.noldus.com>).

## 2.8. Imaged analysis of two-photon images

Two-photon images were exported from the Zen software, preprocessed, and skeletonized (ImageJ Vessel Analysis plugin). The average diameter of the selected vessel segment was measured in an automated manner. For whisker stimulation, images were analyzed every 4 s. Values recorded within the 10 s before the start of the stimulation were averaged and used as baseline. For the CO<sub>2</sub> inhalation experiments, images were analyzed every 30s.

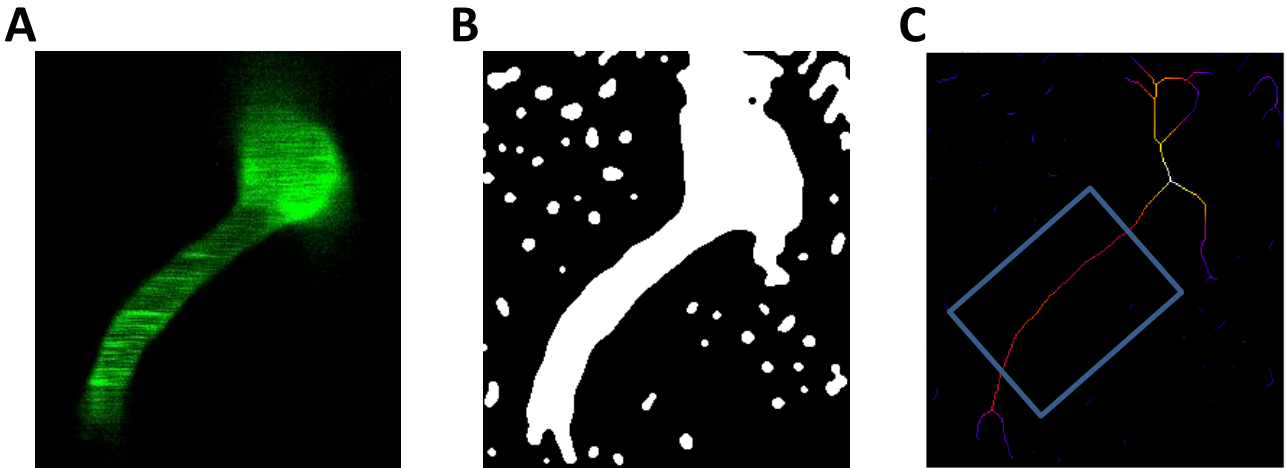


**Figure 12:** Image analysis with ImageJ plug-in. (A) Original image; (B) Preprocessing; (C) Skeletonization and measurement

## 2.9. Statistics

Statistical analyses were performed with GraphPad Prism 7.0 software. Normally distributed data were compared with the Student t-test. Multiple groups were compared with one-way ANOVA or one-way ANOVA on ranks depending on the presence or absence of normal distribution. Differences with  $P < 0.05$  was considered statistically significant.

### 3. Results

#### 3.1. Forepaw stimulation and LDF

Stimulation of the forepaw of 6-8 weeks old C57BL/6N mice resulted in a robust increase in CBF (**Figure 13**). The highest response was observed after the first stimulation (13 +/- 7%), then decreased gradually, and stabilized around 7% until the end of the experiment.

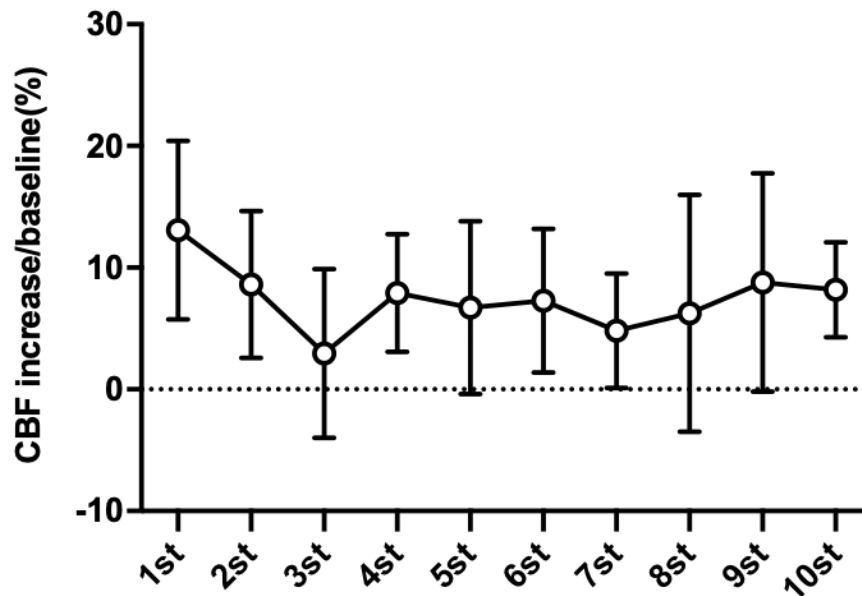


**Figure 13:** CBF in young mice during forepaw stimulation. Data are shown as means  $\pm$  SD (n=5).

#### 3.2. Neuronal activity during forepaw stimulation

To check the spatial specificity of forepaw stimulation, we measured the neuronal field potential during forepaw and hind paw stimulation (**Figure 14**). During forepaw stimulation a constant and prominent neuronal activation was observed, while during hind paw stimulation there was an only sparse response. This result suggests that only forepaw stimulation activates neurons in the forepaw somatosensory area and that unspecific signals, e.g. pain, does not influence this response.

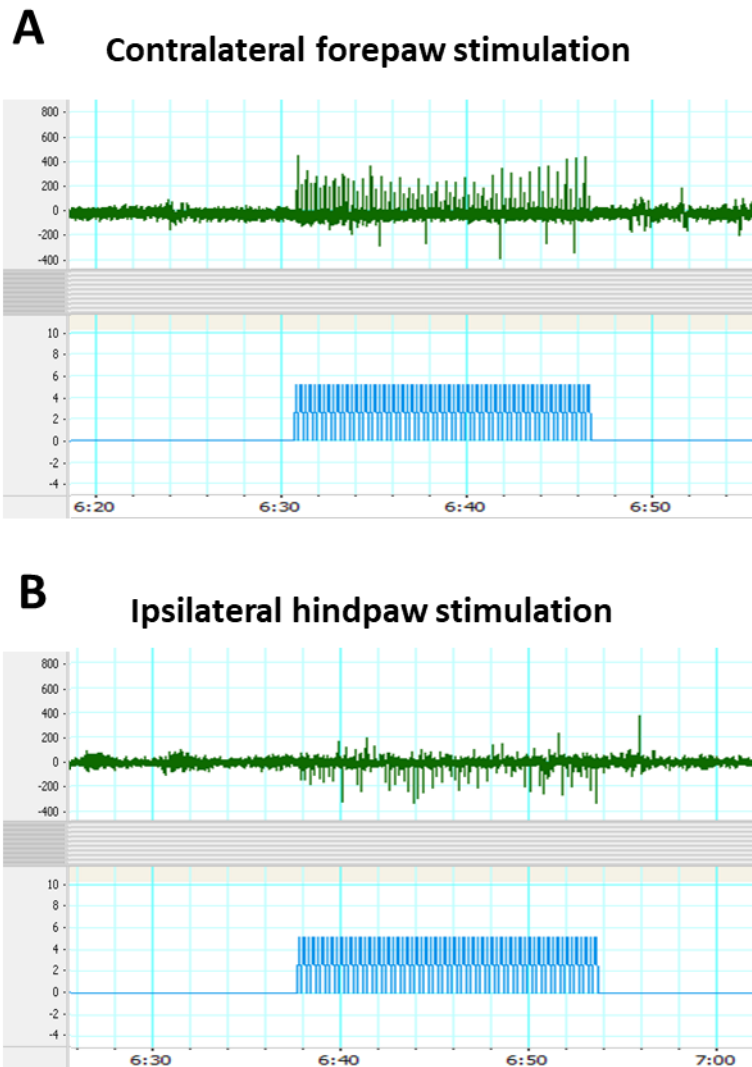


**Figure 14:** Neural field potential recording of forepaw and hindpaw stimulation. (A) Neural field potential recording of contralateral forepaw stimulation; (B) Neural field potential recording of ipsilateral hindpaw stimulation.

### 3.3. Forepaw stimulation and LSI

#### 3.3.1. Forepaw stimulation

LDF and LSI measurements were performed under the same conditions in order to investigate whether these two techniques yield similar results. Indeed, when using the

previously described forepaw stimulation paradigm, LDF and LSI measurements resulted in very similar values and a very similarly shaped temporal profile (**Figure 15**). Only at the beginning of the stimulation LDF resulted in a tendency to somewhat higher CBF values (n.s.).

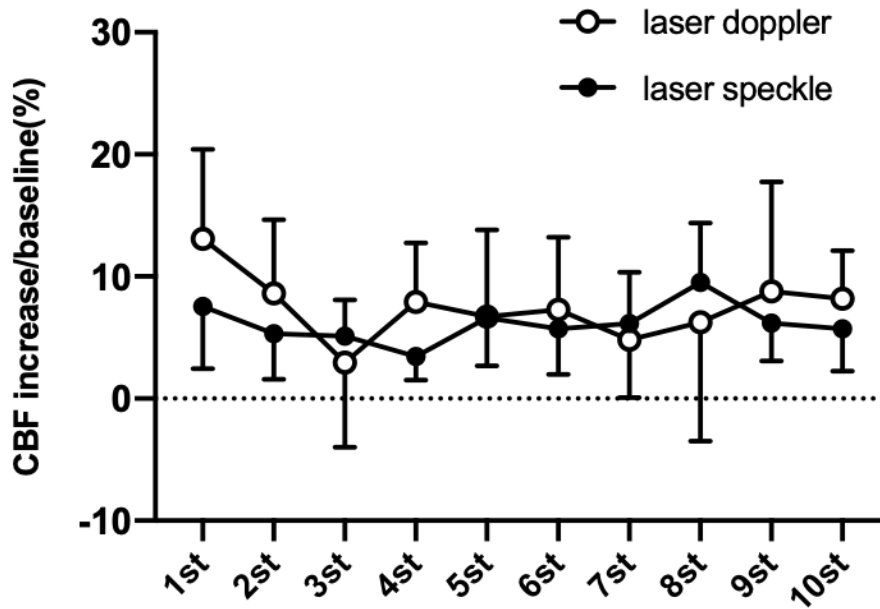


**Figure 15:** CBF response during forepaw stimulation measured with LDF or LSI. Data are shown as Mean  $\pm$  SD; 6-8 weeks C57BL/6N mice, n=5 for LDF group; n=8 for LSI group.

When comparing the CBF response after forepaw stimulation by LSI, the initial response in young and old animals was very similar (**Figure 16A and B**). Only when the responses from the last five stimulations were compared, old mice displayed a significantly lower response (7  $\pm$  2% for the young group and 5  $\pm$  2% for the aged group; P=0.04; **Figure 16D**). Essentially the same results were obtained when instead of the mean response the peak response was used for the comparison between young and old mice: The CBF response was significantly higher in young as compared to aged mice (13  $\pm$  3% for the young group and 10  $\pm$  2% for the aged group; P<0.02; **Figure 17**) and this difference was

mainly due to a significantly lower response of the aged animals to the last five stimulations ( $P < 0.03$ ).

To refine our analysis, we performed area under the curve (AUC) calculations (**Figure 18**). Using this more precise analysis, we got in essence the same results as with the mean or peak analysis. The CBF response was significantly higher in young as compared to aged mice ( $50 \pm 12$  vs.  $35 \pm 13$ ;  $P < 0.02$ ) and this difference was mainly due to a significantly lower response of the aged animals to the last five stimulations ( $P < 0.01$ ).

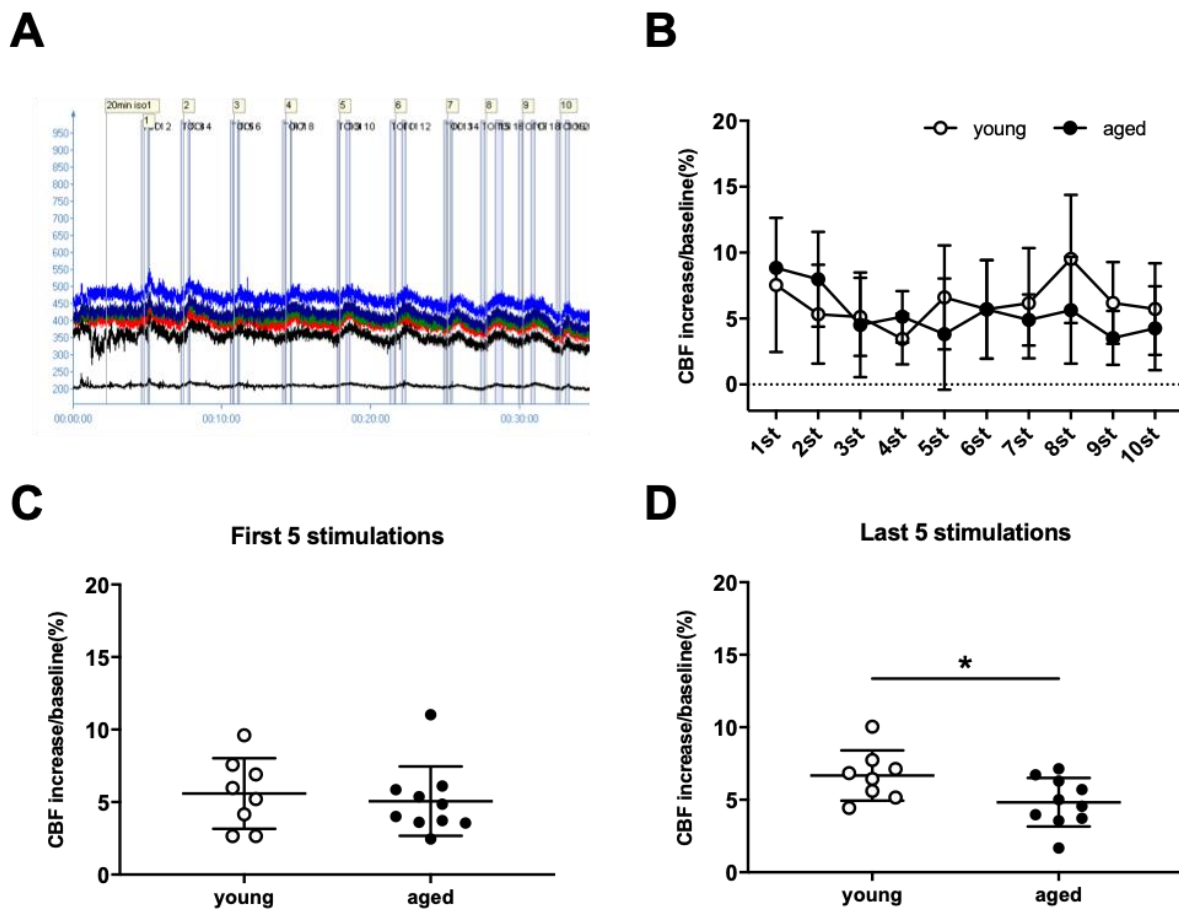


**Figure 16:** Forepaw stimulation of young (6-8 weeks) and 1 year-old mice by LSI. (A) LSI recordings of individual mice; (B) General CBF response; (C) Average CBF response of the first five stimulations; (D) Average CBF response of the last five stimulations. Data are shown as Mean  $\pm$  SD; t-test, \* $p < 0.05$ ; Young:  $n = 8$ ; Aged:  $n = 10$ .

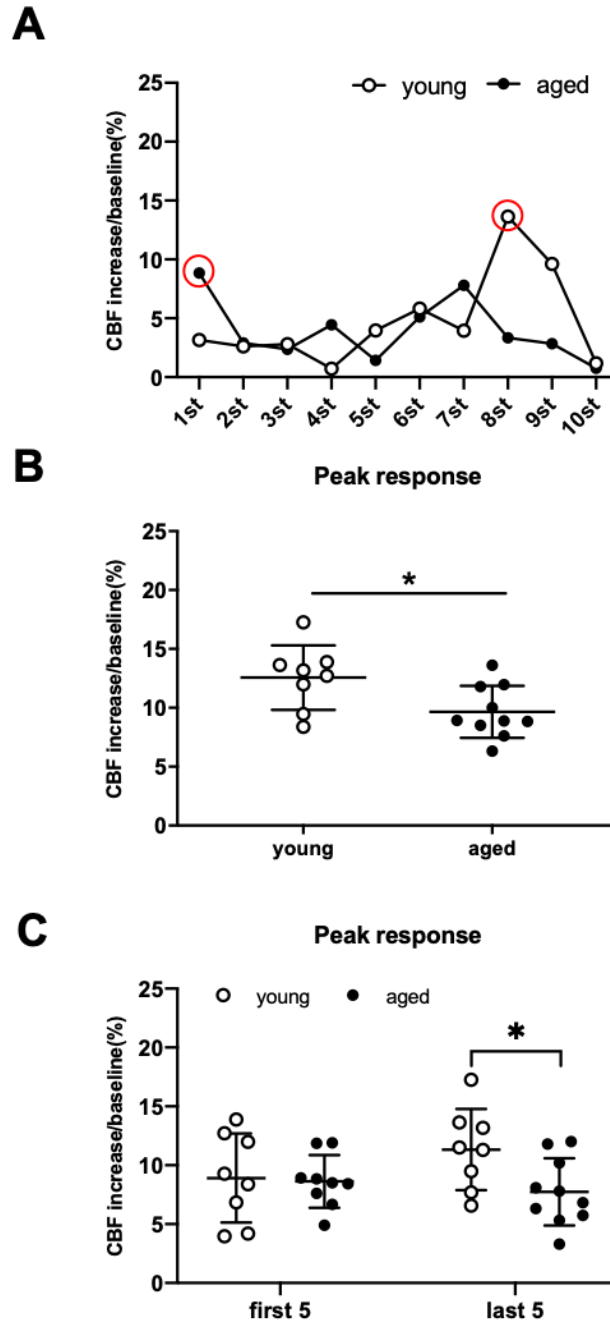


**Figure 17:** CBF in young and aged mice after forepaw stimulation analyzed by peak response. (A) Example of peak response analysis in one young and one aged mouse; (B) Average peak response in young and old mice; (C) Average peak response during the first and five last stimulations in young and old mice. Data are shown as Mean  $\pm$  SD; t-test, \* $p < 0.05$ ; Young:  $n = 8$ ; Aged: 1 year-old,  $n = 10$ .

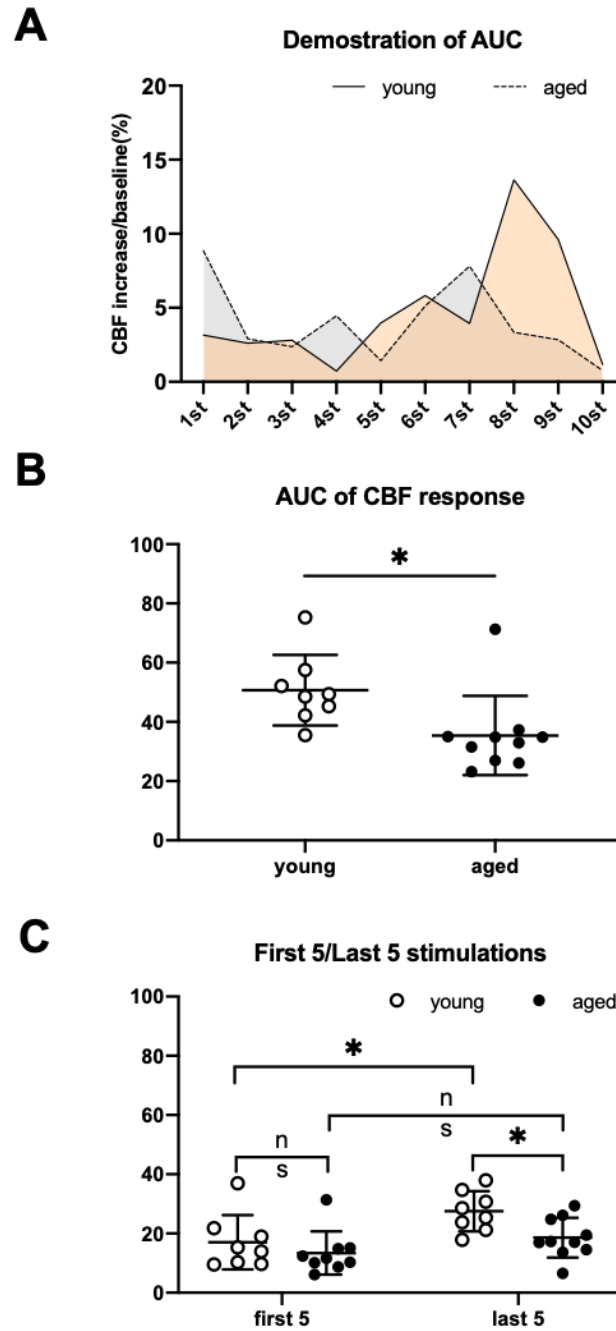


**Figure 18:** CBF response of young and aged mice following forepaw stimulation quantified by area under the curve (AUC) analysis. (A) Example of the CBF response of one young and one aged mouse; (B) AUC of CBF responses; (C) Comparison of CBF responses after the first and last five forepaw stimulations. Mean  $\pm$  SD; t-test, \* $p < 0.05$ ; Young:  $n = 8$ ; Aged: 1 year-old,  $n = 10$ .

### 3.3.2. CO<sub>2</sub> response

We then did the CO<sub>2</sub> inhalation experiment to check the dilation ability of the vessel. Mice were given CO<sub>2</sub> for three minutes and the CBF increase was recorded with LSI (**Figure 19A**). Both young and aged mice showed increased CBF response from the beginning and peaked at the 90s (**Figure 19B**). However, there was no statistical difference between the two groups at any time point. Similar to CBF response by forepaw stimulation, we also measured the peak CO<sub>2</sub> response (**Figure 19B and D**). There was no statistically different response between groups (P=0.33). There was also no difference in the AUC of the CO<sub>2</sub> response between the two groups (**Figure 18E**, P=0.34).

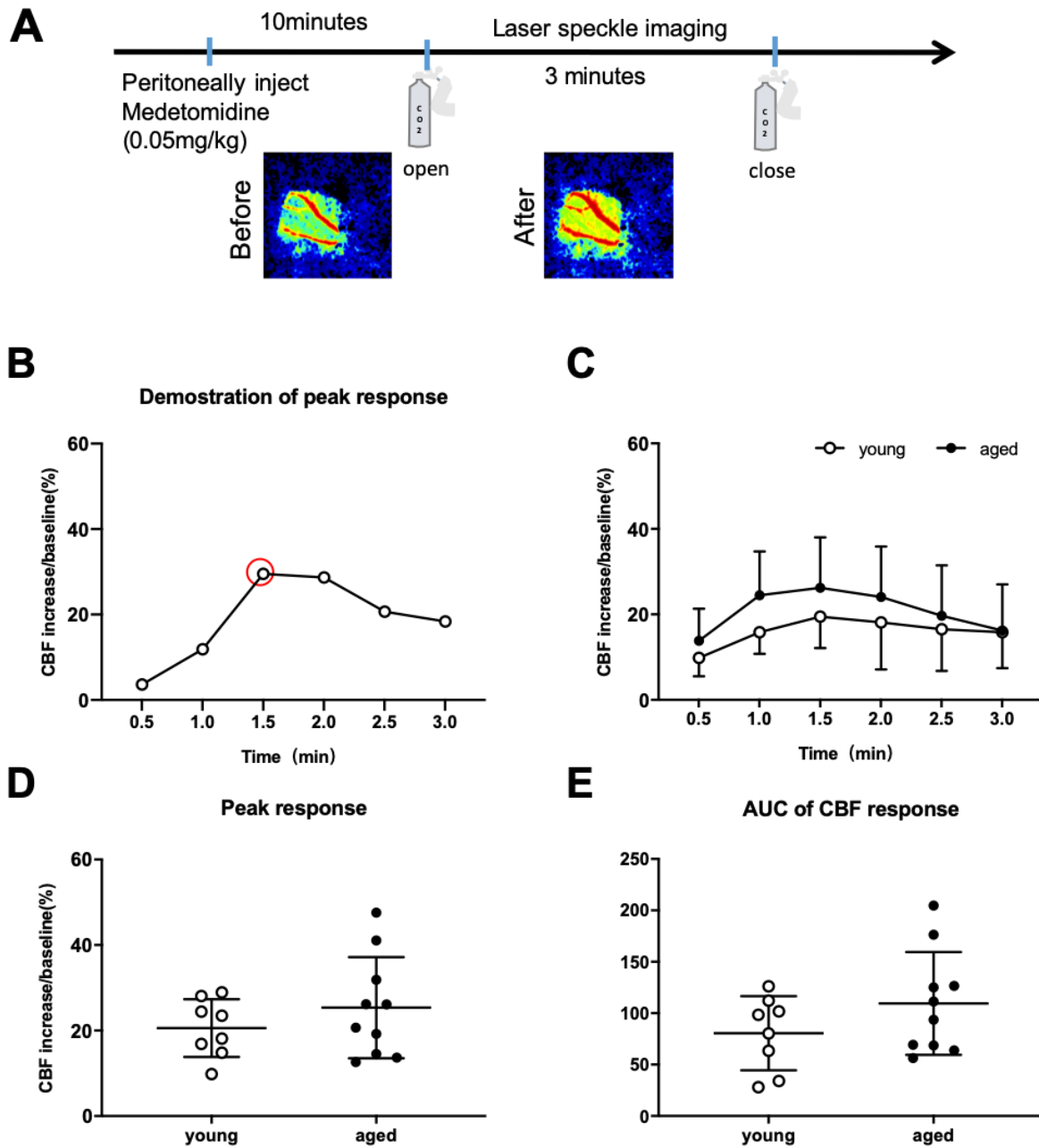


**Figure 19:** CBF response in of young and aged mice during CO<sub>2</sub> inhalation. (A) Experimental protocol of CO<sub>2</sub> inhalation; (B) Example of peak CO<sub>2</sub> response of one young mouse over time; (C) CO<sub>2</sub> response; (D) Peak analysis; (E) AUC analysis. Data are shown as Mean ± SD; t-test, \*p<0.05; Young: 6-8 weeks, n=8; Aged: 1 year-old, n=10.

### 3.3.3. Whisker stimulation

After using forepaw stimulation, we performed whisker stimulation in young and aged mice by LSI. Mice were given three subsequent whisker stimulations (**Figure 20A**). The CBF response of young mice was fast and high, while the response of the 2-year-old mouse was slow and low (**Figure 20B and C**). The CBF response of young mice increased with each stimulation, while the CBF response of 1 year-old mice decreased after the second stimulation. The CBF response of 2 year-old mice remained low the whole time. We found that the CBF response of young mice and 1 year-old mice are larger than the response of 2 year-old mice (**Figure 21A**). There was no statistical difference between the young mice and 1 year-old mice in any of the stimulation. Again, we measured the peak CBF response and the AUC of CBF response (**Figure 21C and D**). The peak CBF response and the AUC of CBF response of young mice and 1 year-old mice were larger than the response of 2 year-old mice ( $P < 0.01$  for young vs. 2 year-old mice;  $P < 0.001$  for 1 year-old vs. 2 year-old mice).

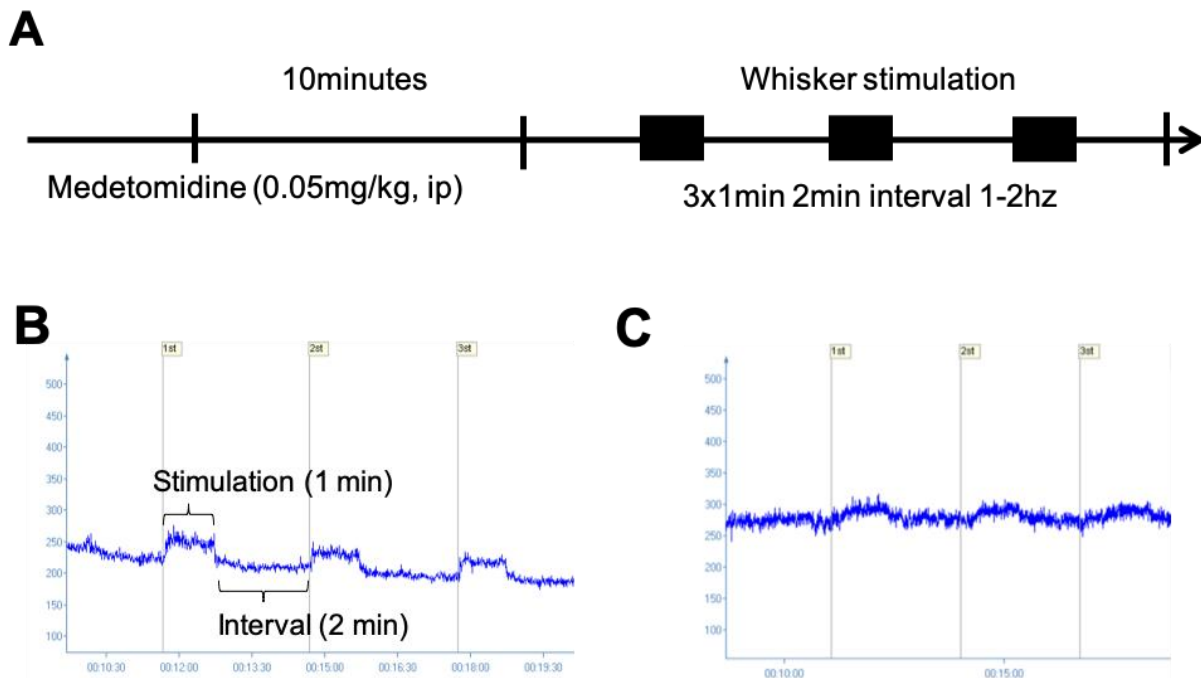


**Figure 20:** Whisker stimulation protocol and example. (A) Experimental protocol for whisker stimulation; (B) CBF response in one young mouse; (C) CBF response of one 2 year-old mouse.

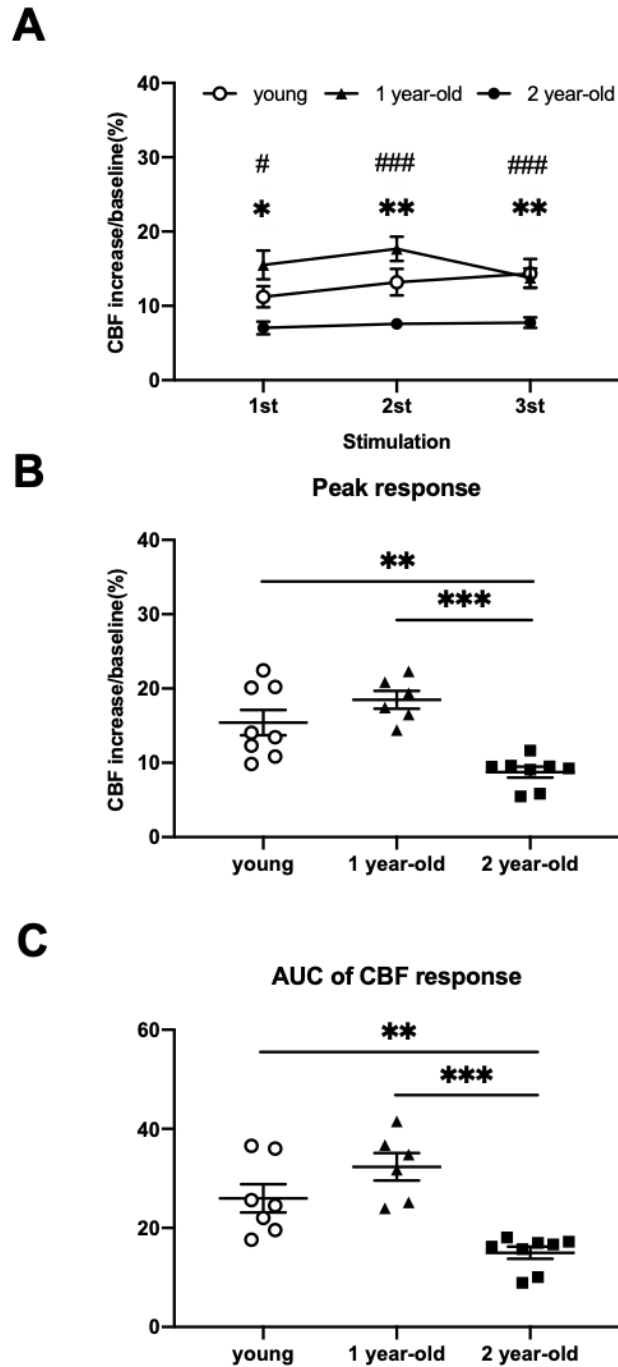


**Figure 21:** Whisker stimulation of young (6-8 weeks), 1 year-old mice and 2 year-old mice by LSI. (A) General CBF response; (B) Averaged peak response; (C) Averaged AUC of CBF response. Data are shown as Mean  $\pm$  SEM; t-test, \*: young mice vs 2y mice, #: 1y aged vs 2y aged(Figure 21A); \* and #= $p < 0.05$ , \*\*=  $p < 0.01$ , \*\*\* and ###= $p < 0.001$ ; Young mice: 6-8 weeks,  $n=8$ ; 1 year-old mice,  $n=6$ ; 2 year-old mice,  $n=8$ .

Furthermore, we analyzed the slope of the CBF response (**Figure 22A**). We found that the slopes of the response in young and 1 year-old mice were higher than the ones in 2 year-old animals (**Figure 22B**, 0.69 +/- 0.25 for young mice, 0.79 +/- 0.66 for 1 year mice, 0.23 +/- 0.11 for the 2 year-old mice;  $P < 0.001$  for young vs. 2 year-old mice,  $P = 0.03$  for 1 year-old mice vs. 2 year-old mice).

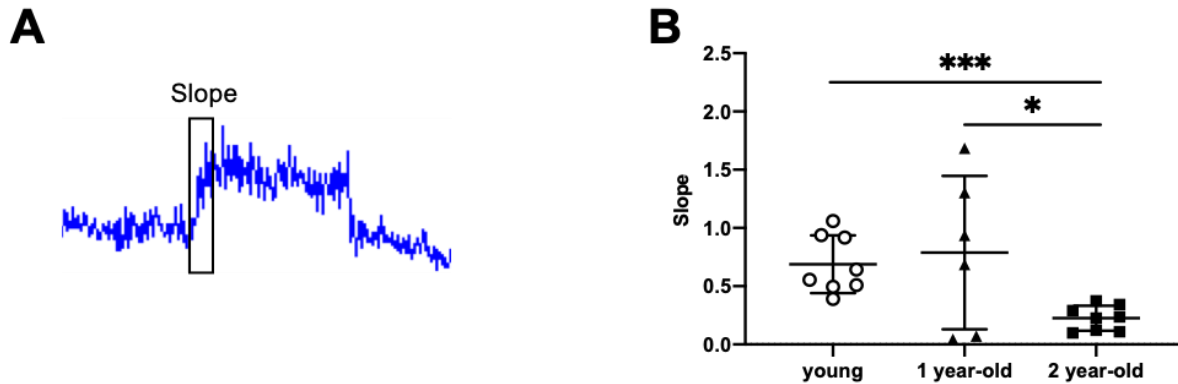


**Figure 22:** Analysis of slope of CBF response of whisker stimulation. (A) Illustration of slope analysis; (B) Slope of whisker stimulation of young (6-8 weeks), 1 year-old mice and 2 year-old mice. Data are shown as Mean  $\pm$  SD; t-test, \*:  $p < 0.05$ , \*\*\*:  $p < 0.001$ ; young mice,  $n = 8$ ; 1 year-old mice:  $n = 6$ ; 2 year-old mice,  $n = 8$ .

We generated heat maps of the LSI data after whisker stimulation. There was a distinctive difference between young, 1 year-old, 2 year-old mice. 36 ROIs were placed on the laser speckle image and analyzed with the Perimed software (**Figure 23A**). For young mice, the higher response (11%) located on the barrel cortex (**Figure 23B**). However, for the 2 year-old mice, the pattern was not so clear, and the highest response (7%) was much smaller (**Figure 23D**). The distribution of heat map data of 1 year-old mice was similar to 2 year-old mice, but the signal (highest: 15%) was much stronger (**Figure 23C**).

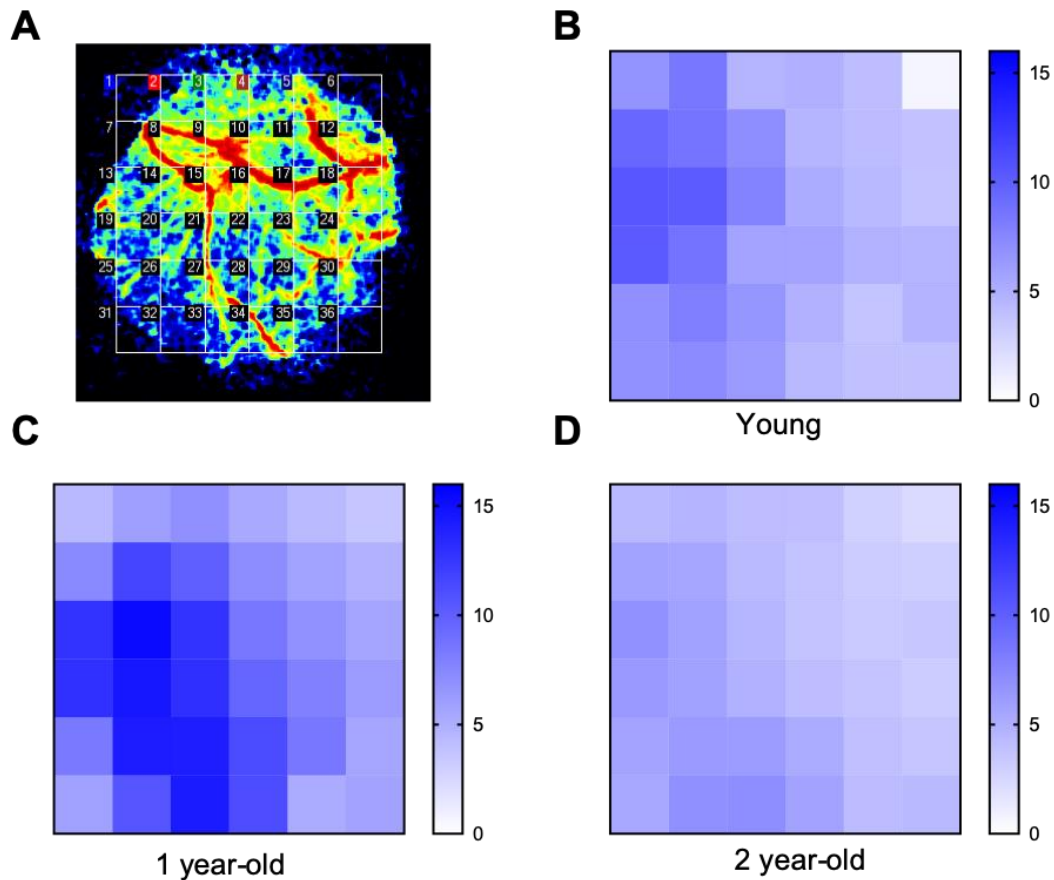


**Figure 23:** Heat map data of LSI of young and aged mice. (A) Illustration of data analysis; (B) Heat map of CBF response in young mice, n=8; (C) Heat map of CBF response of 1 year-old mice, n=6; (D) Heat map of CBF response of 2 year-old aged mice, n=8.

### 3.3.4. CO<sub>2</sub> response

We performed CO<sub>2</sub> inhalation to check neurovascular reactivity. Both young and aged mice showed a good CO<sub>2</sub> response recorded (**Figure 24A and B**). The CO<sub>2</sub> response of all groups was increased from the beginning, peaked between the 60s to 90s, then reduced and remained at a stable level (**Figure 24C**). There was a statistical difference between the responses within the first 30s (**Figure 24D**). In the first 30s, the CO<sub>2</sub> response of 1 year- and 2 year-old mice was significantly smaller compared to young mice (22 +/- 3% for the young mice, 5 +/- 4% for 1 year-old mice, 11 +/- 2% for the 2 year-old mice; P<0.01 for

young mice vs. 1 year-old mice,  $P < 0.05$  for young mice vs. 2 year-old mice). There was no statistical difference between 1 year-old mice and 2 year-old mice in the first 30s ( $P = 0.23$ ). There was also no statistical difference in the peak  $\text{CO}_2$  response ( $P = 0.58$ ) and the AUC of  $\text{CO}_2$  response ( $P = 0.93$ ) between the three groups.

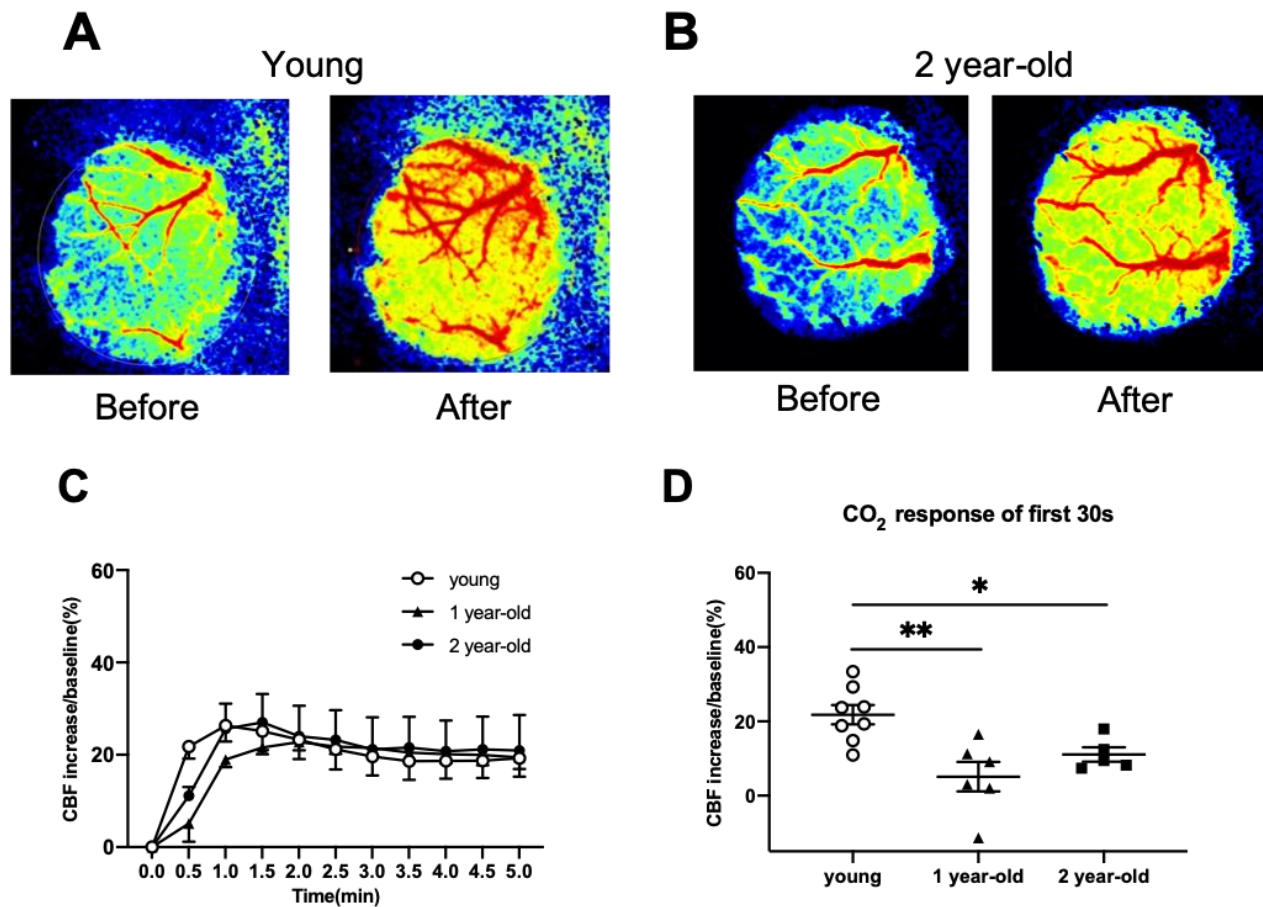


**Figure 24:** CBF response in young (6-8 weeks), 1 year-old mice and 2 year-old mice during  $\text{CO}_2$  inhalation. (A) Example of  $\text{CO}_2$  response of young mice; (B) Example of  $\text{CO}_2$  response of 2 year-old mice; (C)  $\text{CO}_2$  response of young and aged mice; (D)  $\text{CO}_2$  response of first 30 seconds of young and aged mice. Mean  $\pm$  SEM; t-test for comparison between two groups, One way ANOVA for comparison between three groups,  $* = p < 0.05$ ,  $** = p < 0.01$ ; Young: 6-8 weeks,  $n = 8$ ; 1 year-old mice,  $n = 6$ ; 2 year-old mice,  $n = 5$ .

### 3.4. Whisker stimulation and two-photon microscopy

#### 3.4.1. Whisker stimulation

##### 3.4.1.1. Pial arteries

We studied the vascular response of different vessel segments following whisker stimulation by two-photon microscopy. Pial vessels of 1 year-old mice dilated well to whisker stimulation (**Figure 25A**). Young and 2 year-old mice seemed to dilate less; there was a statistically significant difference between three groups at the time points 6s ( $P=0.018$ ), 10s ( $P=0.027$ ), 14s ( $P=0.011$ ), 18s ( $P=0.007$ ), and 22s ( $P=0.017$ ) (**Figure 25B**). The peak response was higher in 1 year-old mice as compared to young mice (**Figure 25C**,  $1 \pm 0.4\%$  for young mice,  $10 \pm 2\%$  for 1 year-old mice,  $4 \pm 2\%$  for 2 year-old mice,  $P=0.006$ ). But there was no statistical difference between young mice and 2 year-old mice ( $P=0.135$ ) or between 1 year- and 2 year-old mice ( $P=0.097$ ). The result of the AUC analysis was quite similar (**Figure 25D**). 1 year-old aged mice reacted stronger than young mice (**Figure 28C**,  $17 \pm 4.8$  for young mice,  $85 \pm 25$  for 1 year-old mice,  $38 \pm 20$  for 2 year-old mice,  $P=0.028$ ). But there was no statistical difference between young mice and 2 year-old mice ( $P=0.3$ ) or between 1 year- and 2 year-old mice ( $P=0.205$ ).

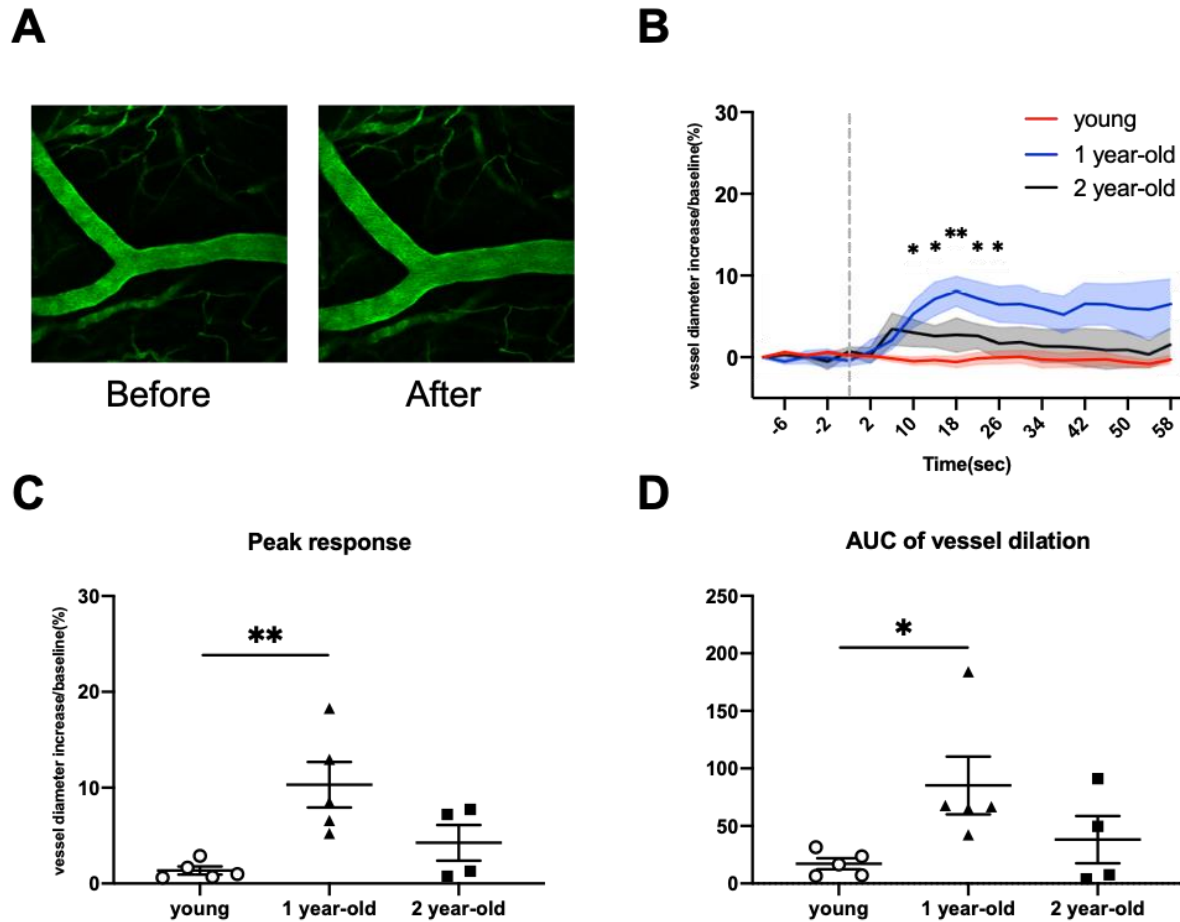


**Figure 25:** Whisker stimulation of the pial artery of young and aged mice in two-photon microscopy. (A) Sample picture of the pial artery in two-photon microscopy; (B) Vessel dilation of whisker stimulation; (C) Peak vessel dilation of whisker stimulation; (D) AUC of vessel dilation of whisker stimulation. Mean  $\pm$  SEM; t-test for comparison of two groups, One-way ANOVA analysis for comparison of three groups, \* =  $p < 0.05$ , \*\* =  $p < 0.01$ ; Young: 6-8 weeks,  $n = 5$ ; 1 year-old mice,  $n = 5$ ; 2 year-old mice,  $n = 4$ .

### 3.4.1.2. Penetrating arteries

The dilation of penetrating arteries following whisker stimulation is shown in Figure 26. Vessel dilation was observed in all groups, but there was no statistical difference between groups at any of the investigated time points (**Figure 26A and B**). There was also no statistical difference in the AUC (**Figure 26C**,  $P = 0.3$ ) or the peak response (**Figure 26D**,  $P = 0.3$ ).

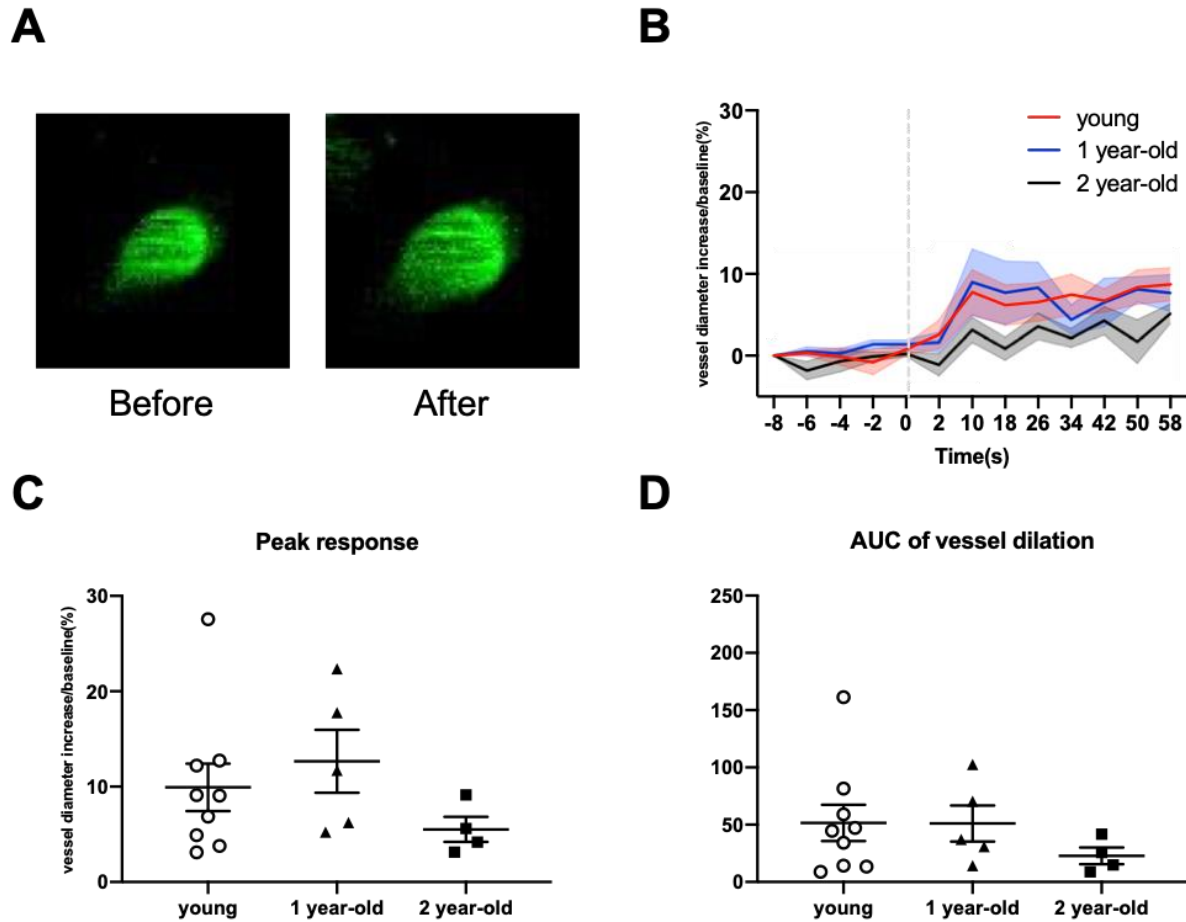


**Figure 26:** Whisker stimulation of the penetrating artery of young and aged mice by two-photon microscopy. (A) Sample picture of a penetrating arteriole by in vivo two-photon microscopy; (B) Vessel dilation after whisker stimulation; (C) Peak vessel dilation after whisker stimulation; (D) AUC analysis after whisker stimulation. Mean  $\pm$  SEM; One-way ANOVA; Young: 6-8 weeks, n=9; 1 year-old mice: n=5; 2 year-old mice, n=4.

### 3.4.1.3. Capillaries

In contrast with pial or penetrating arteries, vessel dilation of capillaries was less pronounced and more variable following whisker stimulation (**Figure 27A and B**). vasodilatation increased from the beginning in young mice, while it remained low in aged mice. There was a statistical significant difference between the three groups at 14s ( $P=0.029$ ), 18s ( $P=0.011$ ) and 58s ( $P=0.038$ ). For the peak response, there was only a

statistical significant difference between young and the 1 year-old mice (**Figure 27C**,  $8 \pm 0.7\%$  for young mice,  $4 \pm 0.6\%$  for 1 year-old mice,  $5 \pm 1\%$  for 2 year-old mice;  $P=0.001$ ). The AUC analysis showed a larger reduction in aged mice. The AUC of young mice was higher than the one in 1 year-old and 2 year-old mice (**Figure 27D**,  $P=0.007$  for young mice vs. 1 year-old mice;  $P=0.041$  for young mice vs. 2 year-old mice). Both 1 year-old and 2 year-old mice remained low and there was no statistical significant difference between these groups ( $P=0.409$ ).

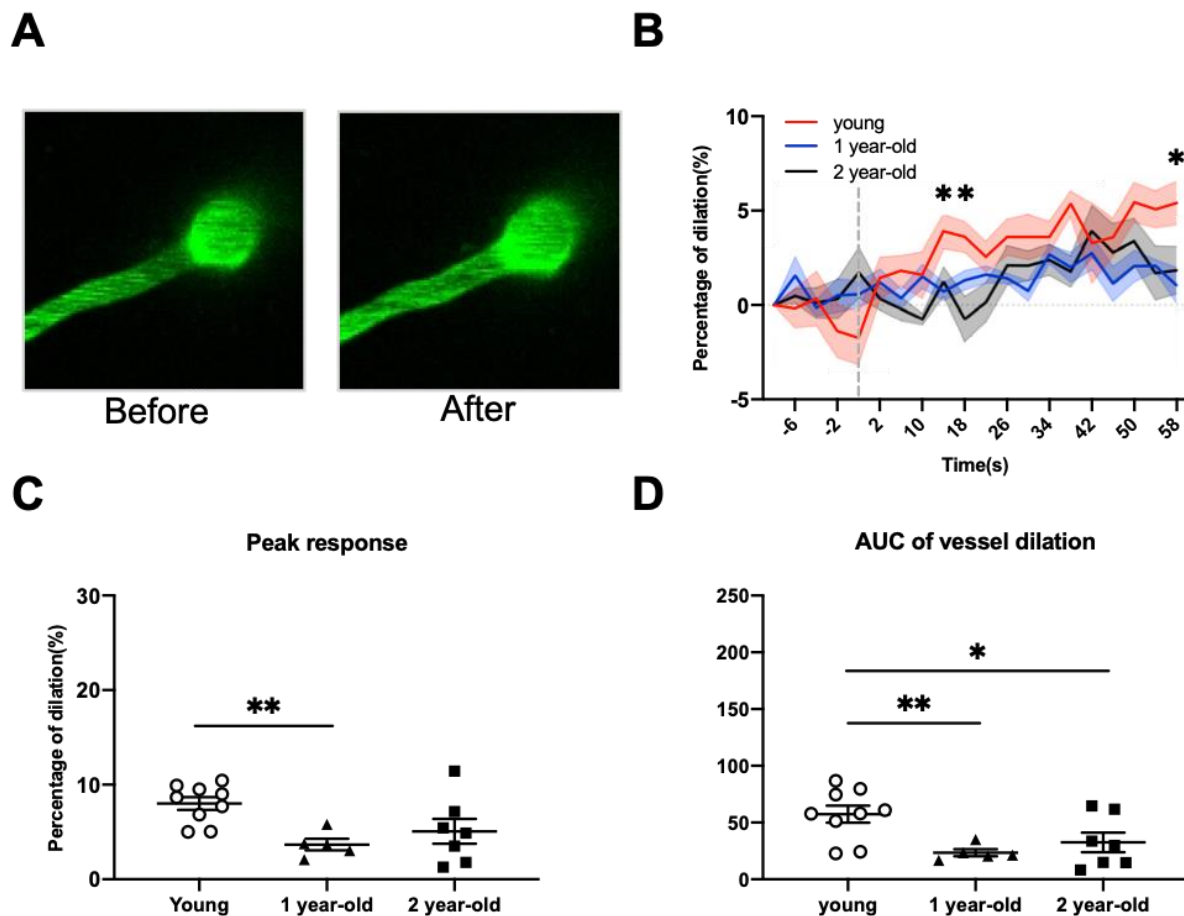


**Figure 27:** Capillary diameter by two-photon microscopy following whisker stimulation. (A) Sample picture of a capillary; (B) Dilated vessel after whisker stimulation; (C) Peak vessel dilation after whisker stimulation; (D) AUC analysis. Mean  $\pm$  SEM; t-test for comparison of two groups,

One-way ANOVA for comparison of three groups,  $*=p<0.05$ ,  $**=p<0.01$ ; Young: 6-8 weeks,  $n=9$ ; Aged: 1 year-old,  $n=5$ ; Aged: 2 year-old,  $n=7$ .

### 3.4.2. CO<sub>2</sub> response

#### 3.4.2.1. Pial arteries

In the end we performed CO<sub>2</sub> inhalation during two-photon microscopy. All mice displayed vessel dilation after inhaling 10% CO<sub>2</sub> for 5 minutes (**Figure 28A and B**). Interestingly, the response of young and aged mice was similar, while 1-year-old animals showed the strongest and quickest response [30s ( $P=0.009$ ), 60s ( $P=0.001$ ) and 90s ( $P=0.02$ )].

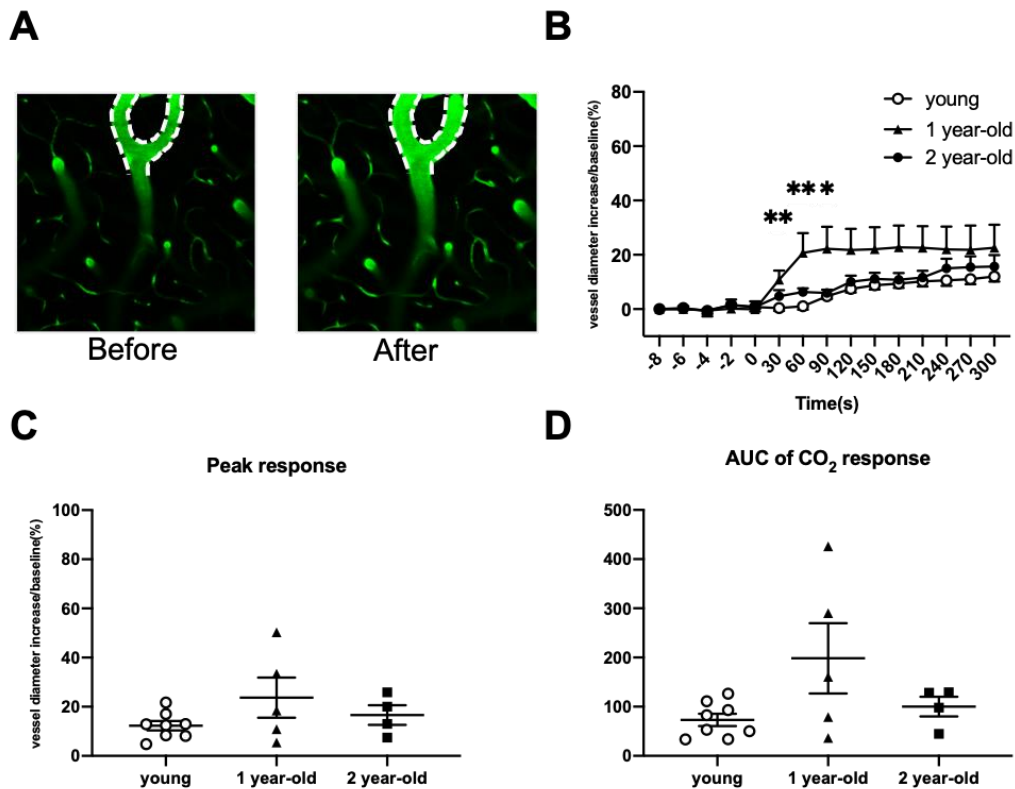


**Figure 28:** CO<sub>2</sub> response of the pial artery of young and aged mice in two-photon microscopy. (A) Sample picture of the pial artery in two-photon microscopy; (B) CO<sub>2</sub> response of the pial artery of young and aged mice; (C) Peak CO<sub>2</sub> response; (D) AUC of CO<sub>2</sub> response. Mean  $\pm$  SEM; t-test for comparison of two groups, One-way ANOVA analysis for comparison of three groups,  $*=p<0.05$ ,  $**=p<0.01$ ; Young: 6-8 weeks,  $n=9$ ; Aged: 1 year-old,  $n=5$ ; Aged: 2 year-olds,  $n=4$ .

### 3.4.2.2. Penetrating arteries

Similar to pial arteries, also penetrating arteries dilated well after CO<sub>2</sub> inhalation. Again, the response of young and aged mice was similarly low, while 1-year-old animals showed the strongest and quickest response. There was statistical significant difference between the 1-year-old group and the other two groups at all time points (P=0.001 for 60s, 0.006 for 120s, 0.022 for 180s, 0.031 for 240s, 0.03 for 300s). For the peak CO<sub>2</sub> response was significantly higher in 1 year-old mice (**Figure 29C**, 18 +/- 3% for young mice, 40 +/- 10% for 1 year-old mice, 16 +/- 3% for 2 year-old mice. P=0.02). The same was observed in the AUC analysis (**Figure 29D**, P=0.003).

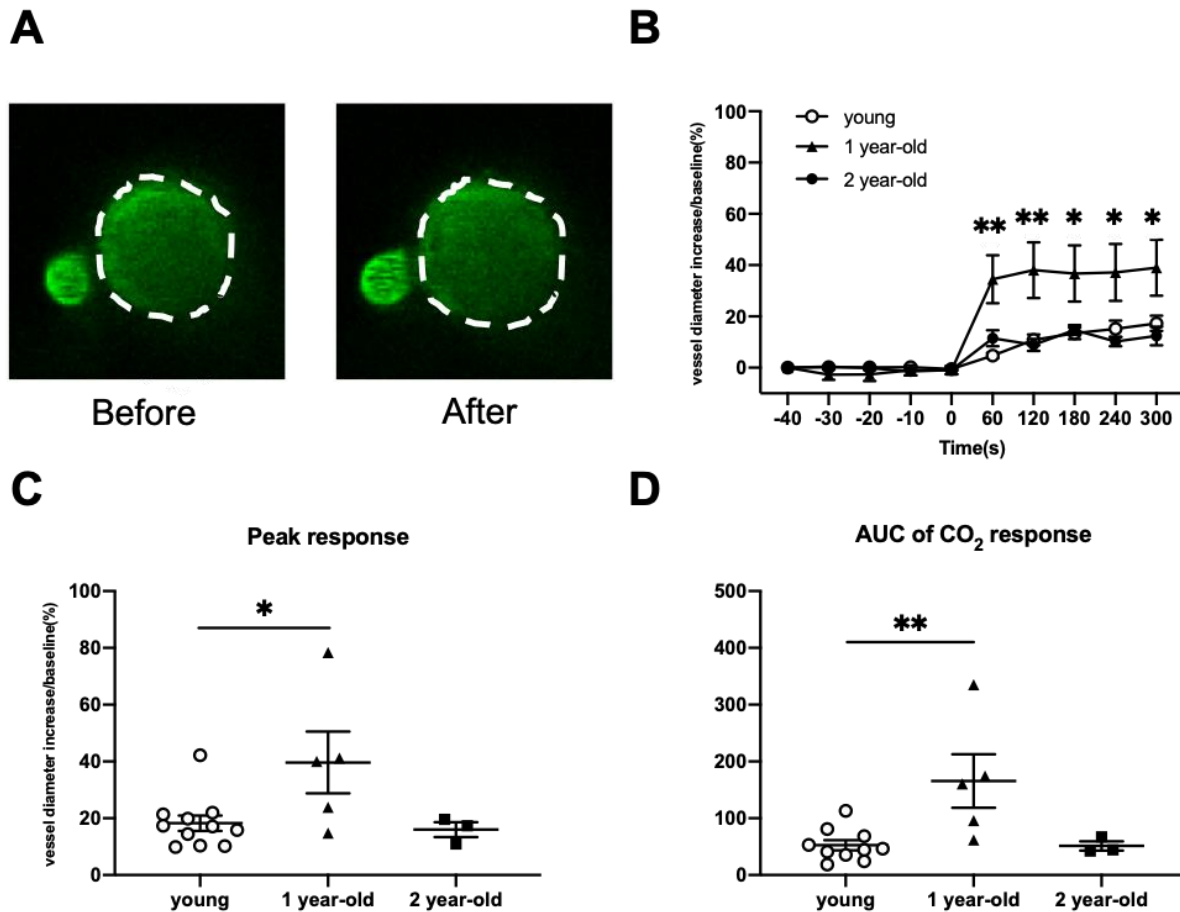


**Figure 29:** CO<sub>2</sub> response of penetrating arteries by two-photon microscopy. (A) Sample picture of a penetrating artery by two-photon microscopy; (B) CO<sub>2</sub> response of penetrating arteries of young

and aged mice; (C) Peak CO<sub>2</sub> response; (D) AUC analysis. Mean ± SEM; t-test for comparison of two groups, One-way ANOVA analysis for comparison of three groups, \**p*<0.05, \*\**p*<0.01; Young: 6-8 weeks, *n*=9; Aged: 1 year-old, *n*=5; Aged: 2 year-olds, *n*=3.

### 3.4.2.3. Capillaries

Similarly, capillaries also dilated well following CO<sub>2</sub> inhalation. There was statistically significant difference between the three groups only in the early phase following 5 minutes of CO<sub>2</sub> inhalation (*P*=0.001 for 60s, 0.003 for 120s, 0.033 for 180s). For the peak CO<sub>2</sub> response in 1 year-old mice was significantly higher than in young mice (**Figure 30C**, 14 ±2 % for young mice, 31 ±5 % for 1 year-old mice, 31 ±16% for 2 years-old mice. *P*=0.002). The same was true for the AUC analysis (**Figure 30D**, *P*=0.006).

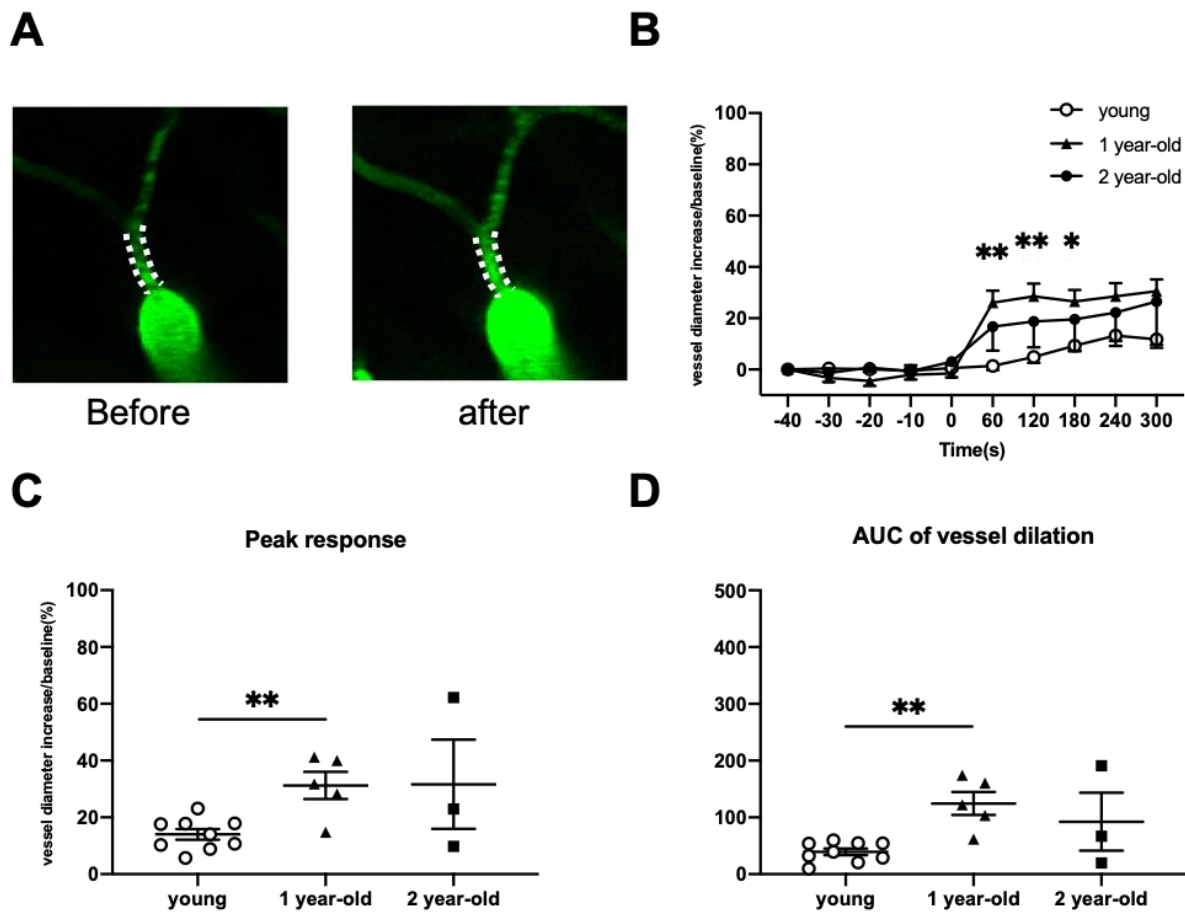


**Figure 30:** CO<sub>2</sub> response of capillaries by two-photon microscopy. (A) Sample picture of a capillary by in vivo two-photon microscopy; (B) CO<sub>2</sub> response of capillaries in young and aged mice; (C)

Peak CO<sub>2</sub> response; (D) AUC analysis. Mean  $\pm$  SEM; t-test for comparison of two groups, One-way ANOVA analysis for comparison of three groups, \*= $p < 0.05$ , \*\*= $p < 0.01$ ; Young: 6-8 weeks, n=9; Aged: 1 year-old, n=5; Aged: 2 year-olds, n=3.

### 3.5. Barnes maze

Besides NVC, we were also interested whether aging affects also behavior in mice. Using the Barnes maze test to study spatial learning and memory formation, we found no statistically significant difference regarding the latency to find the hidden home cage between groups (**Figure 31A**, 79  $\pm$  62s for young mice, 91  $\pm$  75s for 1.5y mice, 99  $\pm$  72s for 2 year-old mice;  $P=0.852$ ) or the speed in the test day (**Figure 31C**, 2.8 $\pm$ 0.3cm/s for young mice, 4.7  $\pm$  2 cm/s for 1.5 year-old mice, 3.7  $\pm$  2.5cm/s for 2 year-old mice;  $P=0.167$ ). Most interestingly, the inter-individual heterogeneity was much larger than the aging affect.

All three groups had a similar learning curve (**Figure 31B**). Only the speed needed to find the home cage was somewhat increased in aged mice (**Figure 31C**).

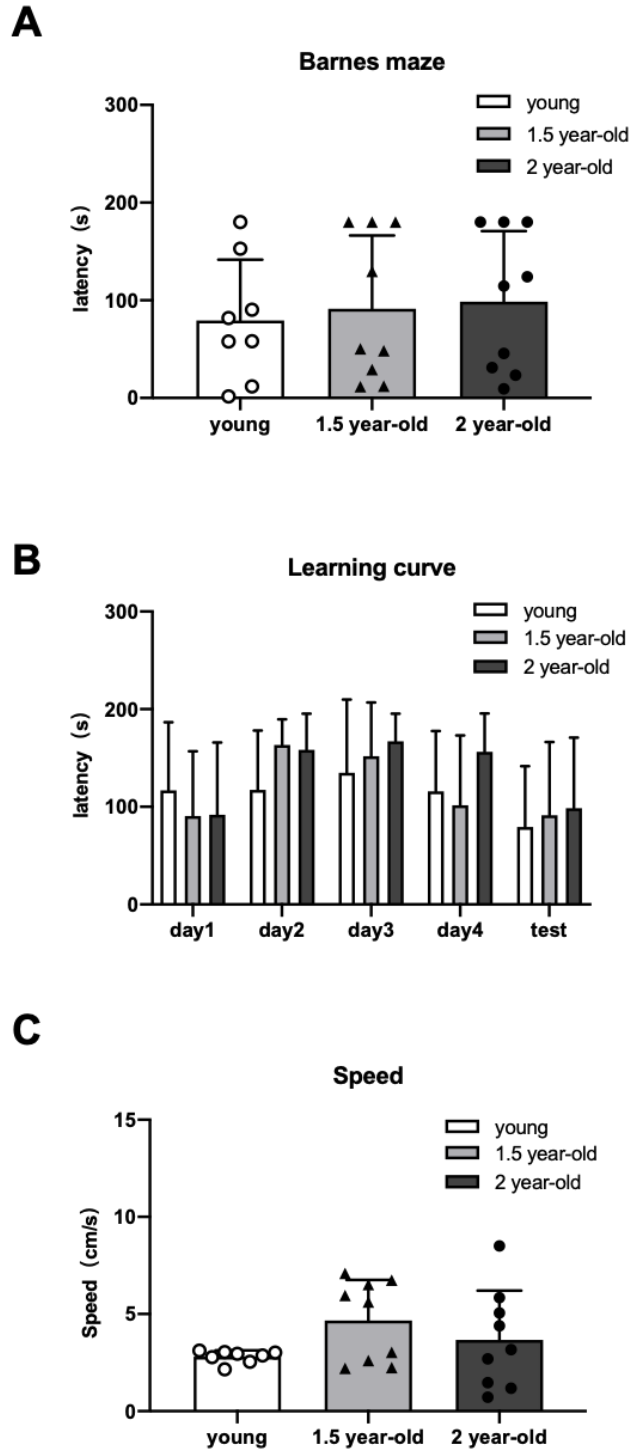


**Figure 31:** Barnes maze test of 6-8 weeks young, 1.5 year-old and 2 year-old mice. (A) Latency on the test day; (B) Learning curve; (C) Speed on the test day. Mean  $\pm$  SD; n=8-9 per group.

#### 4. Discussion

In this study, we aimed to understand the effects of aging on neurovascular coupling. It is known that neurovascular uncoupling frequently happens in the aged brain resulting in not only an unfulfilled energy need to neurons but also an ineffective clearance of metabolic waste products<sup>5</sup>. Moreover, aging often accompanies dementia which is a decline of cognitive function. Vascular dementia is a type of dementia that occurs due to cerebral vascular dysfunction<sup>121</sup>. When neurons do not get sufficient nutrients by the blood stream when activated, their function may deteriorate. Therefore, investigating NVC during aging may improve our understand how the interplay between neurons and vessels may be compromised during pathological conditions. To achieve this goal, we used mice of three different ages to study the NVC. Since different brain regions may change in different ways in response to aging, we studied the NVC response in two different somatosensory areas<sup>122</sup>. We performed electrical forepaw stimulation to induce NVC response in the forepaw area and manual and automated mechanical whisker stimulation to induce NVC in the barrel cortex. We also used LDF and LSI techniques to measure CBF, and in vivo two-photon imaging to measure vessel diameter dynamics of different compartments of brain vascular tree. We showed a significant reduction of NVC in middle-aged (1 year) and old (2 years) mice in comparison with young animals (6-8 weeks). In the end, we examined the spatial memory and learning of aged mice and found no difference between aged and young mice. Since the technique for measuring NVC is of utmost importance for such a study, the discussion of this study will cover mainly two parts: one about establishing an effective and reproducible platform to induce NVC and one using this platform to observe NVC in aged mice.

## **4.1. Discussion of method**

### **4.1.1. In vitro method**

In order to properly invest NVC, the first step is to establish a proper and reproducible method. NVC can be investigated in vitro and in vivo. In vitro mainly acute brain slices are used. Generally, mice are transcardially perfused, then the brain is harvested and sliced acutely. Finally, the slice goes through a recovery period<sup>123</sup>. For NVC experiments, slices are subjected to electrical field stimulation to activate neurons and the vascular response is recorded by infrared-differential interference contrast (IR-DIC) microscopy<sup>124</sup>. This method is particularly common for the study of the role of astrocytes for the maintenance of vascular tone<sup>54,125,126</sup>. The in vitro acute slice model allows to easily investigate different cell types, like neurons or glial cells, and allows single-cell imaging and direct pharmaceutical manipulations. However, since the brain tissue is sliced, tissue damage will always be an issue when interpreting results<sup>127</sup>. Another drawback of this model is the lack of perfusion which results is a lack of basal vascular tone. In order to investigate vasodilatation vessels have therefore to be pre-constricted pharmacologically<sup>8,128</sup>. This procedure makes the interpretation of results on NVC in acute slices even more complicated.

### **4.1.2. In vivo method**

#### **4.1.2.1. Laser Doppler based imaging**

LDF and LSI are both non-invasive in vivo imaging methods for the measurement of tissue perfusion. The basic theory behind is: when moving objects, e.g. red blood cells, are illuminated by constant laser light, movement of the object can be quantified based on the Doppler shift of the wavelength of the reflected light<sup>129</sup>. For LDF, a laser probe is placed or glued on the skull of a mouse and velocity and the concentration of red blood cells are assessed with the help of a monochromatic laser beam<sup>130,131</sup>. The product of red blood

concentration and velocity is defined as laser Doppler flux, a value that changes together with tissue perfusion<sup>132</sup>. The principle of laser speckle contrast imaging is similar. When moving objects are illuminated by dispersed laser light, the scattered light will form an interference pattern called speckle pattern, which is proportional to tissue perfusion<sup>133,134</sup>. This pattern can be converted to 2D tissue perfusion values by laser speckle contrast analysis<sup>135,136</sup>. The laser speckle system composes of a laser and a CCD camera.

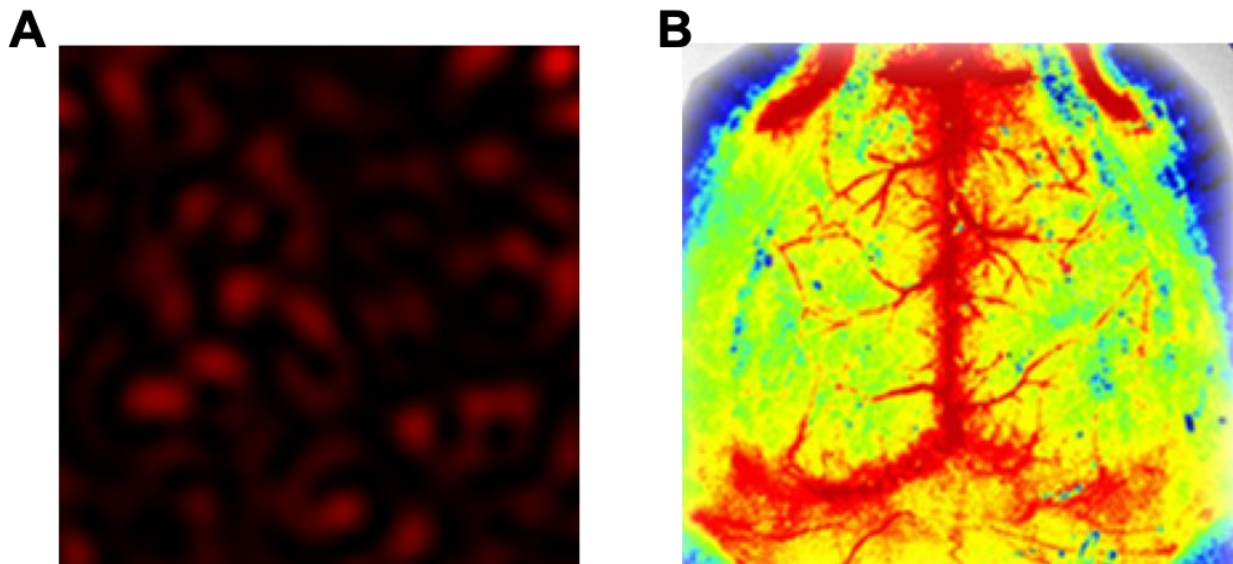


**Figure 32:** (A) Speckle pattern of LSI; (B) Real laser speckle image (adapted from <http://www.perimed-instruments.com>).

LDF has the advantage of penetrating deeper into brain tissue as compared to LSI because of the local single laser beam. Measurement depth of LDF in mouse brain is 300-550  $\mu\text{m}$  beneath the skull<sup>137</sup>. However, LDF can only measure a small brain volume and has therefore a low spatial resolution. LSI, on the other hand, has a far better spatial resolution due to the simultaneous acquisition of flux data from a 2D field of observation<sup>138</sup>. Both techniques can be used to study NVC in mice with or without a cranial window<sup>139,140,138,141</sup>,

or using a thin skull preparation<sup>142</sup>, however, tissue penetration of LSI is less than 100  $\mu\text{m}$ <sup>143</sup>.

#### 4.1.2.2. Fluorescent based imaging

Fluorescent-based in vivo NVC monitoring measures vessel diameter and blood velocity based on direct visualization of red blood cell movements. Unlike epifluorescence microscopy which has almost no tissue penetration and is therefore only used to image superficially located pial vessels, two-photon excitation, which produces fluorescent light only within the focal plane of the objective (**Figure 33**)<sup>144</sup>, is used to image brain tissue down to a depth of 600  $\mu\text{m}$ <sup>145,146</sup>. In order to obtain a better imaging signal, a cranial window is usually needed<sup>145</sup>. Generally, the bone is carefully removed and a glass window is sealed with gel or bone cement to avoid injury of the brain surface and changes in intracranial pressure<sup>147</sup>. For experiments requiring repeated imaging, a chronic cranial window has to be implanted weeks before imaging.

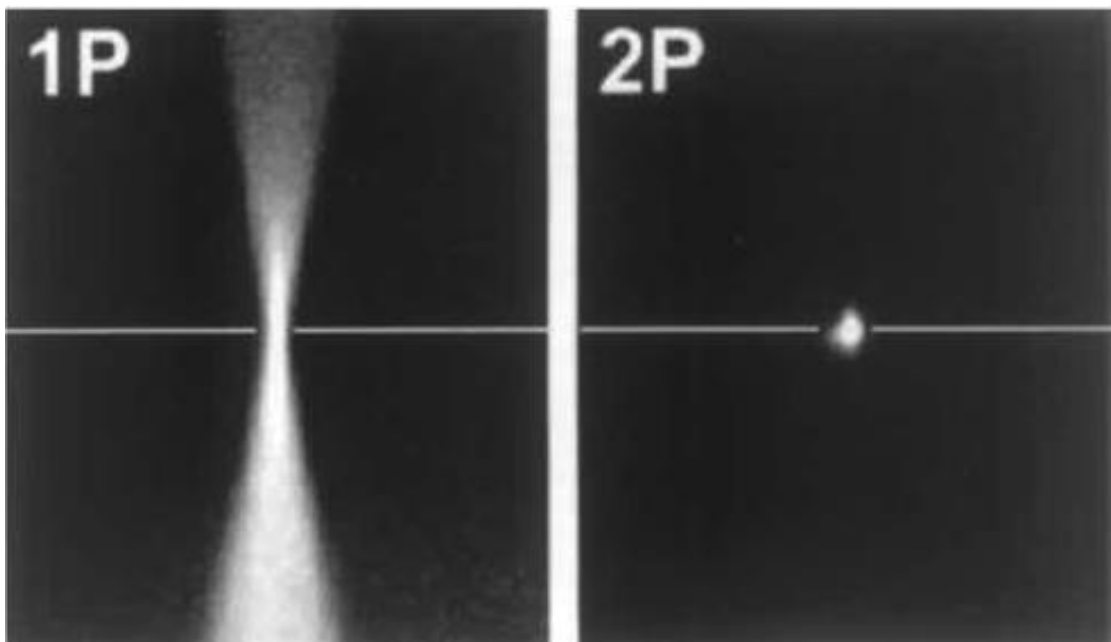


**Figure 33:** Compare of focusing light in epifluorescence microscopy and two-photon microscopy (adapted from <https://www.neurotar.com>).

### **4.1.3. Sensory stimulation**

In order to evoke neuronal activity and subsequent NVC different methods of sensory stimulation are available, such as visual, odor, electrical, or mechanical. Odor stimulation is commonly used when studying the olfactory glomeruli<sup>148</sup>. When the olfactory neuron is activated by odor, for example with amyl acetate, capillaries in olfactory glomeruli will dilate and CBF will increase. Visual stimulation is often combined with BOLD fMRI in human studies<sup>149</sup>. For example, full-field checkerboard stimulation can evoke a 2.9% BOLD signal change and a 20% increase of CBF in the occipital cortex<sup>150</sup>. Electrical fore- or hindpaw stimulation and mechanical whisker stimulation are the main paradigms used to study NVC in rodents.

#### **4.1.3.1. Forepaw stimulation**

To understand why forepaw stimulation can evoke neuronal activation within the somatosensory cortex, the somatosensory pathway needs to be introduced. There are mechano- and thermoreceptors in the forepaw<sup>151</sup>. First-order neurons are responsible for touch sensation and secondary sensory neurons located in the dorsal horn of the spinal cord propagate the signal proximally<sup>152</sup>. Efferent fibers cross the midline and ascent to the ventral posterior lateral nucleus (VPL) in the thalamus and then project to the primary somatosensory cortex<sup>153</sup> (**Figure 5**).

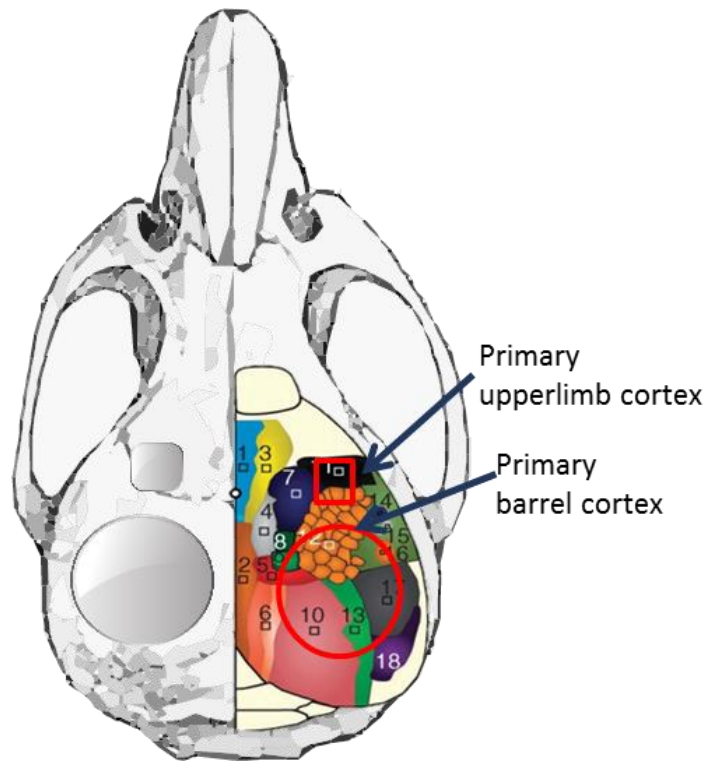


**Figure 34:** Location of primary upper limb sensory cortex and barrel cortex and the location of the cranial window used to expose them (Red round means the size and location of cranial windows)<sup>160</sup>.

Forepaw stimulation can be given both manually and electrically, but usually electrical stimulation is used<sup>154</sup>. Generally, two needle electrodes are inserted into the forepaw and multiple simulations are given with a pulse generator<sup>124</sup>. Parameters like intensity, amplitude, current and frequency can be adjusted. Typical values are 0.5-2.0 mA for intensity and 3 - 10 Hz for frequency<sup>155,156,157,158,159</sup>.

#### 4.1.3.2. Whisker stimulation

Whisker stimulation is a noninvasive method for sensory stimulation by mechanically brushing the whiskers<sup>161</sup> or by using air puffs<sup>162</sup>. The sensory information is carried by the trigeminal nerve to the contralateral trigeminal nerve nuclei, then relay to the ventral posterior medial nucleus (VPM), and finally projects to the barrel cortex (**Figure 9**)<sup>163</sup>. If

the whisker is not available, it is also possible to stimulate the whisker pad electrically<sup>118</sup>. This is of particular importance when investigating aged mice since it is common that the dominant male plucks the whiskers of all other mice in the cage<sup>164</sup>.

#### **4.1.4. Anesthesia**

Besides the imaging technique and the method of neuronal stimulation, another critical determinant for a proper NVC experiment is the use of anesthesia. Anesthesia is usually needed to reduce movement artifacts and stress to the animal<sup>165</sup>.

Commonly used anesthesia protocols for NVC are isoflurane or halothane,  $\alpha$ -chloralose, urethane, or ketamine together with xylazine<sup>166,167,168</sup>. The advantage of inhaled anesthesia is fast induction and recovery. However, isoflurane is also a vessel dilator which acts on calcium and potassium channels of smooth muscle cells<sup>169,170</sup> and therefore affects NVC in a dose- and time-dependent manner<sup>171</sup>.

The disadvantage of using anesthesia is a decrease in cerebral metabolic rate<sup>167,172</sup>. By using special fixation devices and/or augmented reality environments it is nowadays possible to perform imaging in awake, freely moving animals<sup>173,174</sup>. For example, the head of a mouse can be fixed under the microscope and the body can either be restrained in a container<sup>175,176,177</sup> or it is allowed to run freely on a floating plate or ball<sup>178,179,180</sup>. Therefore whisker stimulation induces a higher CBF response in awake mice<sup>120</sup>, however, fine-tuning of the anesthesia protocol can lead to similar results. In fact, a combination of low dosage (0.5 – 0.8%) Isoflurane and hypnorm/hypnovel (0.8 ml/kg, i.p.), exert hemodynamic changes by whisker stimulation similar to the awake state<sup>181</sup>. In general, choosing the right anesthesia combinations is crucial for sensory-evoked NVC experiments.

#### **4.2. Discussion of result**

We first did forepaw stimulation measured CBF with LDF. We tried different published protocols and adjusted our NVC forepaw electrical stimulus settings in parallel to those

studies<sup>155,159</sup>. We used ten times repeated stimulations and adjusted our settings as 2 mA as the stimulation strength which successfully induced NVC response without nociceptive pain. Even though the CBF response was larger in the first stimulation out of the ten times stimulations, it normalized afterward and remained stable. Decreased responses after the first stimulation might be explained with neural adaptation. It has been shown that higher stimulation frequencies (12-24 Hz) induce higher responses but might facilitate the adaption to the stimulus<sup>182</sup>. Thus, smaller frequencies such as 3 Hz to 6 Hz are more preferred for repetitive stimulation paradigms<sup>182</sup>. Ances et al. also found that responses with 5 Hz create higher responses than 1 Hz, 2 Hz, or 10 Hz, which is similar to our setting (6 Hz)<sup>159</sup>.

A disadvantage of this protocol was the use of LDF, since it allows the detection of CBF only in a small region. In order to find the area of the cortex with the strongest response, the LDF probe needed to be moved over the somatosensory cortex. Even though we used a stereotactic frame to fix the LDF probe, this procedure is lengthy and therefore prolongs the duration of anesthesia. Therefore this procedure is often associated with hypotension which is known to affect the CBF response<sup>183</sup>.

Because of the above limitations, we began to optimize the forepaw stimulation platform. We replaced the LDF measurement with a LSI system which allows recording of CBF from larger regions on the cortex and makes time-consuming relocation of probes unnecessary (Figure 7). Since LSI, however, does not penetrate bone and tissue as deep as LDF, a cranial window had to be implanted over the forepaw region of the somatosensory cortex. To obtain a stable and light anesthesia level, we replaced ketamine with medetomidine (i.p.) because ketamine anesthesia increases blood pressure and is relatively hard to control<sup>183</sup>. Medetomidine is an  $\alpha_2$  adrenergic agonist. It is a commonly used anesthesia in NVC experiments with fMRI<sup>184</sup>. Furthermore, medetomidine could effectively reduce isoflurane levels below 1%<sup>169</sup>. To avoid neural adaptation, we adjusted the duration of

forepaw stimulation to 30 seconds and the interval to 3 minutes. Researchers found that forepaw stimulation with longer stimulation duration and interval generated higher CBF responses<sup>185</sup>. The result of forepaw stimulation of young mice on LSI was similar to that of LDF. Although the response by LSI was smaller at the beginning of forepaw stimulation, unlike the LDF recording, the response of LSI constantly increased. This suggests that less neural adaptation occurred with the improved stimulation protocol. This was proven by measuring neural field potentials with fore- and hindpaw stimulation.

After optimizing the method to measure NVC by forepaw stimulation, we examined the effects of aging on NVC. We choose 1 year-old mice for the middle-aged group since this age represents about 50% of the mouse life span<sup>186</sup>. We found a significantly lower NVC response in aged mice (**Figure 16**). The difference was more apparent in the last five stimulations. So that while young mice showed a gradually rising CBF response, 1 year-old aged mice had a reduced response over time. This data indicated that the NVC of 1 year-old aged mice was partially impaired and they had a different dynamic response as compared to the young mice.

The next question was whether there is a difference between the maximal dilation potential of vessels in aged and young mice independent of neuronal activation. We challenged the mice with 10% CO<sub>2</sub> inhalation which is a well-known selective cerebral vessel dilator<sup>187</sup>. Upon application of 10% CO<sub>2</sub> over 3 minutes, CBF increased in young and aged mice. We recorded an approximately 30% increase in CBF as also reported by others<sup>131</sup>. Interestingly aged mice in our experiment seemed to have a hyperactive vessel response. They had a larger mean CBF value, although there was no statistical difference as compared to young mice. This is in line with data from Balbi et al. and Park et al. who did also not find a difference in CBF between young and aged mice upon CO<sub>2</sub> inhalation<sup>94</sup>

188.

Besides the forepaw, whiskers (mystacial vibrissae) play a major role for the acquisition of sensory stimuli in mice. Sensory perception and discrimination of the surrounding factors such as looking for food or avoiding dangers are essential processes for animals in order to appropriately react to their environment<sup>189</sup>. The whiskers are represented in the cerebral cortex in an area called barrel cortex. It is more lateral and larger than that the area where the forepaw is represented. Research also indicated that aged mice had reduced neural numbers in the barrel cortex<sup>190</sup>. Therefore, another important question was, if aged mice have also a significantly reduced NVC response in the barrel cortex area. To answer these questions, we used LSI and two-photon microscopy to study NVC during whisker stimulation.

Before whisker stimulation, mice received a 4 mm glass window above the barrel cortex. The heat map of the stimulated CBF response showed that the most responsive area was mainly located above the somatosensory cortex<sup>179</sup>. This proved the specificity of our stimulation.

We then compared the CBF response of whisker stimulation of young, 1 year-old, and 2 year-old mice using LSI. We found no statistical difference in CBF response between young mice and 1 year-old aged mice. Two year-old mice showed a significantly reduced CBF response as compared to young and 1 year-old mice. The spatial distribution of the CBF response in 1 and 2 year-old mice were slightly different from the one in young. This may suggest functional cortical plasticity and cortical reorganization during aging<sup>191,192</sup>.

Another interesting finding was the slope of the CBF increase after whisker stimulation. We found that the slope, i.e. the velocity of the vascular response of young mice was sharper and higher as compared to the slope of the 2 year-old mice. This was in line with published data showing that 24 months old mice had a slower CBF increase as compared to young animals<sup>76,80</sup>. In the 1 year-old group some of the mice already had a flatter than young mice. This suggests that some aged mice already started to show abnormal NVC

response. Therefore, we speculate that NVC impairment may already start around the age of one year. This is also supported by the fact that 2 year-old mice showed a highly reduced NVC response. This suggest a dose-dependent effect of age on NVC impairment as also observed by others<sup>80,193</sup>.

Upon CO<sub>2</sub> inhalation 1 and 2 year-old mice showed a slow and reduced dilation of cerebral vessels in the first 30 seconds. As discussed previously, this could be explained by a decreased lung functions in aged mice<sup>194,195</sup>. Later on there was no statistical difference between groups as also observed by Balbi et al. by LDF measurements<sup>94</sup>. Other investigators found a significant reduction of CO<sub>2</sub>-induced CBF increase in 2 year-old mice<sup>188,196</sup>, however, our results are corroborated by findings in human subjects showing that normal aging does not lead to the decline of CO<sub>2</sub> response<sup>197,198</sup>. This provides good evidence that our experiments generated translational data.

In order to answer how NVC is affected by age in deeper regions of the cortex, we took advantage of in vivo two-photon microscopy to visualize parenchymal arterioles. In the two-photon experiment, we examined vessel dilation of different vessel segments of pial arteries, penetrating arteries, and capillaries. Even though very few others examined NVC by two-photon microscopy, similar results were observed. Nishino et al. found 5-10% capillary dilation with air puff in awake animals<sup>199</sup>. Cai et al. observed a 20% response with a single stimulation in capillaries<sup>118</sup>. We found a significant decrease of capillary dilatation in 1 and 2 year-old mice, similar to Gutiérrez-Jiménez et al. who observed that 18 months old mice showed abolished vessel dilation<sup>200</sup>. This indicates that NVC is already impaired around one year of age at the level of the capillary.

Previous data suggest that the strongest dilatation following sensory stimulation was observed on the capillary level<sup>118,119</sup>. This is in line with the observation that capillaries dilate earlier than arterioles<sup>70</sup> and contribute to the largest proportion of the CBF increase following sensory stimulation<sup>70</sup>. If capillary dilatation is eliminated, the overall CBF

increase was only 3%<sup>70</sup>. The basis of the response of capillary to a sensory stimulus is their vicinity to astrocytes and neurons, which initiate NVC<sup>201</sup>. Therefore, we believe that the decreased inability of capillaries to dilate upon sensory stimulation with increasing age is the main reason for the reduced CBF response in old mice.

If we combine our observations by LSI and two-photon microscopy, it becomes clear why we did not observe a difference in the CBF response between 1 year-old and young mice following whisker stimulation: in aged mice pial vessels compensate for the reduction of capillary dilation, but with increasing age the compensation was not sufficient and the dysfunction of the whole vascular tree became evident by LSI and by two-photon microscopy.

As mentioned above, aging is often accompanied by cognitive decline or even dementia. The reduction of NVC as observed by us and others could be a possible mechanism for cognitive decline, since a chronic mismatch of flow and metabolism causes repetitive ischemia and possibly neuronal dysfunction. Hence, we were quite surprised not to observe any decline of cognitive function or learning in our cohorts of aged mice. Previous studies, however, provided similar results. Murphy et al. and Harburger et al. found no difference between young and 21-23 months old mice when using Morris water maze to test for learning and memory function<sup>202,203</sup>. Similarly, no cognitive decline was observed when comparing cohorts of mice with increasing age (2, 5, 11, 17 and 18 months)<sup>204,205</sup>. Therefore, we have to conclude that either the cognitive tests we used were not sensitive enough to detect cognitive decline, or that mice are able to maintain their cognitive function despite highly pathological neuro-vascular function. Further research is needed to fully understand this phenomenon.

## 5. Summary

### 5.1. English summary

When neurons are firing, local cerebral blood flow (CBF) increases to deliver more energy substrates and oxygen to the activated neurons. This phenomenon is called neurovascular coupling (NVC). The aim of the current study was to establish effective protocols to study NVC in mice and to investigate the impact of aging on NVC.

We firstly set up a ten times forepaw stimulation protocol based on ketamine anesthesia and Laser Doppler flowmetry (LDF). We then optimized the forepaw stimulation with longer stimulation duration and interval, new anesthesia of medetomidine and Laser speckle imaging (LSI). We compared the NVC of 6-8 weeks young mice and 1 year-old mice and found reduced CBF response in aged mice. The reduction of CBF occurred only after prolonged stimulation suggesting a vascular fatigue phenomenon.

We further studied whisker stimulation with LSI and two-photon microscope comparing 1 year- and 2 year-old mice with young mice. Mice aged for one year were not different from young mice in terms of CBF response following whisker stimulation or CO<sub>2</sub> inhalation. When directly observing capillaries by two-photon imaging, 1 year-old mice had a reduced capillary response, a higher pial vessel response, and a stronger CO<sub>2</sub> response in penetrating arterioles and capillaries as compared to young mice. Further aging the animals to two years resulted in a significant reduction of CBF and capillary dilatation following whisker stimulation while the CO<sub>2</sub> response was unaltered.

In the end, we performed the Barnes maze to test the spatial learning and found no difference between 6-8 weeks, 1.5 year-old and 2 year-old mice.

Taken together, we found a reduced CBF response following sensory stimulation in 1 year- and 2 year-old mice. This impairment was most likely caused by capillary dysfunction. This severe neuro-vascular pathology, however, did not result in reduced cognitive function.

## 5.2. Zusammenfassung und Ausblick

Wenn Neuronen feuern, steigt die lokale zerebrale Durchblutung, um den entstehenden Energiebedarf zu decken. Dieser Prozess wird als neurovaskuläre Kopplung (NVK) bezeichnet. Ziel der vorliegenden Arbeit war Methoden zur Untersuchung der NVK zu entwickeln und damit den Einfluss des Alterungsprozesses auf die NVK zu quantifizieren.

Zuerst haben wir ein Vorderpfoten-Stimulationsprotokoll basierend auf Ketamin-Anästhesie und Laser-Doppler-Durchflussmessungen etabliert. Wir optimierten dann die Vorderpfoten-Stimulation mit längerer Stimulationsdauer und -intervall, verbesserter Anästhesie und 2-D Laser-Speckle Imaging. Wir verglichen die neurovaskuläre Kopplung von jungen Mäusen mit der ein Jahr alten Mäuse und fanden eine reduzierte NVK. Dieser Effekt wurde überwiegend am Ende des Stimulationszyklus beobachtet.

In weiteren Untersuchungen mit mechanischer Stimulation der Barthaare, Messung der zerebralen Durchblutung mit Laser-Speckle Imaging und Bestimmung des Durchmessers zerebraler Mikrogefäße mit Zwei-Photonen-Mikroskopie, haben wir 1- und 2-Jahre alte mit jungen Mäusen verglichen. Bei Mäusen im Alter von einem Jahr fanden wir keinen statistischen Unterschied zu jungen Mäusen in Bezug auf zerebrale Durchblutung und CO<sub>2</sub>-Reaktivität. In der Zwei-Photonen-Bildgebung fanden wir bei Mäuse im Alter von einem Jahr eine verminderte Kapillarreaktion, eine erhöhte Reaktion der pialen Gefäße und eine verstärkte CO<sub>2</sub>-Reaktivität. Bei zwei Jahre alten Mäusen waren diese Effekte verstärkt anzutreffen. Nur die CO<sub>2</sub>-Antwort war unverändert im Vergleich zu jungen Tieren.

Messungen der Lernfähigkeit und des Merkvermögens haben keinen Unterschied zwischen den Gruppen ergeben.

Zusammenfassend haben wir beobachtet, dass Mäuse mit zunehmenden Alter eine Beeinträchtigung der neurovaskulären Kopplung aufweisen, die durch eine Störung der

Kapillarfunktion verursacht wird. Diese Beeinträchtigung führte allerdings nicht zu einer Verringerung der kognitiven Funktion.

## 6. References

1. Raichle ME, Gusnard DA. Appraising the brain's energy budget. *Proc Natl Acad Sci.* 2002. doi:10.1073/pnas.172399499
2. Mathiesen C, Caesar K, Akgören N, Lauritzen M. Modification of activity-dependent increases of cerebral blood flow by excitatory synaptic activity and spikes in rat cerebellar cortex. *J Physiol.* 1998;512(2):555-566. doi:10.1111/j.1469-7793.1998.555be.x
3. Roy CS, Sherrington CS. On the Regulation of the Blood-supply of the Brain. *J Physiol.* 1890. doi:10.1113/jphysiol.1890.sp000321
4. Schmidt, C.F., and Hendrix JP. The action of chemical substances on cerebral blood vessels. *Res Publ Assoc Res Nerv Ment Dis.* 1938;18:229–276.
5. Toth P, Tarantini S, Csiszar A, Ungvari Z. Functional vascular contributions to cognitive impairment and dementia: mechanisms and consequences of cerebral autoregulatory dysfunction, endothelial impairment, and neurovascular uncoupling in aging. *Am J Physiol - Hear Circ Physiol.* 2017;312(1):H1-H20. doi:10.1152/ajpheart.00581.2016
6. Bohlen HG, Harper SL. Evidence of myogenic vascular control in the rat cerebral cortex. *Circ Res.* 1984;55(4):554-559. doi:10.1161/01.res.55.4.554
7. Faraci FM, Heistad DD. Regulation of large cerebral arteries and cerebral microvascular pressure. *Circ Res.* 1990. doi:10.1161/01.RES.66.1.8
8. Garcia-Roldan JL, Bevan JA. Flow-induced constriction and dilation of cerebral resistance arteries. *Circ Res.* 1990;66(5):1445-1448.  
<http://www.ncbi.nlm.nih.gov/pubmed/2335036>. Accessed June 28, 2019.
9. Tiecks FP, Lam AM, Aaslid R, Newell DW. Comparison of static and dynamic cerebral autoregulation measurements. *Stroke.* 1995;26(6):1014-1019. doi:10.1161/01.STR.26.6.1014

10. Liu J, Zhu YS, Hill C, et al. Cerebral autoregulation of blood velocity and volumetric flow during steady-state changes in arterial pressure. *Hypertension*. 2013;62(5):973-979. doi:10.1161/HYPERTENSIONAHA.113.01867
11. Gebremedhin D, Lange AR, Lowry TF, et al. Production of 20-HETE and its role in autoregulation of cerebral blood flow. *Circ Res*. 2000;87(1):60-65. doi:10.1161/01.RES.87.1.60
12. Roman RJ. P-450 metabolites of arachidonic acid in the control of cardiovascular function. *Physiol Rev*. 2002;82(1):131-185. doi:10.1152/physrev.00021.2001
13. Willie CK, Tzeng YC, Fisher JA, Ainslie PN. Integrative regulation of human brain blood flow. *J Physiol*. 2014;592(5):841-859. doi:10.1113/jphysiol.2013.268953
14. Tarasoff-Conway JM, Carare RO, Osorio RS, et al. Clearance systems in the brain - Implications for Alzheimer disease. *Nat Rev Neurol*. 2015;11(8):457-470. doi:10.1038/nrneurol.2015.119
15. Freeman RD, Li B. Neural – Metabolic coupling in the central visual pathway. *Philos Trans R Soc B Biol Sci*. 2016;371(1705):20150357. doi:10.1098/rstb.2015.0357
16. Offenhauser N, Thomsen K, Caesar K, Lauritzen M. Activity-induced tissue oxygenation changes in rat cerebellar cortex: Interplay of postsynaptic activation and blood flow. *J Physiol*. 2005. doi:10.1113/jphysiol.2005.082776
17. Gordon GRJ, Choi HB, Rungta RL, Ellis-Davies GCR, MacVicar BA. Brain metabolism dictates the polarity of astrocyte control over arterioles. *Nature*. 2008. doi:10.1038/nature07525
18. Lin A-L, Fox PT, Hardies J, Duong TQ, Gao J-H. Nonlinear coupling between cerebral blood flow, oxygen consumption, and ATP production in human visual cortex. *Proc Natl Acad Sci*. 2010;107(18):8446-8451. doi:10.1073/pnas.0909711107

19. Lindauer U, Leithner C, Kaasch H, et al. Neurovascular coupling in rat brain operates independent of hemoglobin deoxygenation. *J Cereb Blood Flow Metab.* 2010. doi:10.1038/jcbfm.2009.259
20. Attwell D, Buchan AM, Charpak S, Lauritzen M, Macvicar BA, Newman EA. Glial and neuronal control of brain blood flow. *Nature.* 2010;468(7321):232-243. doi:10.1038/nature09613
21. Longden TA, Dabertrand F, Koide M, et al. Capillary K<sup>+</sup>-sensing initiates retrograde hyperpolarization to increase local cerebral blood flow. *Nat Neurosci.* 2017;20(5):717-726. doi:10.1038/nn.4533
22. Drew PJ, Shih AY, Kleinfeld D. Fluctuating and sensory-induced vasodynamics in rodent cortex extend arteriole capacity. *Proc Natl Acad Sci.* 2011;108(20):8473-8478. doi:10.1073/pnas.1100428108
23. Hosford PS, Gourine A V. What is the key mediator of the neurovascular coupling response? *Neurosci Biobehav Rev.* 2019;96:174-181. doi:10.1016/j.neubiorev.2018.11.011
24. Iadecola C. The Neurovascular Unit Coming of Age: A Journey through Neurovascular Coupling in Health and Disease. *Neuron.* 2017;96(1):17-42. doi:10.1016/j.neuron.2017.07.030
25. Blinder P, Tsai PS, Kaufhold JP, Knutsen PM, Suhl H, Kleinfeld D. The cortical angiome: An interconnected vascular network with noncolumnar patterns of blood flow. *Nat Neurosci.* 2013;16(7):889-897. doi:10.1038/nn.3426
26. Chinta L V., Lindvere L, Dorr A, Sahota B, Sled JG, Stefanovic B. Quantitative estimates of stimulation-induced perfusion response using two-photon fluorescence microscopy of cortical microvascular networks. *Neuroimage.* 2012;61(3):517-524. doi:10.1016/j.neuroimage.2012.04.009

27. Roggendorf W, Cervós-Navarro J. Ultrastructure of arterioles in the cat brain. *Cell Tissue Res.* 1977. doi:10.1007/BF00219571
28. Hamel E. Perivascular nerves and the regulation of cerebrovascular tone. *J Appl Physiol.* 2006. doi:10.1152/jappphysiol.00954.2005
29. physiology EH-J of applied, 2006 undefined. Perivascular nerves and the regulation of cerebrovascular tone. *physiology.org.*  
<https://www.physiology.org/doi/abs/10.1152/jappphysiol.00954.2005>. Accessed June 27, 2019.
30. Cohen ZVI, Bonvento G, Lacombe P, Hamel E. Serotonin in the regulation of brain microcirculation. *Prog Neurobiol.* 1996;50(4):335-362. doi:10.1016/S0301-0082(96)00033-0
31. Dahl E. The fine structure of intracerebral vessels. *Zeitschrift für Zellforsch und Mikroskopische Anat.* 1973;145(4):577-586. doi:10.1007/BF00306725
32. Zhang ET, Inman CB, Weller RO. Interrelationships of the pia mater and the perivascular (Virchow-Robin) spaces in the human cerebrum. *J Anat.* 1990;170:111-123.  
<https://www.ncbi.nlm.nih.gov/pmc/articles/PMC1257067/>. Accessed June 27, 2019.
33. Armulik A, Genové G, Betsholtz C. Pericytes: Developmental, Physiological, and Pathological Perspectives, Problems, and Promises. *Dev Cell.* 2011;21(2):193-215.  
doi:10.1016/j.devcel.2011.07.001
34. Howarth C. The contribution of astrocytes to the regulation of cerebral blood flow. *Front Neurosci.* 2014;8(8 MAY):1-9. doi:10.3389/fnins.2014.00103
35. Morii S, Ngai AC, Ko KR, Winn HR. Role of adenosine in regulation of cerebral blood flow: effects of theophylline during normoxia and hypoxia. *Am J Physiol Circ Physiol.* 2017.  
doi:10.1152/ajpheart.1987.253.1.h165

36. Dirnagl U, Lindauer U, Villringer A. Role of nitric oxide in the coupling of cerebral blood flow to neuronal activation in rats. *Neurosci Lett*. 1993. doi:10.1016/0304-3940(93)90343-J
37. Grienberger C, Konnerth A. Imaging Calcium in Neurons. *Neuron*. 2012;73(5):862-885. doi:10.1016/j.neuron.2012.02.011
38. Bazargani N, Attwell D. Astrocyte calcium signaling: The third wave. *Nat Neurosci*. 2016;19(2):182-189. doi:10.1038/nn.4201
39. Lecrux C, Hamel E. Neuronal networks and mediators of cortical neurovascular coupling responses in normal and altered brain states. *Philos Trans R Soc B Biol Sci*. 2016;371(1705). doi:10.1098/rstb.2015.0350
40. Yang G, Zhang Y, Ross ME, Iadecola C. Attenuation of activity-induced increases in cerebellar blood flow in mice lacking neuronal nitric oxide synthase. *Am J Physiol Circ Physiol*. 2003;285(1):H298-H304. doi:10.1152/ajpheart.00043.2003
41. Takano T, Tian GF, Peng W, et al. Astrocyte-mediated control of cerebral blood flow. *Nat Neurosci*. 2006;9(2):260-267. doi:10.1038/nn1623
42. Lecrux C, Toussay X, Kocharyan A, et al. Pyramidal Neurons Are “Neurogenic Hubs” in the Neurovascular Coupling Response to Whisker Stimulation. *J Neurosci*. 2011;31(27):9836-9847. doi:10.1523/jneurosci.4943-10.2011
43. Anenberg E, Chan AW, Xie Y, LeDue JM, Murphy TH. Optogenetic stimulation of GABA neurons can decrease local neuronal activity while increasing cortical blood flow. *J Cereb Blood Flow Metab*. 2015;35(10):1579-1586. doi:10.1038/jcbfm.2015.140
44. Yaksh TL, Wang JY, Go VLW. Cortical vasodilatation produced by vasoactive intestinal polypeptide (VIP) and by physiological stimuli in the cat. *J Cereb Blood Flow Metab*. 1987;7(3):315-326. doi:10.1038/jcbfm.1987.69

45. Tuor UI, Kelly PAT, Edvinsson L, McCulloch J. Neuropeptide Y and the Cerebral Circulation. *J Cereb Blood Flow Metab.* 1990;10(5):591-601. doi:10.1038/jcbfm.1990.110
46. Cauli B, Tong X-K, Rancillac A, et al. Cortical GABA Interneurons in Neurovascular Coupling: Relays for Subcortical Vasoactive Pathways. *J Neurosci.* 2004;24(41):8940-8949. doi:10.1523/JNEUROSCI.3065-04.2004
47. Cauli B. Revisiting the role of neurons in neurovascular coupling. *Front Neuroenergetics.* 2010;2. doi:10.3389/fnene.2010.00009
48. Cohen Z, Bonvento G, Lacombe P, Hamel E. Serotonin in the regulation of brain microcirculation. *Prog Neurobiol.* 1996;50(4):335-362.  
<http://www.ncbi.nlm.nih.gov/pubmed/9004349>. Accessed July 1, 2019.
49. Lecrux C, Sandoe CH, Neupane S, et al. Impact of Altered Cholinergic Tones on the Neurovascular Coupling Response to Whisker Stimulation. *J Neurosci.* 2017;37(6):1518-1531. doi:10.1523/JNEUROSCI.1784-16.2016
50. Zhang F, Xu S, Iadecola C. Role of nitric oxide and acetylcholine in neocortical hyperemia elicited by basal forebrain stimulation: evidence for an involvement of endothelial nitric oxide. *Neuroscience.* 1995;69(4):1195-1204.  
<http://www.ncbi.nlm.nih.gov/pubmed/8848107>. Accessed July 1, 2019.
51. Zonta M, Angulo MC, Gobbo S, et al. Neuron-to-astrocyte signaling is central to the dynamic control of brain microcirculation. *Nat Neurosci.* 2003;6(1):43-50.  
doi:10.1038/nn980
52. Blanco VM, Stern JE, Filosa JA. Tone-dependent vascular responses to astrocyte-derived signals. *Am J Physiol Circ Physiol.* 2008;294(6):H2855-H2863.  
doi:10.1152/ajpheart.91451.2007

53. Bonder DE, McCarthy KD. Astrocytic Gq-GPCR-Linked IP3R-Dependent Ca<sup>2+</sup> Signaling Does Not Mediate Neurovascular Coupling in Mouse Visual Cortex In Vivo. *J Neurosci*. 2014;34(39):13139-13150. doi:10.1523/jneurosci.2591-14.2014
54. Otsu Y, Couchman K, Lyons DG, et al. Calcium dynamics in astrocyte processes during neurovascular coupling. *Nat Neurosci*. 2015;18(2):210-218. doi:10.1038/nn.3906
55. Jego P, Pacheco-Torres J, Araque A, Canals S. Functional MRI in mice lacking IP3-dependent calcium signaling in astrocytes. *J Cereb Blood Flow Metab*. 2014;34(10):1599-1603. doi:10.1038/jcbfm.2014.144
56. Rosenegger DG, Tran CHT, Wamsteeker Cusulin JI, Gordon GR. Tonic Local Brain Blood Flow Control by Astrocytes Independent of Phasic Neurovascular Coupling. *J Neurosci*. 2015;35(39):13463-13474. doi:10.1523/JNEUROSCI.1780-15.2015
57. Zhang C, Tabatabaei M, Bélanger S, et al. Astrocytic endfoot Ca<sup>2+</sup> correlates with parenchymal vessel responses during 4-AP induced epilepsy: An in vivo two-photon lifetime microscopy study. *J Cereb Blood Flow Metab*. 2017:0271678X1772541. doi:10.1177/0271678X17725417
58. Filosa JA, Bonev AD, Straub S V., et al. Local potassium signaling couples neuronal activity to vasodilation in the brain. *Nat Neurosci*. 2006;9(11):1397-1403. doi:10.1038/nn1779
59. Segal SS. Integration and modulation of intercellular signaling underlying blood flow control. *J Vasc Res*. 2015;52(2):136-157. doi:10.1159/000439112
60. Silva AC, Koretsky AP. Laminar specificity of functional MRI onset times during somatosensory stimulation in rat. *Proc Natl Acad Sci*. 2002;99(23):15182-15187. doi:10.1073/pnas.222561899
61. Longden TA, Dabertrand F, Koide M, et al. Capillary K<sup>+</sup>-sensing initiates retrograde hyperpolarization to increase local cerebral blood flow. *Nat Neurosci*. 2017;20(5):717-726. doi:10.1038/nn.4533

62. Mishra A, Reynolds JP, Chen Y, Gourine A V, Rusakov DA, Attwell D. Astrocytes mediate neurovascular signaling to capillary pericytes but not to arterioles. *Nat Neurosci*. 2016;19(12):1619-1627. doi:10.1038/nn.4428
63. Tallini YN, Brekke JF, Shui B, et al. Propagated endothelial Ca<sup>2+</sup> waves and arteriolar dilation in vivo: Measurements in Cx40BAC-GCaMP2 transgenic mice. *Circ Res*. 2007;101(12):1300-1309. doi:10.1161/CIRCRESAHA.107.149484
64. Hill RA, Tong L, Yuan P, Murikinati S, Gupta S, Grutzendler J. Regional Blood Flow in the Normal and Ischemic Brain Is Controlled by Arteriolar Smooth Muscle Cell Contractility and Not by Capillary Pericytes. *Neuron*. 2015. doi:10.1016/j.neuron.2015.06.001
65. Pournaras CJ, Rungger-Brändle E, Riva CE, Hardarson SH, Stefansson E. Regulation of retinal blood flow in health and disease. *Prog Retin Eye Res*. 2008;27(3):284-330. doi:10.1016/j.preteyeres.2008.02.002
66. Skalli O, Pelte MF, Peclet MC, et al. Alpha-smooth muscle actin, a differentiation marker of smooth muscle cells, is present in microfilamentous bundles of pericytes. *J Histochem Cytochem*. 1989;37(3):315-321. doi:10.1177/37.3.2918221
67. SCHUBERT R, MULVANY MJ. The myogenic response: established facts and attractive hypotheses. *Clin Sci*. 1999;96(4):313. doi:10.1042/CS19980403
68. Chan-Ling T, Page MP, Gardiner T, Baxter L, Rosinova E, Hughes S. Desmin ensheathment ratio as an indicator of vessel stability: evidence in normal development and in retinopathy of prematurity. *Am J Pathol*. 2004;165(4):1301-1313. doi:10.1016/S0002-9440(10)63389-5
69. Bell RD, Winkler EA, Sagare AP, et al. Pericytes control key neurovascular functions and neuronal phenotype in the adult brain and during brain aging. *Neuron*. 2010;68(3):409-427. doi:10.1016/j.neuron.2010.09.043

70. Hall CN, Reynell C, Gesslein B, et al. Capillary pericytes regulate cerebral blood flow in health and disease. *Nature*. 2014;508(1):55-60. doi:10.1038/nature13165
71. Nehls V, Drenckhahn D. Heterogeneity of microvascular pericytes for smooth muscle type alpha-actin. *J Cell Biol*. 1991;113(1):147-154. doi:10.1083/jcb.113.1.147
72. Kisler K, Nelson AR, Rege S V, et al. Pericyte degeneration leads to neurovascular uncoupling and limits oxygen supply to brain. *Nat Neurosci*. 2017;20(3):406-416. doi:10.1038/nn.4489
73. Brown WR, Thore CR. Review: Cerebral microvascular pathology in ageing and neurodegeneration. *Neuropathol Appl Neurobiol*. 2011;37(1):56-74. doi:10.1111/j.1365-2990.2010.01139.x
74. Good CD, Johnsrude IS, Ashburner J, Henson RNA, Friston KJ, Frackowiak RSJ. A voxel-based morphometric study of ageing in 465 normal adult human brains. *Neuroimage*. 2001;14(1 Pt 1):21-36. doi:10.1006/nimg.2001.0786
75. Medina D, deToledo-Morrell L, Urresta F, et al. White matter changes in mild cognitive impairment and AD: A diffusion tensor imaging study. *Neurobiol Aging*. 2006;27(5):663-672. doi:10.1016/j.neurobiolaging.2005.03.026
76. Tarantini S, Valcarcel-Ares NM, Yabluchanskiy A, et al. Treatment with the mitochondrial-targeted antioxidant peptide SS-31 rescues neurovascular coupling responses and cerebrovascular endothelial function and improves cognition in aged mice. *Aging Cell*. 2018;(December 2017):e12731. doi:10.1111/acel.12731
77. Barreto G, Huang TT, Giffard RG. Age-related defects in sensorimotor activity, spatial learning, and memory in c57bl/6 mice. *J Neurosurg Anesthesiol*. 2010;22(3):214-219. doi:10.1097/ANA.0b013e3181d56c98
78. Murman DL. The Impact of Age on Cognition. *Semin Hear*. 2015. doi:10.1055/s-0035-1555115

79. Tucsek Z, Toth P, Tarantini S, et al. Aging exacerbates obesity-induced cerebrovascular rarefaction, neurovascular uncoupling, and cognitive decline in mice. *Journals Gerontol - Ser A Biol Sci Med Sci*. 2014;69(11):1339-1352. doi:10.1093/gerona/glu080
80. Duncombe J, Lennen RJ, Jansen MA, Marshall I, Wardlaw JM, Horsburgh K. Ageing causes prominent neurovascular dysfunction associated with loss of astrocytic contacts and gliosis. *Neuropathol Appl Neurobiol*. 2017;43(6):477-491. doi:10.1111/nan.12375
81. Partridge L, Gems D. Mechanisms of ageing: Public or private? *Nat Rev Genet*. 2002;3(3):165-175. doi:10.1038/nrg753
82. Burke SN, Barnes CA. Neural plasticity in the ageing brain. *Nat Rev Neurosci*. 2006;7(1):30-40. doi:10.1038/nrn1809
83. Farrall AJ, Wardlaw JM. Blood-brain barrier: Ageing and microvascular disease - systematic review and meta-analysis. *Neurobiol Aging*. 2009;30(3):337-352. doi:10.1016/j.neurobiolaging.2007.07.015
84. Sonntag WE, Lynch CD, Cooney PT, Hutchins PM. Decreases in cerebral microvasculature with age are associated with the decline in growth hormone and insulin-like growth factor 1. *Endocrinology*. 1997. doi:10.1210/endo.138.8.5330
85. Wang JC, Bennett M. Aging and atherosclerosis: Mechanisms, functional consequences, and potential therapeutics for cellular senescence. *Circ Res*. 2012. doi:10.1161/CIRCRESAHA.111.261388
86. Ungvari Z, Kaley G, De Cabo R, Sonntag WE, Csiszar A. Mechanisms of vascular aging: New perspectives. *Journals Gerontol - Ser A Biol Sci Med Sci*. 2010;65 A(10):1028-1041. doi:10.1093/gerona/glq113

87. Springo Z, Toth P, Tarantini S, et al. Aging impairs myogenic adaptation to pulsatile pressure in mouse cerebral arteries. *J Cereb Blood Flow Metab.* 2015. doi:10.1038/jcbfm.2014.256
88. Kawamura J, Terayama Y, Takashima S, et al. Leuko-araiosis and cerebral perfusion in normal aging. *Exp Aging Res.* 1993. doi:10.1080/03610739308253935
89. Krejza J, Mariak Z, Walecki J, Szydlak P, Lewko J, Ustymowicz A. Transcranial color Doppler sonography of basal cerebral arteries in 182 healthy subjects: Age and sex variability and normal reference values for blood flow parameters. *Am J Roentgenol.* 1999. doi:10.2214/ajr.172.1.9888770
90. Lipecz A, Csipo T, Tarantini S, et al. Age-related impairment of neurovascular coupling responses: a dynamic vessel analysis (DVA)-based approach to measure decreased flicker light stimulus-induced retinal arteriolar dilation in healthy older adults. *GeroScience.* 2019;41(3):341-349. doi:10.1007/s11357-019-00078-y
91. Lourenço CF, Ledo A, Caetano M, Barbosa RM, Laranjinha J. Age-dependent impairment of neurovascular and neurometabolic coupling in the hippocampus. *Front Physiol.* 2018;9(JUL):913. doi:10.3389/fphys.2018.00913
92. Mayhan WG, Faraci FM, Baumbach GL, Heistad DD. Effects of aging on responses of cerebral arterioles. *Am J Physiol - Hear Circ Physiol.* 1990;258(4 27-4):H1138-H1143. doi:10.1152/ajpheart.1990.258.4.H1138
93. Aanerud J, Borghammer P, Mallar Chakravarty M, et al. Brain energy metabolism and blood flow differences in healthy aging. *J Cereb Blood Flow Metab.* 2012;32(7):1177-1187. doi:10.1038/jcbfm.2012.18
94. Balbi M, Ghosh M, Longden TA, et al. Dysfunction of Mouse Cerebral Arteries during Early Aging. *J Cereb Blood Flow Metab.* 2015;35(9):1445-1453. doi:10.1038/jcbfm.2015.107

95. Fabiani M, Gordon BA, Maclin EL, et al. Neurovascular coupling in normal aging: A combined optical, ERP and fMRI study. *Neuroimage*. 2014;85:592-607. doi:10.1016/j.neuroimage.2013.04.113
96. Toda N. Age-related changes in endothelial function and blood flow regulation. *Pharmacol Ther*. 2012;133(2):159-176. doi:10.1016/j.pharmthera.2011.10.004
97. Finkel T, Holbrook NJ. Oxidants, oxidative stress and the biology of ageing. *Nature*. 2000;408(6809):239-247. doi:10.1038/35041687
98. Toth P, Tarantini S, Tucsek Z, et al. Resveratrol treatment rescues neurovascular coupling in aged mice: role of improved cerebrovascular endothelial function and downregulation of NADPH oxidase. *AJP Hear Circ Physiol*. 2014;306(3):H299-H308. doi:10.1152/ajpheart.00744.2013
99. Park L, Anrather J, Girouard H, Zhou P, Iadecola C. Nox2-derived reactive oxygen species mediate neurovascular dysregulation in the aging mouse brain. *J Cereb Blood Flow Metab*. 2007;27(12):1908-1918. doi:10.1038/sj.jcbfm.9600491
100. Toth P, Csiszar A, Sosnowska D, et al. Treatment with the cytochrome P450  $\omega$ -hydroxylase inhibitor HET0016 attenuates cerebrovascular inflammation, oxidative stress and improves vasomotor function in spontaneously hypertensive rats. *Br J Pharmacol*. 2013;168(8):1878-1888. doi:10.1111/bph.12079
101. Park L, Koizumi K, El Jamal S, et al. Age-dependent neurovascular dysfunction and damage in a mouse model of cerebral amyloid angiopathy. *Stroke*. 2014;45(6):1815-1821. doi:10.1161/STROKEAHA.114.005179
102. Scheltens P, Blennow K, Breteler MMB, et al. Alzheimer's disease. *Lancet*. 2016;388(10043):505-517. doi:10.1016/S0140-6736(15)01124-1
103. Iadecola C. Neurovascular regulation in the normal brain and in Alzheimer's disease. *Nat Rev Neurosci*. 2004;5(5):347-360. doi:10.1038/nrn1387

104. Lourenço CF, Ledo A, Barbosa RM, Laranjinha J. Neurovascular uncoupling in the triple transgenic model of Alzheimer's disease: Impaired cerebral blood flow response to neuronal-derived nitric oxide signaling. *Exp Neurol*. 2017;291:36-43.  
doi:10.1016/j.expneurol.2017.01.013
105. Hock C, Villringer K, Müller-Spahn F, et al. Decrease in parietal cerebral hemoglobin oxygenation during performance of a verbal fluency task in patients with Alzheimer's disease monitored by means of near-infrared spectroscopy (NIRS) - Correlation with simultaneous rCBF-PET measurements. *Brain Res*. 1997. doi:10.1016/S0006-8993(97)00122-4
106. Baloyannis SJ, Baloyannis IS. The vascular factor in Alzheimer's disease: A study in Golgi technique and electron microscopy. *J Neurol Sci*. 2012. doi:10.1016/j.jns.2012.07.010
107. Hunter JM, Kwan J, Malek-Ahmadi M, et al. Morphological and pathological evolution of the brain microcirculation in aging and Alzheimer's disease. *PLoS One*. 2012.  
doi:10.1371/journal.pone.0036893
108. Roher AE, Esh C, Rahman A, Kokjohn TA, Beach TG. Atherosclerosis of cerebral arteries in Alzheimer disease. In: *Stroke*. ; 2004. doi:10.1161/01.STR.0000143317.70478.b3
109. Schneider JA, Arvanitakis Z, Bang W, Bennett DA. Mixed brain pathologies account for most dementia cases in community-dwelling older persons. *Neurology*. 2007.  
doi:10.1212/01.wnl.0000271090.28148.24
110. Park L, Anrather J, Zhou P, et al. NADPH-oxidase-derived reactive oxygen species mediate the cerebrovascular dysfunction induced by the amyloid beta peptide. *J Neurosci*. 2005;25(7):1769-1777. doi:10.1523/JNEUROSCI.5207-04.2005
111. Park L, Zhou P, Pitstick R, et al. Nox2-derived radicals contribute to neurovascular and behavioral dysfunction in mice overexpressing the amyloid precursor protein. *Proc Natl Acad Sci U S A*. 2008;105(4):1347-1352. doi:10.1073/pnas.0711568105

112. Tarantini S, Tran CHT, Gordon GR, Ungvari Z, Csiszar A. Impaired neurovascular coupling in aging and Alzheimer's disease: Contribution of astrocyte dysfunction and endothelial impairment to cognitive decline. *Exp Gerontol*. 2017;94:52-58.  
doi:10.1016/j.exger.2016.11.004
113. Tarantini S, Hertelendy P, Tucsek Z, et al. Pharmacologically-induced neurovascular uncoupling is associated with cognitive impairment in mice. *J Cereb Blood Flow Metab*. 2015;35(11):1871-1881. doi:10.1038/jcbfm.2015.162
114. Chen W, Liu P, Volkow ND, Pan Y, Du C. Cocaine attenuates blood flow but not neuronal responses to stimulation while preserving neurovascular coupling for resting brain activity. *Mol Psychiatry*. 2016. doi:10.1038/mp.2015.185
115. Uchida S, Bois S, Guillemot JP, Leblond H, Piché M. Systemic blood pressure alters cortical blood flow and neurovascular coupling during nociceptive processing in the primary somatosensory cortex of the rat. *Neuroscience*. 2017;343:250-259.  
doi:10.1016/j.neuroscience.2016.12.014
116. Sekiguchi Y, Takuwa H, Kawaguchi H, et al. Pial arteries respond earlier than penetrating arterioles to neural activation in the somatosensory cortex in awake mice exposed to chronic hypoxia: An additional mechanism to proximal integration signaling? *J Cereb Blood Flow Metab*. 2014;34(11):1761-1770. doi:10.1038/jcbfm.2014.140
117. Watanabe N, Sasaki S, Masamoto K, Hotta H. Vascular gap junctions contribute to forepaw stimulation-induced vasodilation differentially in the pial and penetrating arteries in isoflurane-anesthetized rats. *Front Mol Neurosci*. 2018;11:446.  
doi:10.3389/fnmol.2018.00446
118. Cai C, Fordsmann JC, Jensen SH, et al. Stimulation-induced increases in cerebral blood flow and local capillary vasoconstriction depend on conducted vascular responses. *Proc Natl Acad Sci*. 2018;115(25):E5796-E5804. doi:10.1073/pnas.1707702115

119. Rungta RL, Chaigneau E, Osmanski BF, Charpak S. Vascular Compartmentalization of Functional Hyperemia from the Synapse to the Pia. *Neuron*. 2018;99(2):362-375.e4. doi:10.1016/j.neuron.2018.06.012
120. Drew PJ, Shih AY, Kleinfeld D. Fluctuating and sensory-induced vasodynamics in rodent cortex extend arteriole capacity. *Proc Natl Acad Sci*. 2011;108(20):8473-8478. doi:10.1073/pnas.1100428108
121. Shabir O, Berwick J, Francis SE. Neurovascular dysfunction in vascular dementia, Alzheimer's and atherosclerosis. *BMC Neurosci*. 2018;19(1). doi:10.1186/s12868-018-0465-5
122. Beason-Held LL, Kraut MA, Resnick SM. II. Temporal patterns of longitudinal change in aging brain function. *Neurobiol Aging*. 2008. doi:10.1016/j.neurobiolaging.2006.11.011
123. Ting JT, Lee BR, Chong P, et al. Preparation of Acute Brain Slices Using an Optimized N-Methyl-D-glucamine Protective Recovery Method. *J Vis Exp*. 2018;(132):e53825. doi:10.3791/53825
124. Balbi M, Koide M, Wellman GC, Plesnila N. Inversion of neurovascular coupling after subarachnoid hemorrhage in vivo. *J Cereb Blood Flow Metab*. 2017;37(11):3625-3634. doi:10.1177/0271678X16686595
125. Mulligan SJ, MacVicar BA. Calcium transients in astrocyte endfeet cause cerebrovascular constrictions. *Nature*. 2004;431(7005):195-199. doi:10.1038/nature02827
126. Xu H-L, Mao L, Ye S, Paisansathan C, Vetri F, Pelligrino DA. Astrocytes are a key conduit for upstream signaling of vasodilation during cerebral cortical neuronal activation in vivo. *Am J Physiol Heart Circ Physiol*. 2008;294(2):H622-32. doi:10.1152/ajpheart.00530.2007
127. Filosa. Vascular tone and neurovascular coupling: considerations toward an improved in vitro model. *Front Neuroenergetics*. 2010;2. doi:10.3389/fnene.2010.00016

128. Armstead WM, Mirro R, Busija DW, Leffler CW. Vascular responses to vasopressin are tone-dependent in the cerebral circulation of the newborn pig. *Circ Res*. 1989;64(1):136-144. <http://www.ncbi.nlm.nih.gov/pubmed/2909297>. Accessed June 28, 2019.
129. Draijer M, Hondebrink E, Van Leeuwen T, Steenbergen W. Review of laser speckle contrast techniques for visualizing tissue perfusion. *Lasers Med Sci*. 2009;24(4):639-651. doi:10.1007/s10103-008-0626-3
130. Hungerhuber E, Zausinger S, Westermaier T, Plesnila N, Schmid-Elsaesser R. Simultaneous bilateral laser Doppler fluxmetry and electrophysiological recording during middle cerebral artery occlusion in rats. *J Neurosci Methods*. 2006;154(1-2):109-115. doi:10.1016/j.jneumeth.2005.12.004
131. Ances BM, Detre JA, Takahashi K, Greenberg JH. Transcranial laser Doppler mapping of activation flow coupling of the rat somatosensory cortex. *Neurosci Lett*. 1998;257(1):25-28. doi:10.1016/S0304-3940(98)00796-4
132. Ances BM, Greenberg JH, Detre JA. Laser Doppler imaging of activation-flow coupling in the rat somatosensory cortex. *Neuroimage*. 1999;10(6):716-723. doi:10.1006/nimg.1999.0510
133. Kazmi SS, Richards LM, Schrandt CJ, Davis MA, Dunn AK. Expanding Applications, Accuracy, and Interpretation of Laser Speckle Contrast Imaging of Cerebral Blood Flow. *J Cereb Blood Flow Metab*. 2015;35(7):1076-1084. doi:10.1038/jcbfm.2015.84
134. Yuan S, Devor A, Boas DA, Dunn AK. Determination of optimal exposure time for imaging of blood flow changes with laser speckle contrast imaging. *Appl Opt*. 2005;44(10):1823. doi:10.1364/AO.44.001823
135. Kazmi SMS, Richards LM, Schrandt CJ, Davis MA, Dunn AK. Expanding applications, accuracy, and interpretation of laser speckle contrast imaging of cerebral blood flow. *J Cereb Blood Flow Metab*. 2015;35(7):1076-1084. doi:10.1038/jcbfm.2015.84

136. Bo B, Li Y, Li W, Wang Y, Tong S. Optogenetic excitation of ipsilesional sensorimotor neurons is protective in acute ischemic stroke: a laser speckle imaging study. *IEEE Transactions on Biomedical Engineering*. 2018.
137. Fredriksson I, Larsson M, Strömberg T. Measurement depth and volume in laser Doppler flowmetry. *Microvasc Res*. 2009;78(1):4-13. doi:10.1016/j.mvr.2009.02.008
138. Cho A, Yeon C, Kim D, Chung E. Laser Speckle Contrast Imaging for Measuring Cerebral Blood Flow Changes Caused by Electrical Sensory Stimulation. 2016;20(1):88-93. doi:10.3807/JOSK.2016.20.1.088
139. Yuan Y, Zhao Y, Jia H, et al. Cortical hemodynamic responses under focused ultrasound stimulation using real-time laser speckle contrast imaging. *Front Neurosci*. 2018;12(APR):1-8. doi:10.3389/fnins.2018.00269
140. Shin P, Choi WJ, Joo JY, Oh WY. Quantitative hemodynamic analysis of cerebral blood flow and neurovascular coupling using optical coherence tomography angiography. *Journal of Cerebral Blood Flow and Metabolism*. <https://doi.org/10.1177/0271678X18773432>. Published 2018.
141. Ayata C, Dunn AK, Gursoy-Özdemir Y, Huang Z, Boas DA, Moskowitz MA. Laser speckle flowmetry for the study of cerebrovascular physiology in normal and ischemic mouse cortex. *J Cereb Blood Flow Metab*. 2004;24(7):744-755. doi:10.1097/01.WCB.0000122745.72175.D5
142. Tarantini S, Fulop GA, Kiss T, et al. Demonstration of impaired neurovascular coupling responses in TG2576 mouse model of Alzheimer's disease using functional laser speckle contrast imaging. *GeroScience*. 2017;39(4):465-473. doi:10.1007/s11357-017-9980-z
143. Davis MA, Kazmi SMS, Dunn AK. Imaging depth and multiple scattering in laser speckle contrast imaging. *J Biomed Opt*. 2014;19(8):086001. doi:10.1117/1.JBO.19.8.086001

144. Shih AY, Driscoll JD, Pesavento MJ, Kleinfeld D. Two-photon microscopy to measure blood flow and concurrent brain cell activity. In: *Neuromethods*. Vol 85. ; 2014:273-290. doi:10.1007/978-1-62703-785-3\_16
145. Shih AY, Driscoll JD, Drew PJ, Nishimura N, Schaffer CB, Kleinfeld D. Two-photon microscopy as a tool to study blood flow and neurovascular coupling in the rodent brain. *J Cereb Blood Flow Metab*. 2012;32(7):1277-1309. doi:10.1038/jcbfm.2011.196
146. Kleinfeld D, Blinder P, Drew PJ, et al. A guide to delineate the logic of neurovascular signaling in the brain. *Front Neuroenergetics*. 2011;(APRIL):1-9. doi:10.3389/fnene.2011.00001
147. Holtmaat A, Bonhoeffer T, Chow DK, et al. Long-term, high-resolution imaging in the mouse neocortex through a chronic cranial window. *Nat Protoc*. 2009;4(8):1128-1144. doi:10.1038/nprot.2009.89
148. Belluscio L, Katz L, Lecoq J, Ducros M, Knöpfel T, Charpak S. Symmetry, Stereotypy, and Topography of Odorant Representations in Mouse Olfactory Bulbs. *J Neurosci*. 2007;21(6):2113-2122. doi:10.1523/jneurosci.3141-06.2007
149. Uludağ K, Dubowitz DJ, Yoder EJ, Restom K, Liu TT, Buxton RB. Coupling of cerebral blood flow and oxygen consumption during physiological activation and deactivation measured with fMRI. *Neuroimage*. 2004;23(1):148-155. doi:10.1016/j.neuroimage.2004.05.013
150. Riva CE, Logean E, Falsini B. Visually evoked hemodynamical response and assessment of neurovascular coupling in the optic nerve and retina. *Prog Retin Eye Res*. 2005;24(2):183-215. doi:10.1016/j.preteyeres.2004.07.002
151. Johnson KO. The roles and functions of cutaneous mechanoreceptors. *Curr Opin Neurobiol*. 2001;11(4):455-461. <http://www.ncbi.nlm.nih.gov/pubmed/11502392>. Accessed June 28, 2019.

152. Vallbo AB, Johansson RS. Properties of cutaneous mechanoreceptors in the human hand related to touch sensation. *Hum Neurobiol.* 1984;3(1):3-14.  
<http://www.ncbi.nlm.nih.gov/pubmed/6330008>. Accessed June 28, 2019.
153. Hoover JE, Hoffer ZS, Alloway KD. Projections from primary somatosensory cortex to the neostriatum: the role of somatotopic continuity in corticostriatal convergence. *J Neurophysiol.* 2003;89(3):1576-1587. doi:10.1152/jn.01009.2002
154. Uchida S, Kagitani F. Effect of acupuncture-like stimulation on cortical cerebral blood flow in aged rats. *J Physiol Sci.* 2015;65(1):67-75. doi:10.1007/s12576-014-0340-9
155. Gutiérrez-Jiménez E, Cai C, Mikkelsen IK, et al. Effect of electrical forepaw stimulation on capillary transit-time heterogeneity (CTH). *J Cereb Blood Flow Metab.* 2016;36(12):2072-2086. doi:10.1177/0271678X16631560
156. Shih YYI, Huang S, Chen YY, et al. Imaging neurovascular function and functional recovery after stroke in the rat striatum using forepaw stimulation. *J Cereb Blood Flow Metab.* 2014;34(9):1483-1492. doi:10.1038/jcbfm.2014.103
157. Urban A, Mace E, Brunner C, Heidmann M, Rossier J, Montaldo G. Chronic assessment of cerebral hemodynamics during rat forepaw electrical stimulation using functional ultrasound imaging. *Neuroimage.* 2014;101:138-149.  
doi:10.1016/j.neuroimage.2014.06.063
158. Adamczak JM, Farr TD, Seehafer JU, Kalthoff D, Hoehn M. High field BOLD response to forepaw stimulation in the mouse. *Neuroimage.* 2010;51(2):704-712.  
doi:10.1016/j.neuroimage.2010.02.083
159. Ances BM, Greenberg JH, Detre JA. Activation-flow coupling with forepaw stimulation in female and male rats. *Neurosci Res.* 1999;35(1):37-41. doi:10.1016/S0168-0102(99)00065-6

160. Lim DH, Mohajerani MH, Ledue J, Boyd J, Chen S, Murphy TH. In vivo large-scale cortical mapping using channelrhodopsin-2 stimulation in transgenic mice reveals asymmetric and reciprocal relationships between cortical areas. *Front Neural Circuits*. 2012. doi:10.3389/fncir.2012.00011
161. Vogel J, Kuschinsky W. Decreased heterogeneity of capillary plasma flow in the rat whisker- barrel cortex during functional hyperemia. *J Cereb Blood Flow Metab*. 1996;16(6):1300-1306. doi:10.1097/00004647-199611000-00026
162. Lecrux C, Sandoe CH, Neupane S, et al. Impact of Altered Cholinergic Tones on the Neurovascular Coupling Response to Whisker Stimulation. *J Neurosci*. 2017;37(6):1518-1531. doi:10.1523/JNEUROSCI.1784-16.2016
163. Cox SB, Woolsey TA, Rovainen CM. Localized dynamic changes in cortical blood flow with whisker stimulation corresponds to matched vascular and neuronal architecture of rat barrels. *J Cereb Blood Flow Metab*. 1993;13(6):899-913. doi:10.1038/jcbfm.1993.113
164. Sarna JR, Dyck RH, Whishaw IQ. The Dalila effect: C57BL6 mice barber whiskers by plucking. *Behav Brain Res*. 2000;108(1):39-45. doi:10.1016/S0166-4328(99)00137-0
165. Masamoto K, Kanno I. Anesthesia and the quantitative evaluation of neurovascular coupling. *J Cereb Blood Flow Metab*. 2012;32(7):1233-1247. doi:10.1038/jcbfm.2012.50
166. Lindauer U, Villringer A, Dirnagl U. Characterization of CBF response to somatosensory stimulation: model and influence of anesthetics. *Am J Physiol Circ Physiol*. 1993;264(4):H1223-H1228. doi:10.1152/ajpheart.1993.264.4.H1223
167. Hyder F, Rothman DL, Shulman RG. Total neuroenergetics support localized brain activity: Implications for the interpretation of fMRI. *Proc Natl Acad Sci*. 2002;99(16):10771-10776. doi:10.1073/pnas.132272299
168. Ueki M, Mies G, Hossmann KA. Effect of alpha-chloralose, halothane, pentobarbital and nitrous oxide anesthesia on metabolic coupling in somatosensory cortex of rat. *Acta*

*Anaesthesiol Scand.* 1992;36(4):318-322.

<http://www.ncbi.nlm.nih.gov/pubmed/1595336>. Accessed June 28, 2019.

169. Akata T, Kanna T, Yoshino J, Takahashi S. Mechanisms of direct inhibitory action of isoflurane on vascular smooth muscle of mesenteric resistance arteries. *Anesthesiology*. 2003;99(3):666-677. doi:10.1097/00000542-200309000-00023
170. Kokita N, Stekiel TA, Yamazaki M, Bosnjak ZJ, Kampine JP, Stekiel WJ. Potassium Channel-mediated Hyperpolarization of Mesenteric Vascular Smooth Muscle by Isoflurane. *Anesthesiology*. 1999;90(3):779-788. doi:10.1097/00000542-199903000-00021
171. Masamoto K, Fukuda M, Vazquez A, Kim SG. Dose-dependent effect of isoflurane on neurovascular coupling in rat cerebral cortex. *Eur J Neurosci*. 2009;30(2):242-250. doi:10.1111/j.1460-9568.2009.06812.x
172. Dudley RE, Nelson SR, Samson F. Influence of chloralose on brain regional glucose utilization. *Brain Res*. 1982;233(1):173-180. doi:10.1016/0006-8993(82)90938-6
173. Gao YR, Ma Y, Zhang Q, et al. Time to wake up: Studying neurovascular coupling and brain-wide circuit function in the un-anesthetized animal. *Neuroimage*. 2017;153(April):382-398. doi:10.1016/j.neuroimage.2016.11.069
174. Wright PW, Brier LM, Bauer AQ, et al. Functional connectivity structure of cortical calcium dynamics in anesthetized and awake mice. *PLoS One*. 2017;12(10):1-27. doi:10.1371/journal.pone.0185759
175. Balbi M, Vanni MP, Silasi G, et al. Targeted ischemic stroke induction and mesoscopic imaging assessment of blood flow and ischemic depolarization in awake mice. *Neurophotonics*. 2017;4(3):035001. doi:10.1117/1.nph.4.3.035001
176. Silasi G, Xiao D, Vanni MP, Chen ACN, Murphy TH. Intact skull chronic windows for mesoscopic wide-field imaging in awake mice. *J Neurosci Methods*. 2016;267:141-149. doi:10.1016/j.jneumeth.2016.04.012

177. Tajima Y, Takuwa H, Nishino A, et al. Cerebral hemodynamic response to acute hyperoxia in awake mice. *Brain Res.* 2014;1557:155-163. doi:10.1016/j.brainres.2014.01.053
178. Tran CHT, Gordon GR. Astrocyte and microvascular imaging in awake animals using two-photon microscopy. *Microcirculation.* 2015;22(3):219-227. doi:10.1111/micc.12188
179. Takuwa H, Autio J, Nakayama H, et al. Reproducibility and variance of a stimulation-induced hemodynamic response in barrel cortex of awake behaving mice. *Brain Res.* 2011;1369:103-111. doi:10.1016/j.brainres.2010.11.007
180. Dombeck DA, Khabbaz AN, Collman F, Adelman TL, Tank DW. Imaging Large-Scale Neural Activity with Cellular Resolution in Awake, Mobile Mice. *Neuron.* 2007;56(1):43-57. doi:10.1016/j.neuron.2007.08.003
181. Sharp PS, Shaw K, Boorman L, et al. Comparison of stimulus-evoked cerebral hemodynamics in the awake mouse and under a novel anesthetic regime. *Sci Rep.* 2015;5(March). doi:10.1038/srep12621
182. Kim T, Masamoto K, Fukuda M, Vazquez A, Kim SG. Frequency-dependent neural activity, CBF, and BOLD fMRI to somatosensory stimuli in isoflurane-anesthetized rats. *Neuroimage.* 2010;52(1):224-233. doi:10.1016/j.neuroimage.2010.03.064
183. Krystal JH. Subanesthetic Effects of the Noncompetitive NMDA Antagonist, Ketamine, in Humans. *Arch Gen Psychiatry.* 1994;51(3):199. doi:10.1001/archpsyc.1994.03950030035004
184. Zhao F, Zhao T, Zhou L, Wu Q, Hu X. BOLD study of stimulation-induced neural activity and resting-state connectivity in medetomidine-sedated rat. *Neuroimage.* 2008;39(1):248-260. doi:10.1016/j.neuroimage.2007.07.063
185. Ances BM, Greenberg JH, Detre JA. Effects of variations in interstimulus interval on activation-flow coupling response and somatosensory evoked potentials with forepaw

- stimulation in the rat. *J Cereb Blood Flow Metab.* 2000;20(2):290-297.  
doi:10.1097/00004647-200002000-00010
186. Dutta S, Sengupta P. Men and mice: Relating their ages. *Life Sci.* 2016;152:244-248.  
doi:10.1016/j.lfs.2015.10.025
187. Pelligrino DA, Koenig HM, Albrecht RF. Nitric oxide synthesis and regional cerebral blood flow responses to hypercapnia and hypoxia in the rat. *J Cereb Blood Flow Metab.* 1993;13(1):80-87. doi:10.1038/jcbfm.1993.10
188. Park L, Anrather J, Girouard H, Zhou P, Iadecola C. Nox2-derived reactive oxygen species mediate neurovascular dysregulation in the aging mouse brain. *J Cereb Blood Flow Metab.* 2007;27(12):1908-1918. doi:10.1038/sj.jcbfm.9600491
189. Helmchen F, Gilad A, Chen JL. Neocortical dynamics during whisker-based sensory discrimination in head-restrained mice. *Neuroscience.* 2018.  
doi:10.1016/j.neuroscience.2017.09.003
190. Flood DG, Coleman PD. Neuron numbers and sizes in aging brain: Comparisons of human, monkey, and rodent data. *Neurobiol Aging.* 1988;9(C):453-463. doi:10.1016/S0197-4580(88)80098-8
191. Liguz-Leczna M, Siucinska E, Zakrzewska R, Kossut M. Impairment of experience-dependent cortical plasticity in aged mice. *Neurobiol Aging.* 2011;32(10):1896-1905.  
doi:10.1016/j.neurobiolaging.2009.11.009
192. Coq JO, Xerri C. Sensorimotor experience modulates age-dependent alterations of the forepaw representation in the rat primary somatosensory cortex. *Neuroscience.* 2001;104(3):705-715. doi:10.1016/S0306-4522(01)00123-3
193. Park L, Anrather J, Girouard H, Zhou P, Iadecola C. Nox2-derived reactive oxygen species mediate neurovascular dysregulation in the aging mouse brain. *J Cereb Blood Flow Metab.* 2007. doi:10.1038/sj.jcbfm.9600491

194. Sharma G, Goodwin J. Effect of aging on respiratory system physiology and immunology. *Clin Interv Aging*. 2006;1(3):253-260. doi:10.2147/cia.2006.1.3.253
195. Janssens JP, Pache JC, Nicod LP. Physiological changes in respiratory function associated with ageing. *Eur Respir J*. 1999;13(1):197-205. doi:10.1034/j.1399-3003.1999.13a36.x
196. Desjardins M, Berti R, Pouliot P, Dubeau S, Lesage F. Multimodal study of the hemodynamic response to hypercapnia in anesthetized aged rats. *Neurosci Lett*. 2014;563:33-37. doi:10.1016/j.neulet.2014.01.027
197. Stefanidis KB, Askew CD, Klein T, Lagopoulos J, Summers MJ. Healthy aging affects cerebrovascular reactivity and pressure-flow responses, but not neurovascular coupling: A cross-sectional study. Mogi M, ed. *PLoS One*. 2019;14(5):e0217082. doi:10.1371/journal.pone.0217082
198. Nowak-Flück D, Ainslie PN, Bain AR, et al. Effect of healthy aging on cerebral blood flow, CO<sub>2</sub> reactivity, and neurovascular coupling during exercise. *J Appl Physiol*. 2018;125(6):1917-1930. doi:10.1152/jappphysiol.00050.2018
199. Nishino A, Takuwa H, Urushihata T, Ito H, Ikoma Y, Matsuura T. Vasodilation Mechanism of Cerebral Microvessels Induced by Neural Activation under High Baseline Cerebral Blood Flow Level Results from Hypercapnia in Awake Mice. *Microcirculation*. 2015;22(8):744-752. doi:10.1111/micc.12250
200. Gutiérrez-Jiménez E, Angleys H, Rasmussen PM, et al. Disturbances in the control of capillary flow in an aged APP<sup>swE</sup>/PS1<sup>ΔE9</sup> model of Alzheimer's disease. *Neurobiol Aging*. 2018;62:82-94. doi:10.1016/j.neurobiolaging.2017.10.006
201. Peppiatt CM, Howarth C, Mobbs P, Attwell D. Bidirectional control of CNS capillary diameter by pericytes. *Nature*. 2006;443(7112):700-704. doi:10.1038/nature05193

202. Murphy GG, Rahnama NP, Silva AJ. Investigation of age-related cognitive decline using mice as a model system: Behavioral correlates. *Am J Geriatr Psychiatry*. 2006;14(12):1004-1011. doi:10.1097/01.JGP.0000209405.27548.7b
203. Harburger LL, Lambert TJ, Frick KM. Age-dependent effects of environmental enrichment on spatial reference memory in male mice. *Behav Brain Res*. 2007;185(1):43-48. doi:10.1016/j.bbr.2007.07.009
204. Baraldi T, Schöwe NM, Balthazar J, et al. Cognitive stimulation during lifetime and in the aged phase improved spatial memory, and altered neuroplasticity and cholinergic markers of mice. *Exp Gerontol*. 2013;48(8):831-838. doi:10.1016/j.exger.2013.05.055
205. Barreto G, Huang TT, Giffard RG. Age-related defects in sensorimotor activity, spatial learning, and memory in c57bl/6 mice. *J Neurosurg Anesthesiol*. 2010;22(3):214-219. doi:10.1097/ANA.0b013e3181d56c98

## 7. Abbreviations

A $\beta$	Amyloid beta
AD	Alzheimer's disease
AMPA	$\alpha$ -amino-3-hydroxy-5-methyl-4-isoxazole propionic acid
AUC	Area under the curve
BBB	Blood brain barrier
BOLD	Blood-oxygen-level-dependent
CBF	Cerebral blood flow
CGRP	Calcitonin gene-related peptide
COX-2	Cyclooxygenase 2
DTI	Diffusion tensor imaging
fMRI	Functional magnetic resonance imaging
GABA	$\gamma$ -aminobutyric acid
IP3	Inositol triphosphate
IR-DIC	Infrared-differential interference contrast
K <sup>+</sup>	potassium
K <sub>ir</sub>	Inward-rectifier potassium
LDF	Laser Doppler flowmetry
LSI	Laser speckle imaging

LTP	Long-term potentiation
MRI	Magnetic resonance imaging
NVC	Neurovascular coupling
NVU	Neurovascular unite
NMDA	N-methyl-D-aspartate
nNOS	Neuronal nitric oxide synthase
NADPH	Nicotinamide adenine dinucleotide phosphate
NO	Nitric oxide
NPY	Neuropeptide Y
NG2	Neuron-glia antigen 2
PDGFR- $\beta$	Platelet-derived growth factor receptor $\beta$
PGE2	Prostaglandin E2
PLA2	Phospholipase A2
ROS	Reactive oxygen species
ROI	Region of interest
SMC	Smooth muscle cell
VPL	Ventral posterior lateral nucleus
VPM	Ventral posterior medial nucleus
VIP	Intestinal peptide

20-HETE

20-Hydroxyeicosatetraenoic acid

$\alpha$ -SMA

$\alpha$ -smooth muscle actin

## **8. Acknowledgments**

First of all, I want to express my gratitude to my supervisor Dr. Nikolaus Plesnila. Thank you for offering me the opportunity to study and work in the lab and the general support and guidance throughout the whole project. Next, I want to thank my advisor Dr. Burcu Şeker for her daily help to me in the experiment whether big or small and each time of discussion that helps me improve myself and progress. I want to thank all the AG Plesnila members for the kind help and the friendly working environment. I want to thank our animal caretakers for the help in animal experiments. I also want to thank Mihail Todorov for his kindly offer of some 1 year-old aged mice.

I want to thank my parents and other family members for their care, support, and encouragement. I want to thank all my friends in Munich for the time we spend together.

In the end, I want to thank my wife. The best thing in my life is meeting you here.

## **Affidavit**

I, Ziyu Fan, hereby confirm that my thesis entitled

The effect of age on neuro-vascular reactivity in mice

is the result of my own work. I did not receive any help or support from commercial consultants. All sources and/or materials applied are listed and specified in the thesis.

Furthermore, I confirm that this thesis has not yet been submitted as part of another examination process neither in identical nor in similar form.

Place and date: Munich, 05.03.2021

Name: Ziyu Fan